DISSERTATION

ELECTROPHYSIOLOGICAL ANALYSIS OF KV2 CHANNEL REGULATION VIA NON-CANONICAL AND CANONICAL MECHANISMS

Submitted by

Emily E. Maverick

Department of Biomedical Sciences

In partial fulfillment of the requirements

For the Degree of Doctor of Philosophy

Colorado State University

Fort Collins, Colorado

Fall 2020

Doctoral Committee:

Advisor: Michael Tamkun

Gregory Amberg
Diego Krapf
Susan Tsunoda
Jozsef Vigh

ABSTRACT

ELECTROPHYSIOLOGICAL ANALYSIS OF KV2 CHANNEL REGULATION VIA NON-CANONICAL AND CANONICAL MECHANISMS

Kv2 channels are the most abundant voltage-gated potassium channels in the mammalian nervous system and entire body. These channels regulate action potential firing and apoptosis via their canonical conducting functions. However, Kv2 channels also play a non-conducting role in the cells in which they are expressed. Specifically, they form junctions between the endoplasmic reticulum and plasma membranes, and these junctions regulate a myriad of cellular process. Several studies have now shown that many Kv2.1 channels expressed on the plasma membranes of mammalian cells do not respond canonically to changes in membrane voltage. Instead of opening to allow potassium efflux, the pores of these non-canonical channels are locked in a non-conducting state. This state has likely evolved to prevent electrical paralysis that would otherwise be conferred upon cells expressing high levels of completely functional Kv2 channels. The mechanism bringing about the non-conducting state of Kv2.1 channels is unknown.

The work described in the first part of this dissertation was carried out with the ultimate goal of revealing the mechanism of the Kv2.1 channel non-conducting state. I describe an improved, all-electrophysiological method to quantify the numbers of non-conducting Kv channels expressed in heterologous systems. I validate this approach by measuring the fraction of non-conducting Kv2.1 channels that arise when expressed in HEK293 cells. I go on to use this approach to show evidence for a non-conducting state in the second Kv2 isoform, Kv2.2, for the first time. I find that like Kv2.1, the Kv2.2 non-conducting state is dependent on the density of channels in the membrane. Surprisingly, I also find that two *Shaker*-related channels, Kv1.4 and Kv1.5 also show density depen-

dence in the fraction of channels that conduct. These results suggest that the mechanism underlying the non-conducting state is more common than we thought, and I discuss hypotheses that should be tested in the future.

In the last part of this dissertation I describe the effects of the assembly of Kv2 channels with a newly discovered family of Kv β subunits, the AMIGOs. The experiments in this portion of the dissertation focus on AMIGO's ability to modulate canonical, conducting Kv2 channels, as well as Kv2's ability to alter AMIGO trafficking and localization. I find that both Kv2.1 and Kv2.2 promote AMIGO trafficking to the plasma membrane and alter their localization there. I also find that while all three AMIGO isoforms promote Kv2 channel opening, AMIGO2 confers an additional stabilizing effect on the open state by slowing inactivation and deactivation.

In all, the work in this dissertation expands on our current understanding of Kv channel function. These findings should guide future experiments to probe both canonical and non-canonical functions of Kv channels.

ACKNOWLEDGEMENTS

First and foremost, I would like to acknowledge my adviser, Dr. Mike Tamkun for harboring a lab environment that allowed me to flourish. I knew before I came to CSU that Mike's lab would be my top choice, and he enthusiastically agreed to take me on. I don't think he understood the depths of my obsession with ion channel structure/function at the time, although I don't know that I did either. It is a testament to Mike's character as a mentor and a scientist that he allowed me to pursue a project that truly stirred the workings of my mind, despite his warnings of its difficulty and its tangential relationship to other ongoing lab projects. Thank you also, Mike, for sharing so many good backpacking spots and for always being excited to see pictures from my adventures.

Next, I would like to thank my lab mates. Ashley and Laura, we have been Tamkunites together for so many years! It has truly been a privilege to work alongside you both. Each of you brings unique strengths to the lab and I have relied on you both countless times for protocol advice, cell feedings, and general lab wisdom, but also equally important things like chocolate, ibuprofen, alcohol, Hot Chicken and good company. Laura, you taught me how to do electrophysiology, which is one of the greatest gifts I have ever received. I am endlessly impressed by your knowledge of lab techniques and experimental design, and I have learned so much from working with you. Ashley, we have shared so many moments in our PhD journeys. I can't imagine having anyone else to celebrate the tiny joys with and to mourn the many failures. Your support has been unwavering, and working closely with you on our joint project over the past year has truly been a highlight of my graduate career. Ben, Liz and Phil, I have not forgotten about you and never will. You three embody the spirit of the Tamkun lab in my mind and have each imparted your wisdom on me in different ways. I am a better scientist having worked with you three.

I would also like to acknowledge the members of my thesis committee, for their prompt responses to Doodle polls and their universal willingness to consult with me

about my project. I cannot think of a time when I needed one of your advice and did not get it. Jozsef, thank you for the lengthy and sometimes philosophical discussions about electrophysiology. I will never forget that the first gigaseal I ever made was in your lab. Susan and Greg, thank you for sharing so many reagents with me without expectation of repayment. There were many a preliminary (or emergency) experiment that were done because you or your students made them possible. Diego, thank you for consulting with me on so many projects over the years. You have always been generous with your time in explaining mathematical concepts or giving your opinion on various types of analysis.

Next I would like to thank my family, especially my mom and dad for their endless support of my lifelong pursuit of learning. You two were always excited to hear about my experiences in graduate school, scientific or otherwise, and were quick to offer advice, ask questions or simply provide a listening ear. Thank you for your support throughout this long journey and for not asking "When will you graduate?" too many times.

Lastly, but most importantly, I would like to acknowledge you, Stephen, as my rock and most crucial supporter. On hard days, you were always the first to remind me that my PhD was not about the outcome, but the journey. On the good days you always wanted to hear the details. Thank you for the many electronics lessons and for taking a true interest in the technicalities of my field. I love you.

DEDICATION

To all the teachers I've ever had, within school and without, for instilling in me a love of learning and curiosity about the world

TABLE OF CONTENTS

LIST OF TABLES

LIST OF FIGURES

Chapter 1

Introduction

1.1 Excitable membranes and membrane potential

1.1.1 "Animal electricity" and the dawn of electrophysiology

The systematic study of excitable tissues began in the late 18th century with Luigi Galvani, an Italian surgeon and anatomist with an interest in the physiological basis of the interaction between electricity and the human body. Doctors of the day used electricity to treat ailments ranging from "paralysis, sciatic pain, deafness and rheumatic afflictions" and this branch of medicine termed "medical electricity" was quite popular [1]. However, at the time no one understood how electricity elicited such dramatic effects on the human body as accelerated heart rate, perspiration and muscle contraction. It was common knowledge among physicians at the time that a dissected frog muscle could contract upon electrical stimulation long after the animal had died. Galvani's methodical approach to the study of the frog neuro-muscular preparation led to his hypothesis that electricity – from conducting wires or even lightning – interacted with some intrinsic excitability in the preparation that in turn led to muscle contraction. And thus, Galvani proposed the idea of animal electricity, the means by which "the animal…maintains [the electrical fluid] in a state of disequilibrium, ready to be set in motion by means of…external or internal influences" [1]. This insight sparked further exploration of electrical conduction in the nervous system and gave rise to the field of electrophysiology as we know it today.

1.1.2 Ionic gradients underlie neuronal signaling

By the early 1900s, it was clear that ionic salts were required for muscle and nerve excitability. Julius Bernstein formalized a hypothesis regarding nerve conduction, suggesting that "excitable cells are surrounded by a membrane selectively permeable to K^+ ions at rest and that during excitation the membrane permeability to other ions increases" [2].

Although he was correct in his description of resting permeability, Berstein was incorrect in his suggestion that the membrane lost selective permeability during excitation. However, Bernstein's membrane hypothesis drove experimentation in the 1930's, 40's and 50's and should be given significant credit. Out of a desire to formally test the membrane hypothesis, Hodgkin and Huxley devised an innovative recording apparatus and made the first intracellular recording of an action potential (AP) from a squid axon (Figure 1.1) [3].

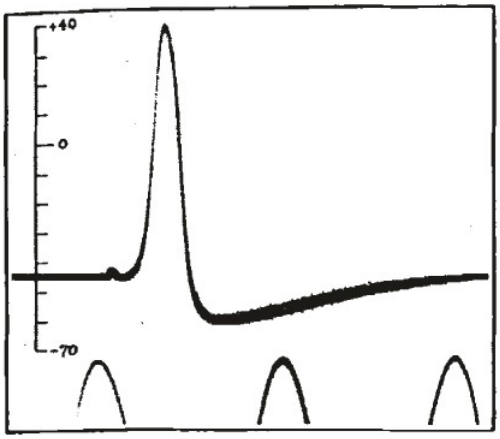

Figure 1.1: The first intracellular recording of an action potential. The membrane potential is given on the y-axis in reference to the extracellular solution. Note that the membrane potential does not simply collapse during the action potential, but reverses sign. The time scale is given by the cycles along the bottom of the figure which are each 2 ms apart. Figure from [3].

They were surprised to see the membrane potential reverse, surpassing the zero potential condition predicted for a membrane permeable to all ions. This observation was confirmed a few years later by Curtis and Cole at Woods Hole using a slightly different apparatus [4]. In this same work Curtis and Cole investigated the dependence of the AP on different ionic species and noted that the resting potential depended strongly on K^+ while the action potential did not. This led them to conclude "that a separate mechanism [was] responsible for the production of each" [4].

1.1.3 Selective permeability is key to nerve impulses

Two breakthroughs were paramount to a deeper understanding of the phenomena Hodgkin, Huxley, Curtis and Cole had observed. First was Goldman's mathematical treatment of the Nernst-Planck equation, which relates ion flow in a solution to the concentration of the ions and the strength of the electric field they feel [5, 6]. Using a few key assumptions – that the electric field is constant across the axon membrane and that ion activity near the membrane is proportional to the bulk ion concentration – Goldman explicitly related membrane current to the membrane potential and bulk ion concentrations:

$$I_i = \frac{P_i z_i^2 F^2 V}{RT}\left(\frac{C_{i,in} e^{z_i FV/RT} - C_{i,out}}{e^{z_i FV/RT} - 1}\right) \tag{1.1}$$

where I is the current density of the ionic species i, P refers to that ion's membrane permeability, z is the ion's valence, and $C_{i,in}$ and $C_{i,out}$ are the concentrations of that ion inside and outside the cell, respectively. This relation was key in the interpretation of a new observation that the speed and magnitude of the AP depended greatly on Na^+ [7]. A rearrangement of Equation (1.1) led to the concept of relative permeability, and takes the form now known as the Goldman-Hodgkin-Katz voltage equation:

$$V_m = \frac{RT}{F} ln \frac{P_K[K]_{out} + P_{Na}[Na]_{out} + P_{Cl}[Cl]_{in}}{P_K[K]_{in} + P_{Na}[Na]_{in} + P_{Cl}[Cl]_{out}} \tag{1.2}$$

where V_m is the membrane potential, P_K, P_{Na}, P_{Cl} are relative permeabilities of the membrane to different ion species, and $[K]$, $[Na]$, and $[Cl]$ are ion concentrations in the bulk solutions. Hodgkin and Katz used Equation (1.2) to first propose that the "separate mechanism" underlying resting and action potentials was in fact a switch in the *relative* permeability of the membrane to K^+ and Na^+ [5].

The second breakthrough was the invention of the space-clamp circuit, a new electronic configuration that enabled researchers to control the current flowing across a finite area of membrane and record the resulting changes in membrane potential [8]. The

squid axon is said to be an "active" membrane because beyond a certain threshold voltage, changes in membrane potential are propagated in space and time. This property made it extremely difficult to measure the current or voltage of the membrane in response to suprathreshold stimuli. Marmont solved this problem with his space-clamp system by electrically isolating a cylindrical portion of the membrane and preventing propagation [8]. Two innovative aspects of his recording apparatus allowed this. First, he found that coating a thin platinum wire with silver-chloride greatly reduced the impedance between the electrode and the axoplasm such that longitudinal currents through the wire were almost eliminated. Therefore, once inserted into the axon, the response of the axon would instantaneously be recorded from the entire length of the coated electrode. Second, he physically and electrically isolated a segment of the axon length to further limit spatial propagation of electrical signals. This was accomplished by passing the axon through three liquid filled chambers, each containing its own electrolyte solution and electrode. Current was prevented from passing from the central chamber electrode to the two "guard" electrodes on either side by maintaining zero voltage between the central and guard electrodes. This configuration allowed Marmont to pass defined current stimuli to the axon segment and record the membrane voltage from the area contacted by the center electrode only, solving the problem of spatial propagation. Hodgkin, Huxley and Katz used a modified version of Marmont's recording circuit to clamp the voltage of the isolated section of axon membrane while recording the current flowing across it [9]. This so-called "voltage-clamp" allowed the researchers to observe the time course of the membrane currents at different command potentials, even those above threshold. Using this information Hodgkin and Huxley were able to produce a mathematical description of the AP, as we shall see below.

1.1.4 A numerical understanding of the action potential

Hodgkin and Huxley began a methodical investigation of the time- and voltage-dependence of the current that flowed across the membrane during an action potential

using the voltage-clamp method. They found they could isolate K^+ and Na^+ currents by bathing the squid axon preparation in either normal sea water or a solution similar to sea water but with choline replacing the Na^+ ions. These experiments revealed the voltage-dependence and time course of both the Na^+ and K^+ currents that flowed when the axon membrane was depolarized. Hodgkin and Huxley found that in response to membrane depolarization, the potassium conductance rose exponentially after an initial delay and did not decay appreciably within tens of milliseconds (Figure 1.2A). In contrast, the sodium conductance rose and decayed abruptly after a depolarizing step was applied to the membrane (Figure 1.2B). In the final paper of a 5-part series, they presented the equations that explicitly described K^+ and Na^+ conductance as a function of time and voltage [11]. They found that the sum of these two conductances (plus a leak

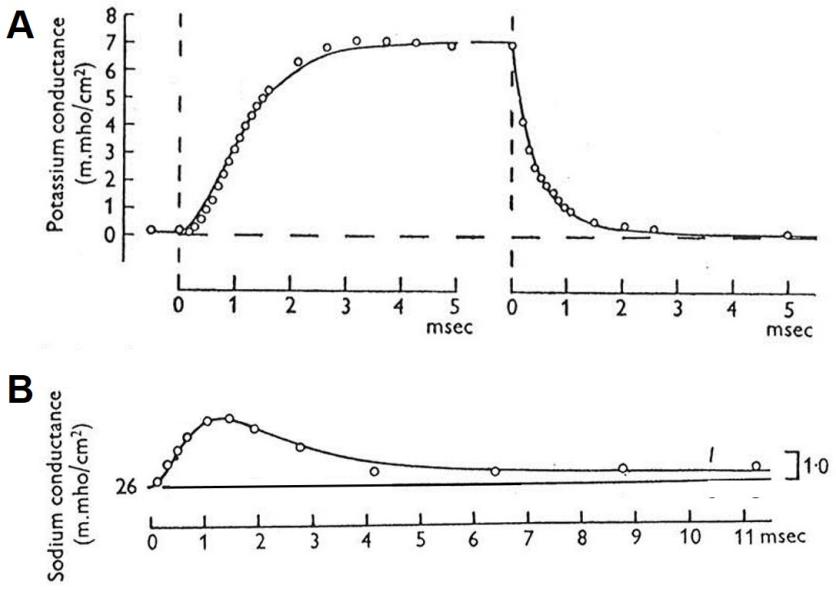

Figure 1.2: Time course of the squid giant axon membrane conductance carried by **A)** potassium and **B)** sodium. Potassium conductance was recorded using the voltage-clamp technique in the absence of Na^+ ions in the extracellular solution. Sodium conductance was also measured using voltage clamp and was taken as the difference between membrane conductance in sea water and extracellular solution without Na^+ ions. The direction of the currents (inward/outward) cannot be appreciated from this figure because the units were converted to conductance. However, the reader can appreciate the difference in the time dependence of membrane conductance carried by either ion. Adapted from [10].

conductance) resulted in a total membrane current that took the form:

$$I = C_M \frac{dV}{dt} + g_K n^4 (V - V_K) + g_{Na} m^3 h (V - V_{Na}) + g_l (V - V_l) \tag{1.3}$$

where C_M is the membrane capacitance, V is the membrane potential, g_K is the potassium conductance, g_{Na} is the sodium conductance, g_l is the leak conductance, V_K, V_{Na}, and V_l are the equilibrium potentials of each conductance, and n, m, and h are each additional time- and voltage-dependent parameters. They went on to show that this expression could reproduce the currents that flowed during an action potential waveform quite well. Although they offered some speculation, Hodgkin and Huxley were careful not to over-interpret their equations in terms of their physical meaning. After all, "the success of the equations is no evidence in favour of the mechanism of permeability change that we tentatively had in mind when formulating them." [11] It would take a new scientific field, the field of molecular biology, to prove that some of their ideas were in fact correct.

1.1.5 Ion channels gate membrane permeability

Hodgkin and Huxley's equations described the way that changes in membrane permeability depended on voltage. They reasoned that this mechanism required that a charged component in the membrane sense voltage and bring about the changes in permeability. Such a mechanism should give rise to a current that preceded a change in permeability. Since they saw no evidence in their recordings of this voltage-sensor current, they concluded that it must be extremely small. From here they postulated that the number of charged sensors would be distributed rather sparsely in the membrane, and that upon activation, many ions would cross the membrane at the site of each sensor [11]. By 1955, Hodgkin had conceptualized the sites in the membrane as "channels" where many ions traversed the membrane in single file [12]. This nomenclature shows up in the literature in the 1950s and 60s [13] despite a lack of understanding regarding what these "channels" were made of. In the 1970's accumulating evidence suggested that

the sodium "channel" was likely a protein embedded in the phospholipid membrane bilayer [14–16]. The sodium channel protein complex was eventually purified from electric eel using tetrodotoxin (TTX), a toxin in Japanese puffer fish known to selectively block the Na^+ conductance in nerve [17]. Subsequent studies found that the largest peptide purified from the complex was sufficient to produce Na^+ currents in artificial lipid bilayers [18–20] and therefore it was assumed to be the sodium channel. The amino acid sequence of the electric eel sodium channel was finally deduced from cDNA in 1984 [21]. By 1987, peptide sequences of potassium selective channels were identified from *Drosophila melanogaster* behavioral mutants and found to share some of the key features seen in sodium channel sequences [22–24]. For example, both sodium and potassium channel peptides had several hydrophobic regions that were predicted to span the fatty plasma membrane (Figure 1.3). While potassium channel peptides had a single set of these six putative transmembrane segments, sodium channel peptides were made up of four repeats of the sets of six, giving them 24 predicted transmembrane segments in total. It was suspected and is now known that a single functional potassium channel requires the assembly of four peptides, while a functional sodium channel is made up of a single peptide with four repeated domains. Also apparent in the amino acid sequences was that the fourth transmembrane

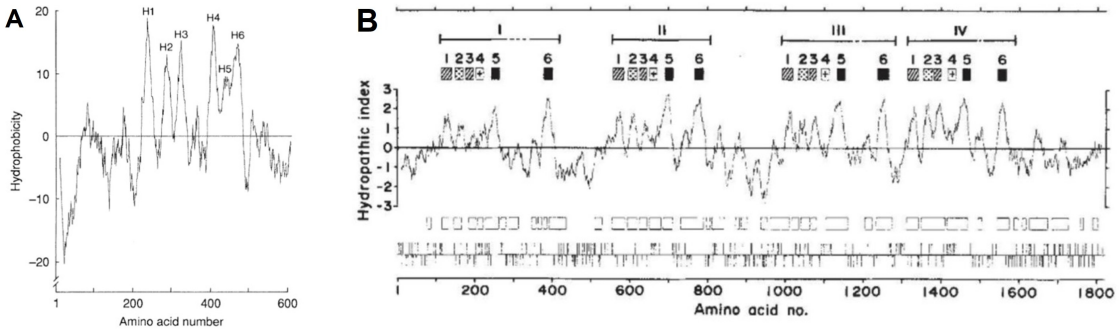

Figure 1.3: Hydropathy plots of **A)** *Shaker* and **B)** sodium channel peptide sequences. Peaks above the x-axis represent hydrophobic regions of the sequence that are predicted to span the membrane. Note that the *Shaker* sequence has six putative transmembrane segments while the sodium channel has 4 repeats of the same six segments. Figures modified from [21, 22].

segment in each domain contained more positively charged amino acid residues than the others, and the positions of the positive charges were conserved between and among channel families. Researchers immediately predicted that the positive charges in segment four (S4) represented the voltage sensors that Hodgkin and Huxley had conceptualized in 1952 [22].

As more potassium ion channel sequences were identified, it became clear that one string of five amino acids was absolutely conserved across all potassium selective channels (Figure 1.4). Naturally, this region was assumed to be responsible for the channels' ability to select for potassium over other cations. At this point the working model of voltage-dependent ion channels assumed that the charged S4 helix acted as a voltage sensor and somehow communicated membrane voltage to the selectivity sequence, which in turn controlled ion flow across the membrane. However, the functional relationship between these events was difficult to imagine without a picture of an ion channel's structure. Near the turn of the millennium, the MacKinnon lab solved several X-ray crystal structures of potassium channels; first for two prokaryotic channels [25–27] and for two mammalian channels soon after [28–30]. These breakthroughs confirmed many hypothe-

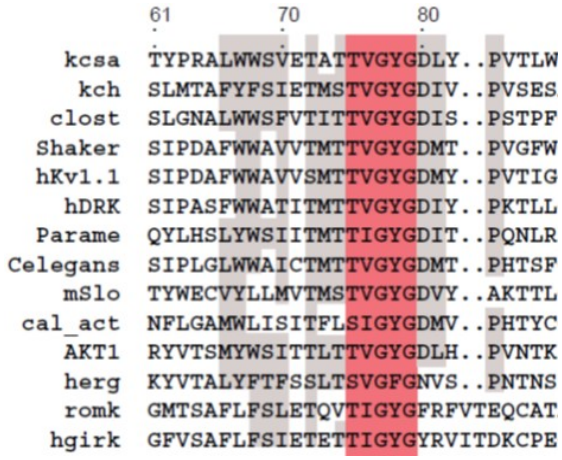

Figure 1.4: Alignment of the putative selectivity sequence from several potassium channel peptides. Five residues (red) were exquisitely conserved among potassium selective channels and were predicted to form the selectivity filter. Adapted from [25].

ses regarding voltage-gated ion channel structure and function and led to our current understanding of voltage-dependent channel gating and conduction.

1.2 Voltage-gated potassium channels

1.2.1 Structure and Gating

The first x-ray crystal structure of a potassium channel was of a two-transmembrane domain channel (KcsA) from the soil bacterium *Streptomyces lividans* (Figure 1.5) [25].

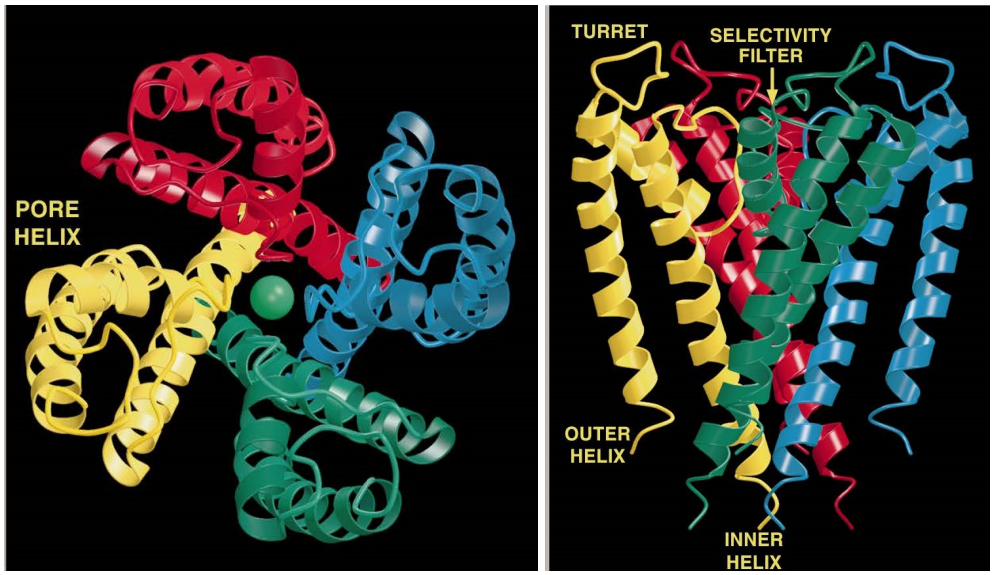

Figure 1.5: First structural model of an ion channel, KcsA, viewed from the extracellular side of the membrane looking down the pore of of the channel (left) or from the side (right). Four subunits, each colored differently, come together to form the pore through the membrane. The green sphere on the left represents a potassium ion in the pore. Figure from [25].

Although not a voltage-dependent channel, the KcsA structure provided the first three-dimensional picture of a potassium selective pore. As predicted by Tempel and colleagues [22], KcsA was made up of four subunits, each containing helical segments embedded in the membrane. In the KcsA structure, Doyle et al. found that the amino acids of the putative selectivity sequence from each subunit were located at the intersection of the four subunits, in the central part of the complex [25]. Upon closer inspection, it was clear that the five amino acids of the selectivity sequence lined the channel pore and provided

two coordination sites for potassium ions deep within the lipid membrane. These sites were close enough together that ions occupying them would exert repulsive forces on one another and this mechanism was proposed to underlie the efficient conduction of ions through the pore. The authors also found that the pore was perfectly sized to stabilize dehydrated K^+ ions but would be too large to coordinate dehydrated Na^+ ions. This confirmed that ion selectivity was a property determined deep in the channel pore, at the structure now known as the selectivity filter [25]. Doyle and colleagues also noted a narrow constriction at the intracellular side of the membrane formed by crossing of the last KcsA transmembrane segments. They called this site the "bundle crossing" and predicted that it was the site of channel gating; widening of this constriction would allow K^+ ions to access the selectivity filter and the channel to conduct, while narrowing would create a barrier to conduction. This conclusion was strongly based on previous studies that identified amino acids in the homologous region of the *Shaker* channel that were differentially accessible to the intracellular solution when the channel was either open or closed [31, 32]. While the KcsA structure answered questions related to K^+ channel selectivity and conduction, it could not address questions regarding voltage-dependent gating. This issue was solved over the next decade when the MacKinnon lab successfully crystalized three voltage-gated K^+ channels and proposed a model of voltage-dependent gating.

The first voltage-dependent channel structure was of KvAP from the archaebacterium *Aeropyrum pernix* [26, 27]. Soon after, the structure of the mammalian channel Kv1.2 was solved, first in complex with a β subunit then as a chimera with another related channel, Kv2.1 [28–30]. Unlike KcsA, KvAP and Kv1.2 each have six transmembrane helices. However, the new structures revealed that the pore architecture of these voltage-dependent channels was quite similar to that of KcsA (Figure 1.6) [28]. For example, Kv1.2 also had four subunits arranged symmetrically around a central pore. Segments five and six of Kv1.2, which share homology to KcsA's two helices, came together at the central part of

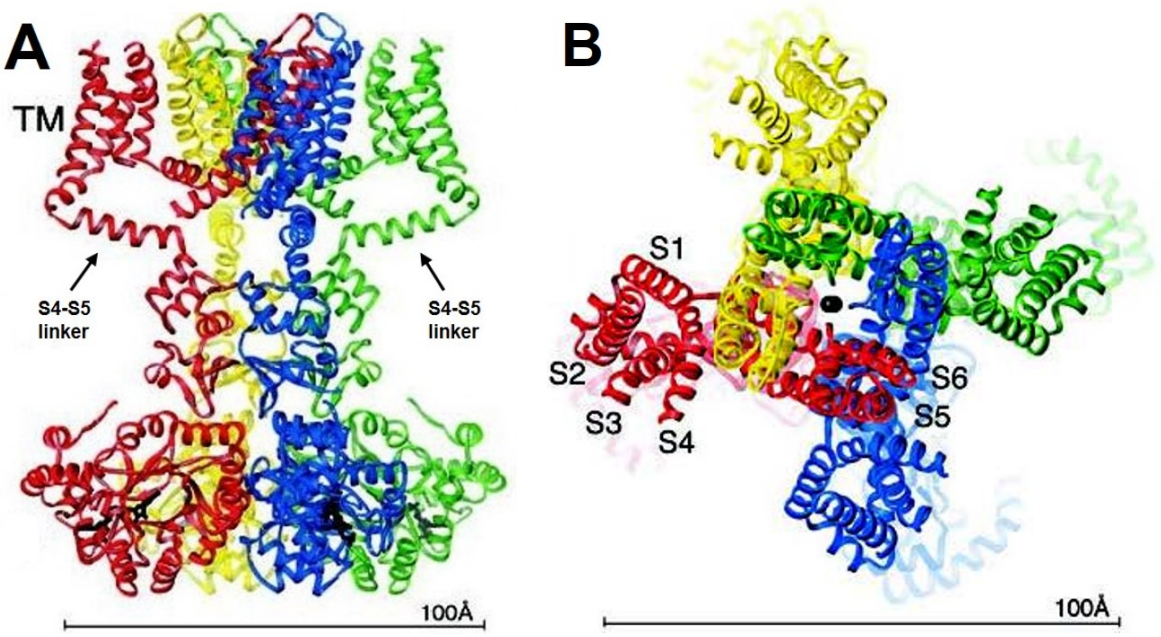

Figure 1.6: Crystal structure of the voltage-dependent channel Kv1.2. **A)** Side view of Kv1.2. Each subunit is colored differently. The transmembrane segments (TM) are embedded in the plasma membrane, while the N- and C-termini of the channel are intracellular. The S4-S5 linkers from two subunits are indicated with arrows. **B)** Top down view of Kv1.2. Colors are as in A. The voltage-sensing and pore modules are clearly distinguished by their location relative to the pore. Transmembrane segments 1-4 form the voltage-sensing module, while segments 5-6 form the pore. Black spheres represent K^+ ions in the pore. Adapted from [28].

the complex and formed a channel through the membrane lined by the selectivity filter. Segments 1-4, which contained the charged voltage sensor residues, were found on the periphery of the pore-forming domain of the channel. This arrangement immediately suggested that the voltage-sensing and pore domains were separate modules. Indeed, they were only covalently linked through the main amino acid chain and shared minimal non-covalent contacts [26]. These observations led to the idea that the voltage sensing module was flexible in relation to the pore module and that motion of the voltage-sensing domain would have to be transmitted to the pore domain in order to open the channel. But how would this transduction occur? The helical linker region between the two modules (S4-S5 linker) was a likely candidate. The Kv1.2 structures showed that the S4-S5 linker made contacts with the site of the bundle crossing, the narrow constriction at the base of the channel which was identified in KcsA and was conserved

in voltage-dependent channels. Long and colleagues suggested that movement of the voltage-sensing module would change the position of the S4-S5 linker, prying open the bundle crossing at the base of S6 to allow K^+ ions to access the selectivity filter [29]. This interpretation was consistent with functional studies from the Yellen lab showing that voltage-dependence could be imparted onto the KcsA channel by splicing in the voltage sensing module, the S4-S5 linker and the bundle crossing from a Kv1.2-like channel [33]. The coupling between the S4-S5 linker and lower S6 activation gate is thought to be the major mechanism by which canonical voltage-gated channels gate, although other channel structures can modulate this coupling and distinct mechanisms are certainly present in different Kv channel families [34, 35].

The current basic model of Kv channel gating is given in Figure 1.7. This model shows a Kv channel in each of four states which represent the major steps of the gating cycle from closed to open to inactivated. These four states are not meant to accurately depict all the possible conformational states of Kv channels. Indeed, some modern mathematical models of Kv gating require upwards of 12 distinct states to capture the nuances of channel function [36, 37]. However, Figure 1.7 gives an overview of the process.

At resting membrane potentials, most Kv channels are closed. As seen in Figure 1.7 on the left, the channel's voltage sensors (blue) are in the resting conformation and the channel pore is closed. A depolarizing stimulus leads to the activated state, which is distinguished from the closed state by a conformational change in the voltage sensors. Voltage-sensor activation favors conformational changes in the pore domains and leads to the open state of the channel, which conducts potassium ions. Once open, most Kv channels undergo some sort of inactivation. Figure 1.7 depicts two major types of inactivation: N-type (lower) and C-type (upper). N-type inactivation occurs when a specific sequence in the channel N-terminus physically occludes the ion conducting pore. This type of inactivation is relatively fast and is relieved by a return to the closed state, usually via membrane repolarization [38]. C-type inactivation is less well-understood, but is thought

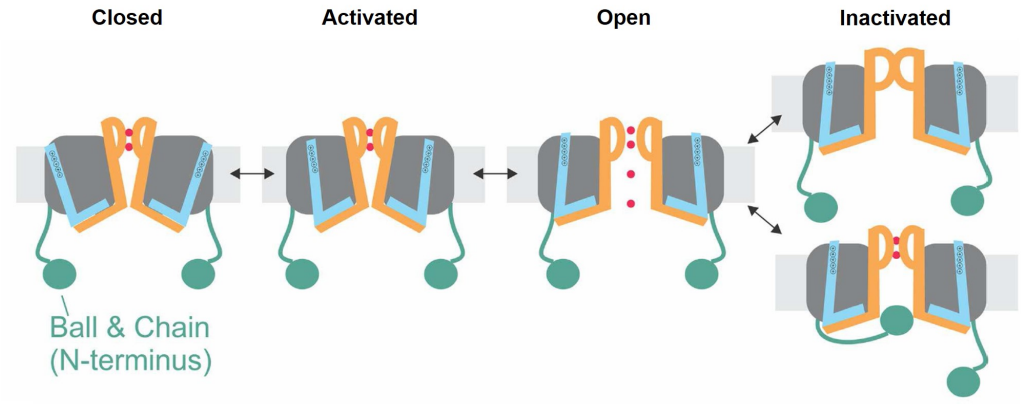

Figure 1.7: A four state model describing the major steps in the Kv channel gating cycle. On the left, the channel's voltage sensors (blue) are in the resting position and the channel is closed. A depolarizing stimulus leads to a rearrangement of the charged residues in the voltage sensors, and the channel is said to be activated. Voltage sensor activation then favors the opening of the constriction at the base of the channel called the bundle crossing (yellow). When this gate opens the channel conducts potassium. Opening of the bundle crossing favors channel inactivation, which can occur via two major mechanisms. The upper mechanism represents C-type inactivation, in which the selectivity filter collapses. The lower mechanism represents N-type inactivation, in which a moiety in the channel N-terminus physically blocks conduction. After membrane repolarization, the channels return to the closed state and the cycle can repeat. Figure adapted from [34].

to represent rearrangements in the selectivity filter that are allosterically coupled to the inner and outer pore [39, 40]. Again, relief from C-type inactivation is favored by return of the bundle crossing and voltage sensors to their closed and resting states, respectively. The model of Kv channel gating shown here is the result of decades of work by hundreds of investigators using powerful methods, including single-channel and macroscopic electrophysiology, cysteine accessibility, scanning mutagenesis, voltage-clamp fluorometry, and mathematical modeling. A comprehensive explanation of each of these studies is not practical here.

1.2.2 Nomenclature and diversity

Voltage-dependent potassium channels represent the most diverse class of ion channel proteins in mammals. As discussed in Section 1.1, the first voltage-gated potassium channel gene was identified in *Drosophila*. It was named *Shaker* because of the characteristic behavioral abnormalities that mutations in the gene conferred to fruit flies. Soon after

the *Shaker* gene was found, four other *Drosophila* voltage-gated potassium channel genes were identified; they were named *Shab*, *Shaw*, and *Shal*, paying homage to the scientists who identified them, Alice Butler and Aguan Wei. [41,42]. Around the same time, potassium channel genes were being mapped in vertebrates [43–47]. It was quickly apparent that each of the four *Drosophila* genes had multiple variants in mammalian systems, and based on phylogenetic trees we believe that the four major families evolved in invertebrates and then underwent massive gene duplication in vertebrate systems [42].

There are currently twelve distinct families of vertebrate voltage-gated potassium channels which are delineated by their evolutionary origins [48]. Members of these families are considered canonical channels in that they share the general 6-TM domain structure and open in response to membrane depolarization. The four families identified in *Drosophila* (*Shaker, Shab, Shaw, and Shal*) correspond to vertebrate Kv1, Kv2, Kv3 and Kv4 respectively [49]. They are each expressed heavily in the nervous system and are partially responsible for the extreme variability in the shape, frequency and duration of action potential waveforms found in the brain [49]. Some members of the Kv7, Kv10, Kv11 and Kv12 are also found in the brain, while others are specifically localized to peripheral tissues. For example, Kv7.1 (KCNQ1) and Kv11.1 (hERG) are well-known for their roles in regulating the cardiac action potential [48]. Kv5, Kv6, Kv8 and Kv9 are known as the "silent" Kv channel subunits, because when expressed alone they do not form functional channels. Instead, these subunits assemble specifically with members of the Kv2 family and modify their behavior. The sheer number of unique Kv channel genes imparts diversity to cellular behaviors throughout the body. Indeed, even within families, different Kv channel isoforms can have wildly different properties [50]. However, additional mechanisms contribute even further to Kv channel functional diversity, such as association with modulatory proteins, post-translational modifications, or alternative splicing, but a comprehensive discussion of each of these is beyond the scope of this dissertation [48,49].

An additional, and relevant, source of diversity among Kv channels is their ability to heteromultimerize. In 1992, the Jan lab identified a region in the cytoplasmic N-terminus that mediated the subunit interactions required to form functional tetrameric channels [51]. Li and colleagues found that a 114 amino acid fragment from the *Shaker* N-terminus bound to both the full length *Shaker* peptide or the same 114 amino acid fragment immobilized on nitrocellulose. This result suggested that homophilic interactions between the N-termini of Kv channel subunits regulated their assembly. Further supporting this conclusion, Li found that the amino acid sequence in this so called tetramerization domain, or T1 domain, was well conserved within Kv channel families but not between them, and indeed, functional channels were only formed between subunits from the same family [51]. Some exceptions to this general rule are found in vertebrate Kv channel assembly. Most notably, the Kv2 family subunits can heteromultimerize with members of the "silent" Kv families, as mentioned above.

1.2.3 Measuring Kv channel function

Voltage-gated potassium channels are not only defined by their evolutionary origins, but by their electrical function. Indeed, throughout the literature, clones of putative Kv channels are often published along with an electrophysiological characterization of the channel. The classical way of assaying cloned Kv channel electrical function is via expression in heterologous systems followed by voltage clamp experiments. In this method, cells that are easily grown in the lab are used to express Kv channel peptides-of-interest from introduced nucleic acids (either mRNA or cDNA, depending on the cell type). Ideally these cells express very few voltage-dependent channels endogenously and so you are free to study your channel-of-interest in an approximately null background. After inducing expression, the cells are subject to voltage-clamp protocols and various parameters describing the observed currents are reported. For example, Figure 1.8 shows the currents carried by *Shaker*, *Shab*, *Shal* and *Shaw* when introduced into *Xenopus oocytes*, a common heterologous system.

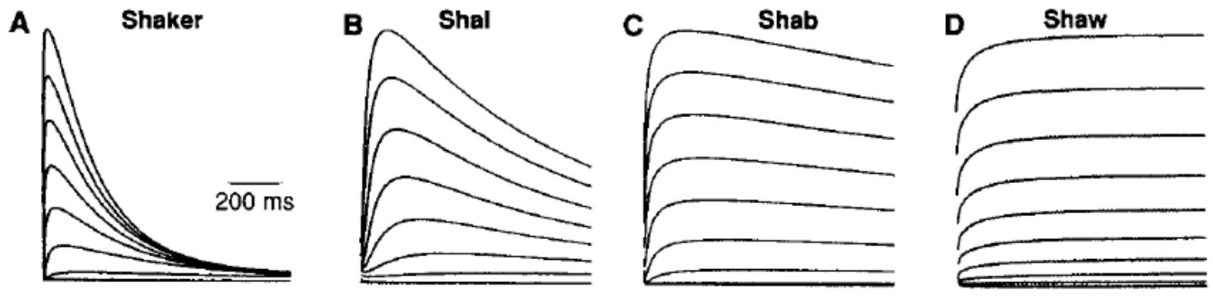

Figure 1.8: Currents carried by *Drosophila* Kv channels expressed in *Xenopus oocytes*. Voltage-clamp experiments reveal the shape of K^+ currents carried by **A)** *Shaker*, **B)** *Shal*, **C)** *Shab*, and **D)** *Shaw* channels. Note the differences in activation and inactivation kinetics. The pulse protocol was a 1 second step to voltages between -80 and +20 in 10 mV increments. The holding potential was -90 mV. Figure from [42].

The waveforms in Figure 1.8 represent current flowing across the oocyte membrane in response to various membrane potentials, which are commanded by the voltage-clamp apparatus. To save space, the responses to several command potentials are stacked on top of each other. Recordings like those shown in Figure 1.8 are used to characterize each channel's **voltage-dependence** - how the magnitude of the current changes with membrane potential, **activation kinetics** - the time course of the rising phase of the currents, and **inactivation kinetics** - the time course of the falling phase of the currents, among other parameters. It is immediately obvious in Figure 1.8 that the four *Drosophila* genes encode potassium channels with unique characteristics. For example, the currents carried by *Shaker* reach a peak rather quickly, then decay, or inactivate, substantially within 500 milliseconds (Figure 1.8A). In contrast, *Shab* currents reach their peak relatively slowly then undergo slow inactivation (Figure 1.8C). *Shaw* currents also activate slowly and undergo no inactivation over the time course shown (Figure 1.8D).

In addition to their ionic currents, activation of Kv channels produces another type of current, the gating current. Gating current is the current associated with the movement of the S4 voltage sensors during channel activation. Gating currents can also be detected using the voltage-clamp technique. However, gating currents are at least an order of magnitude smaller than ionic currents and have much faster kinetics, and thus were extremely difficult to detect in the early days of voltage-clamp recordings. Armstrong and Bezanilla

were the first to publish recordings of sodium channel gating currents from squid axons, which they did in 1973 (Figure 1.9) [52]. To do this, they used extensive signal averaging and an innovative subtraction procedure that removed the capacitive current associated with charging the axon membrane from their recordings. These modifications, along with the replacement of all permeant ions in the internal and external solutions allowed them to resolve small, transient currents with properties consistent with those of the voltage sensors predicted by Hodgkin and Huxley [11]. In fact, these recordings were made more than a decade before the first sodium channel gene was cloned and were paramount in our understanding of ion channel function prior to the molecular genetics and ion channel crystallography eras.

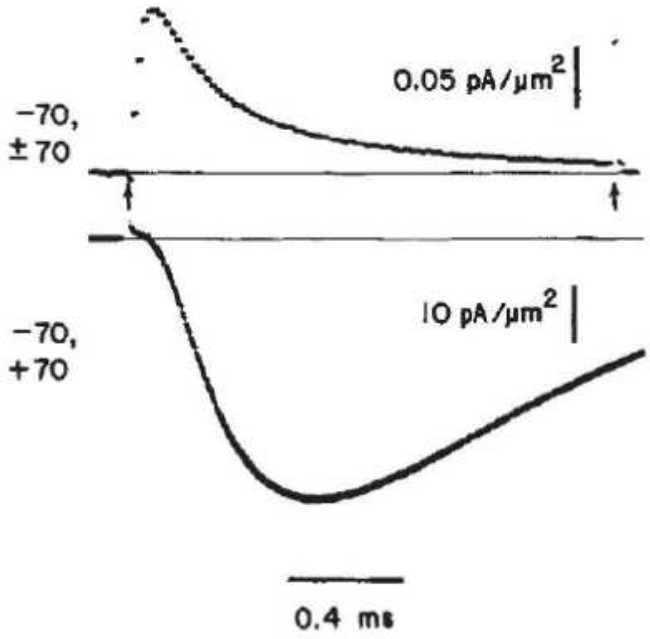

Figure 1.9: Sodium channel gating currents from the squid axon. *Top* - Current from the axon membrane in the absence of permeant ions during a step to +70 mV. The membrane capacitive current has been subtracted from the recording. Therefore, this transient current was thought to be carried by the voltage sensors of sodium channels in the axon. The authors estimated that the axon in this recording had about 50 sodium channels/μm^2. *Bottom* - Current from the axon membrane in the presence of sodium but not potassium. Note that the rise of the gating current in the upper trace is faster than rise of the ionic current in the lower trace, which is consistent with the gating current's role in channel activation. Note the difference in scale between the two recordings. Taken from [52].

A comparison between the molecular events underlying the gating and ionic currents is shown in Figure 1.10. Gating current is brought about by the movement of charged amino acids in the channel helices in response to a change in membrane potential. This event is depicted as the transition between the closed and activated states in Figure 1.10A.

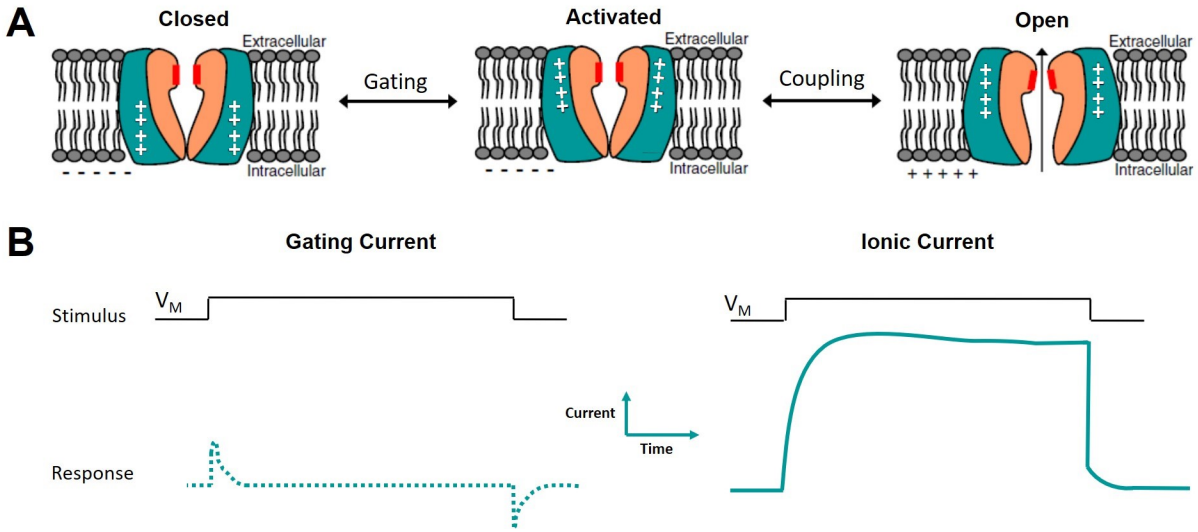

Figure 1.10: The origin of Kv channel gating and ionic current. **A)** *Left*: Under resting conditions, the membrane is polarized such that the inside is more negative than the outside. The voltage sensors, which are positively charged, are in their resting state and the channel pore is closed. *Middle*: A depolarizing stimulus, whether caused by neuronal input or an experimenter, induces activation of the channel's voltage sensors. This step in the activation cycle is called gating. The motion of these charges through the membrane's electric field can be measured as gating current as shown in B. *Right*: The new conformation of the voltage sensors is coupled to a conformational change in the channel pore, which opens to allow potassium ions to flow. This step in the cycle is called coupling. The flow of ions through the pore can be measured as ionic current as shown in B. **B)** General forms of the gating (left) and ionic (right) currents that can be recorded from voltage-gated potassium channels. Note that these are not drawn to scale, as the gating current is at least an order of magnitude smaller than the ionic current. Panel A is from [53].

As we saw in the previous figure, this event gives rise to small, transient currents that can be recorded using voltage-clamp. The left side of Figure 1.10B shows what gating currents might look like in a typical voltage-clamp experiment. Once activated, a coupling mechanism occurs between the ion channel voltage sensing and pore domains, which is depicted as the transition between the activated and open states in Figure 1.10A. The

current associated with channel opening is the ionic current, as discussed previously. A typical recording of potassium current is depicted on the right side of Figure 1.10B.

Because gating currents directly report the activation of voltage sensors while ionic currents directly report the opening of the pore, studies of gating and ionic currents together can give insight about the coupling of voltage sensor activation to pore opening. Indeed, coupling in channels from the Kv1 family is relatively strong, and therefore the gating and ionic currents have overlapping voltage dependencies [54]. In contrast, channels of the Kv2 family have weaker coupling as evidenced by a separation in the voltage dependence of channel gating vs. pore opening [54, 55].

Interestingly, the voltage dependencies of *Shaker* gating and pore opening can be separated by mutating hydrophobic amino acids in the S4 segment [56, 57]. Indeed, the Aldrich laboratory found that replacing only three non-charged residues in the *Shaker* S4 segment with analogous residues from the *Shaw* S4 segment drastically altered the voltage-dependence and kinetics of *Shaker* ionic currents. This mutant, called *Shaker*-ILT for the three mutated residues, had a left-shifted gating charge activation curve (Q-V curve) and a right shifted ionic current activation curve (G-V curve). These two curves report the voltage-dependence of gating charge movement and pore opening, respectively, and in total the two curves are separated by approximately 200 mV in *Shaker*-ILT. One hypothesis for the mechanism underlying this massive uncoupling of channel activation and pore opening is a stabilization of the S4 segment in a conformation that does not promote channel opening [58]. Since the electrostatics and hydrophobicity of the mutated residues are not drastically changed in *Shaker*-ILT, it is difficult to predict why the pre-open state is stabilized. One hypothesis is that the mutated S4 has altered interactions with membrane lipids [58].

It is important to note that data like that in Figure 1.8, Figure 1.9, and Figure 1.10 come from ensembles of channels. In fact, voltage-clamp recordings from whole cells report the collective behavior of all channels in the cell membrane. Therefore, the parameters

extracted from such data necessarily describe population characteristics. There is an entire section in this chapter (Section 1.5) devoted to a discussion of methods investigating the behavior of individual Kv channels. Discrepancies between data obtained from single channels vs. channel populations is a major theme of this dissertation, and therefore it is worth drawing attention to the methodological distinctions here.

1.3 Kv2 potassium channels

1.3.1 Kv2.1 and Kv2.2 are ubiquitous potassium channels

Kv2 channels are slowly-inactivating channels that are the mammalian corollaries to *Drosophila Shab* channels. Rolf Joho's lab cloned the first member of the vertebrate Kv2 family, Kv2.1, in 1989 [45]. The authors noted the high degree of homology between Kv2.1 and *Shab*, especially in functionally important regions such as S4. Perhaps most importantly, when expressed in *Xenopus oocytes* these newly identified Kv2.1 subunits generated currents that were reminiscent of the slowly-activating and non-inactivating potassium currents found in some neurons. In the 1980's and 90's, studies on potassium channels *in situ* lagged behind those of sodium channels, partially due to a lack of highly specific and selective toxins against Kv channels (recall from section 1.1 that the first sodium channel was isolated using TTX). In 1991, James Trimmer developed an antibody against the C-terminus of the Joho lab's newly cloned Kv2.1 channel [59]. This antibody was specific to Kv2.1 and could be used to detect the channel in various biochemical studies, including immunoblotting, immunoprecipitation and immunohistochemistry. Trimmer found that Kv2.1 channels were highly expressed in pyramidal neurons of the rat cortex and he noted the "punctate, membrane-associated nature of the staining." [59] Subsequent studies using similar immunological methods have found Kv2.1 all over the body, in central [60–62] and peripheral neurons [63], pancreatic beta cells [64, 65], cardiac [66] and smooth muscle [67, 68], for example.

In 1992, a second member of the Kv2 family, Kv2.2, was identified from a rat tongue cDNA library based on its homology to Kv2.1 [69]. Hwang and colleagues localized Kv2.2 to the hippocampus and other brain regions using *in situ* hybridization and concluded that its localization pattern was reciprocal to that of Kv2.1. However, in 2010 Kihira *et. al.* found that the Kv2.2 sequence reported in 1992 was much shorter than the genomic sequence predicted. Indeed, these authors showed that the long form of Kv2.2 predicted by the genomic sequence was actually the predominant form expressed in the brain. They suggested that the earlier reported short Kv2.2 sequence had been the result of some sort of cloning artifact [70]. Kihira et al. performed immunolocalization of the long Kv2.2 peptide *in vivo* and found that Kv2.1 and Kv2.2 were co-localized in many brain regions. They went on to show that the long form of Kv2.2 could form heteromeric channels with Kv2.1 both *in vivo* and when expressed in heterologous systems [62, 70, 71]. Therefore, studies of Kv2.2 pre-dating the 2010 discovery of the long sequence should be interpreted carefully, especially in the context of the channel's localization.

1.3.2 Kv2 channels have unique sub-cellular localization

The punctate immunostaining of Kv2.1 in cortical neurons was later confirmed to be associated with the neuronal plasma membrane (PM) using immunogold labeling and electron microscopy (EM) [60]. Du and colleagues noted several interesting aspects of Kv2.1 localization in this EM study. Firstly, they found that immunogold particles bound to Kv2.1 were often found on sections of the PM that were associated with sub-surface cisternae (SSC). These SSC were known to be portions of the endoplasmic reticulum that came into close apposition with the plasma membrane, although their prevalence and physiological functions were not well-known at the time. Du and colleagues suggested that these sites may correspond to the punctate Kv2.1 labeling that had already been seen using light microscopy, a prediction that would prove to be correct. Secondly, Kv2.1 labeling was found on parts of the neuronal PM adjacent to astrocytic membranes, as if Kv2.1 defined a locale where neurons and astrocytes interact. Furthermore, a high

percentage of labeling was found near symmetrical synapses. These latter findings were strong indications that Kv2.1 might play a role in cell-cell communication, an area of study that is currently active in our lab and others.

Over the years, immunolabeling of endogenous Kv2 channels or microscopy of fluorescently tagged Kv2 expressed in heterologous systems has proven that the punctate pattern seen by Trimmer and Du is a ubiquitous characteristic of both Kv2.1 and Kv2.2 channels. Indeed, Kv2 channels form large clusters when transfected into several different cell lines, including HEK293 [70, 72–74], MDCK [75] and Cos [76] cells. Figure 1.11 shows confocal images of Kv2.1 clusters on the basal surface of a HEK293 cell expressing a GFP-tagged Kv2.1 construct. The construct also encodes a biotin-acceptor epitope in an extracellular loop of the channel, which enables specific labeling of channels in the PM (as opposed to those that are synthesized but remain intracellular). This work confirmed the findings of the earlier EM studies by showing that Kv2.1 channels that make up clusters are in fact embedded in the PM.

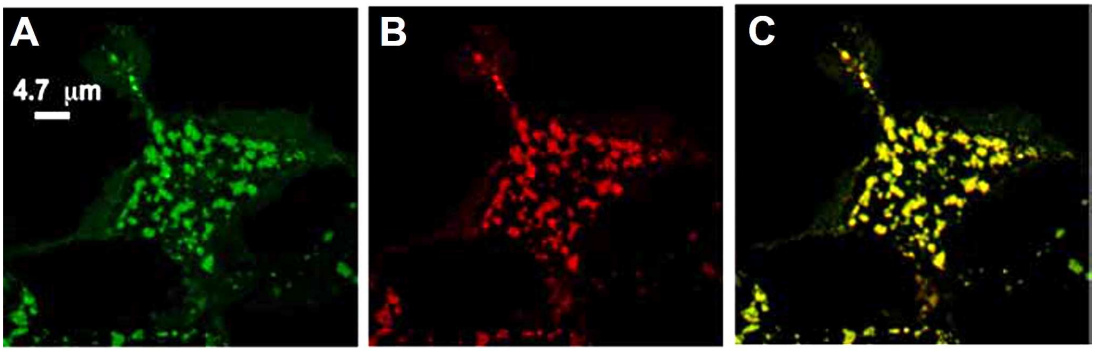

Figure 1.11: Confocal images of a HEK293 cell transiently expressing Kv2.1 with GFP fused to its N-terminus. **A)** GFP fluorescence of the cell's basal membrane showing clusters of channels. Note that some clusters have diameters of up to 1 micron. **B)** Fluorescent streptavidin labeling of the same cell in A reveals that clustered Kv2.1 channels are in the PM. **C)** Merge of the images from A and B showing perfect colocalization between the two signals. Adapted from [77].

Our lab was the first to apply live-cell imaging to Kv2.1 in order to study its lateral mobility in the PM. Fluorescence recovery after photobleaching (FRAP) experiments sug-

gested that a large fraction of Kv2.1 channels, but not other Kv channels, was immobile in the PM. These data, along with the observation that photo-activated Kv2.1 was also partially immobile led to the hypothesis that clustered Kv2.1 channels were somehow restricted in their ability to diffuse in the PM [72]. Higher resolution FRAP studies and single-molecule tracking indicated that while Kv2.1 channels within clusters were freely diffusive, they seemed to be corralled within the cluster perimeter [66, 77, 78]. It would be 8 more years before our lab showed definitively that Kv2.1 clusters are sites where the endoplasmic reticulum (ER) forms a junction with the PM, harkening back to the EM studies showing SSC near Kv2.1. Our lab performed experiments in live-cells to visualize both Kv2.1 and the cortical ER and found that transfection of Kv2.1 into HEK293 cells increased both the size and stability of junctions between the two membranes [79]. Furthermore, disruption of Kv2.1 clusters led to retraction of the ER from the PM, a process that we could image in real-time. These data confirmed that not only are Kv2.1 clusters equivalent to ER-PM junctions, the stable interaction between the two membranes requires Kv2 channels [79–81].

The finding that Kv2.1 induced ER-PM junctions suggested that Kv2.1 was restricted to clusters by interacting with a protein in the ER, instead of being corralled by a fence at the cluster perimeter. Several pieces of evidence from earlier work in the Trimmer lab provided some hints regarding the mechanism of this interaction. Quite early on, the Trimmer lab determined that the long C-terminus of Kv2.1 was required for the channel's clustered localization [75]. In 2000, Lim and coworkers used truncation mutants to narrow down the important region to just 26 amino acids, and then further identified four absolutely critical residues using alanine scanning of that region. The four amino acids required for Kv2.1 clustering were S583, S586, F587 and S589 [82]. It was no coincidence that three of these four residues were serines, as Misonou and coworkers showed soon after that calcineurin, a Ca^{2+}-dependent phosphatase, regulated Kv2.1 clustering [83]. The ability to control the Kv2.1 clustering phenotype by introducing point mutations in its

sequence was extremely important for the subsequent molecular characterization of the ER-PM junction. After years of failed attempts to co-immunoprecipitate an ER protein interactor with Kv2.1, our lab finally identified a candidate using a proximity-biotinylation assay [74]. In this assay, a promiscuous biotin ligase was fused to a Kv2 auxiliary subunit and this chimera was co-expressed in HEK293 cells with either wild-type or a non-clustering mutant Kv2.1. Biotinylation of a 33 kDa protein was observed in whole cell lysates when the ligase was expressed with wild-type Kv2.1, but not the non-clustering Kv2.1 mutant, suggesting that Kv2.1's proximity to this 33 kDa protein depended on its ability to cluster. We now know that the 33 kDa protein is Vamp-associated protein, or VAP, a protein embedded in the ER membrane that interacts with the critical amino acids in the Kv2.1 C-terminus originally identified by the Trimmer lab. We went on to show that these residues define a non-canonical FFAT (two phenylalanines in an acidic tract) motif whose interaction with VAP is exquisitely regulated by phosphorylation and neuronal electrical activity [74]. A model of the Kv2 interaction with ER VAPs that underlies ER-PM junction formation is shown in Figure 1.12.

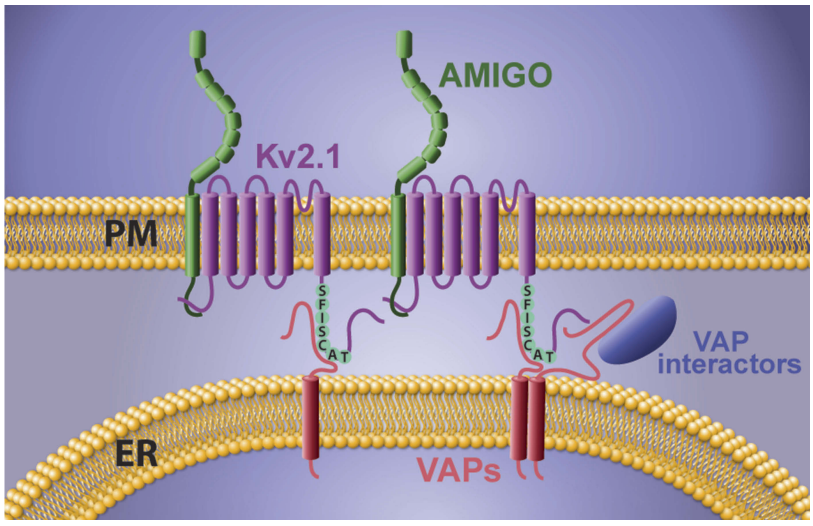

Figure 1.12: Model of Kv2 ER-PM junction. Kv2.1 channels (purple) embedded in the PM bind to VAP (red) in the ER via a non-canonical FFAT motif (green amino acids). The FFAT motif is located in the Kv2 C-terminus and binds to a basic groove in the VAP cytosolic domain. VAPs are known to oligomerize, suggesting that the ER-PM junction acts as a hub for VAP-interacting proteins (blue). Also shown is AMIGO (green), a Kv2 β subunit with cell adhesion molecule-like properties. Figure from [84].

1.3.3 Kv2 electrical function

As mentioned previously, the two Kv2 channels encode delayed rectifier currents in many cell types. The activation threshold of Kv2 currents is relatively high compared with other Kv channels. Indeed, in voltage clamp experiments Kv2 pore opening begins around -20 mV and saturates near +40 mV. Kv2 channel kinetics are also relatively slow, often requiring tens of milliseconds to reach maximal magnitudes [55]. These properties limit the activation of Kv2 channels during single action potentials, which typically have thresholds near -40 mV and are over within 2 ms. However, experiments in cultured neurons have shown that Kv2 channel currents are activated under conditions of repetitive firing, especially at high frequency. For example, Du et al. found that knock-down of Kv2.1 in cultured hippocampal neurons led to depolarization block in response to 1 Hz stimulation but not 0.2 Hz stimulation [85]. Similarly, Guan and colleagues found that transfection of a dominant-negative Kv2.1 construct in cortical neuron slices interfered with the transfected neurons' ability to maintain high frequency AP firing in response to current injection [86]. These data, and others, suggest that the Kv2 channels' main electrical function *in vivo* is to facilitate membrane repolarization in the inter-spike-interval during high frequency firing.

1.3.4 Relationship between Kv2 localization and function

In the same work showing that Kv2.1 phosphorylation state was linked to clustering, Misonou and colleagues also found a link between channel phosphorylation and function. Namely, stimuli that induced Kv2.1 de-clustering also caused the currents carried by the channels to activate and inactivate at more hyperpolarized potentials [83]. For example, in central neurons, a 10 minute application of 10 µM glutamate was sufficient to induce both de-clustering and a -20 mV shift in Kv2.1 voltage dependence. These effects were prevented by removing Ca^{2+} from the extracellular solution or by blocking calcineurin, the phosphatase that regulates the Kv2.1-VAP interaction [83]. Treat-

ment of hippocampal neurons with carbachol (a muscarinic agonist) induced a similar calcineurin-dependent effect on Kv2.1 voltage-dependence [73]. However, this effect was mediated by Ca^{2+} released from intracellular stores as opposed to Ca^{2+} from the extracellular medium and required additional residues in the channel C-terminus [73]. Along with the aforementioned shifts in voltage dependence, de-clustering via glutamate or carbachol led to changes in neuronal excitability. For example, after glutamate treatment hippocampal neurons fired fewer APs in response to injected current steps [87], consistent with the idea that enhanced Kv2.1 voltage sensitivity lead to a reduction in overall excitability.

At the time of the above studies, the connection between Kv2.1 and the ER had not been established. The obvious hypothesis regarding Kv2.1 localization and function was that clustered channels had a high activation threshold, and upon declustering they took on the low threshold phenotype [83]. Our lab set out to test this idea using on-cell patch clamp of Kv2.1 expressed in HEK293 cells. This method allowed us to measure currents from clustered or non-clustered channels independently. To our surprise, when expressed in HEK293 cells, non-clustered Kv2.1 channels had a voltage-dependence of activation in the normal range, not the hyperpolarized range associated with de-phosphorylated channels [88]. This was the first suggestion that phosphorylation state in the C-terminus of Kv2.1 that regulates clustering was independent of channel electrical function. This conclusion was later supported by the finding that the voltage-dependence of a Kv2.1 mutant lacking the non-canonical FFAT motif was still sensitive to calcineurin-dependent dephosphorylation [89]. Perhaps more surprisingly, using on-cell patch clamp, O'Connell and colleagues found that clustered channels did not activate at all, even at voltages up to +150 mV. Consistent with the separation between channel localization and electrical function, stimuli that disrupted Kv2.1 clustering, such as alkaline phosphatase and actin depolymerizing drugs, did not result in any increase in Kv2.1 current as would be expected if these silent channels became active when they escaped from clusters. Together

these data were strong evidence that 1) channel clustering and voltage dependence were controlled by separate phosphorylation events and 2) some Kv2.1 channels were held in a non-functional, or non-conducting state, and the mechanism that silenced these channels was independent of their phosphorylation state and localization. These non-conducting Kv2.1 channels are a major focus of this dissertation, and therefore will be given a more thorough treatment in section 1.4.

1.3.5 Pathophysiology of Kv2 channels

Kv2 channels have been implicated in several pathophysiological contexts. The Aizenman laboratory has spent decades characterizing the contribution of Kv2 current to injury-induced apoptosis, or programmed cell death. In 2003, Pal and coworkers found that Kv2.1 dominant negative constructs expressed in cortical neurons ameliorated the increase in K^+ current that usually precedes apoptosis [90]. This was the first indication that Kv2 channels carried this well-known pro-apoptotic K^+ surge that kicks off caspase-mediated cell death. In this same work, the authors showed that the dominant negative Kv2.1 construct offered protection to neurons exposed to DTDP, a drug that can induce apoptosis. Follow-up studies have identified two residues, Y124 and S800, whose phospho-states regulate the Kv2.1 current surge. It appears that DTDP leads to increased phosphorylation of these residues, promoting the insertion of new Kv2.1 channels into the membrane via SNARE-dependent mechanisms. The Aizenman lab recently reported that preventing the expression of the Kv2.1 apoptotic current is neuroprotective after an ischemic insult [91–93].

Like many other voltage-gated potassium channels, Kv2 channel function has also been implicated in neuronal excitability disorders, such as epilepsy. In 2014 Speca and coworkers characterized a Kv2.1 knock-out mouse line and found that it was more susceptible to epileptic seizures in the face of convulsant administration, although it did not have spontaneous seizures. These mice also had general hyperactivity and deficits in some learning paradigms, but overall had no gross morphological or behavioral pheno-

types [94]. More recently, *de novo* mutations in Kv2 channels have been implicated in human epilepsies and developmental delay. Some 20 gene variants have been found in Kv2.1 that lead to missense mutations, frameshifts or truncated subunits [95]. DeKovel and co-authors characterized patients carrying one of these mutations and found that 100% of patients had developmental delay and more than 90% had epileptic encephalopathy. Another group of scientists carefully studied several of the documented mutations in a heterologous system using automated patch clamp [96]. They found variable effects of each mutation on channel function, but in most cases a complete loss of electrical function was attributed to reduced channel trafficking to the cell surface. Interestingly, at least 3 of the characterized mutations occur in the C-terminus of the channel protein and are not predicted to alter Kv2 channel conductance or trafficking [96]. Instead these mutations remove the C-terminal FFAT motif, inhibiting Kv2.1's ability to interact with ER VAPs. It is intriguing to speculate on how these mutations could lead to excitability disorders by altering ER-PM junction formation yet without altering channel conducting functions. Therefore, in some cases the relationship between channel function and disease is still unclear.

1.4 Non-conducting Kv2 channels

1.4.1 Evidence for nonconducting Kv2.1 channels

As mentioned above, in 2010 our lab showed with on-cell patch clamp that clustered Kv2.1 channels expressed in HEK293 cells did not conduct potassium in response to depolarization [88]. This result was consistent with an older observation from the Pongs laboratory that had largely been overlooked in the literature. In that experiment, Bendorf et. al. expressed Kv2.1 in *Xenopus oocytes* and recorded currents from the entire cell membrane using the whole-cell patch clamp method. They observed something strange. Not only did they see the normal slowly activating and inactivating ionic currents carried by Kv2.1 channels, but at the beginning of each recording they also saw fast, tran-

sient currents that were much smaller than the ionic currents whose time- and voltage-dependence resembled that of gating currents as shown in Figure 1.13 [97]. Based on the relative magnitudes of the whole-cell ionic current and presumptive gating current, the authors estimated that less than 1% of the gating channels actually opened and conducted potassium. This is the only time gating and ionic Kv2.1 currents have been observed in the same voltage clamp trace. The author's did not speculate on what may have caused so many non-conducting channels in their preparation.

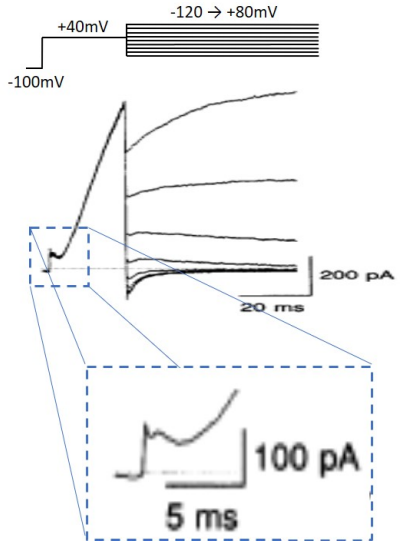

Figure 1.13: Whole-cell voltage-clamp recording from Kv2.1 expressed in *Xenopus oocytes* revealed gating currents and ionic currents in the same recording. Note in the *inset* the "hump" in the current that occurs after the initial capacitive spike but precedes the majority of the ionic current. The "hump" was proposed by the authors to be carried by Kv2.1 gating charges. Adapted from [97].

A few more indirect pieces of data from the literature further support the existence of a silent population of Kv2.1 channels. For example, a recent study by O'Dwyer of Kv2.1 in mesenteric arterial myocytes also showed a mismatch between the magnitude of Kv2.1 gating charge and macroscopic K^+ conductance [98]. These authors used Kv2-specific spider toxins to block channel gating and conductance. However, they measured either gating charge or conductance from a single cell, but did not measure both parameters from the same cell. Nevertheless, measurements before and after toxin application

revealed that Kv2 gating currents were carried by 75,000 channels/myocyte in males and 180,000 channels/myocyte in females. In contrast, the toxin-sensitive ionic currents were only a few hundred picoamps in magnitude. This level of Kv2 ionic current was estimated to represent a few hundred fully functioning Kv2 channels. Therefore O'Dwyer and coworkers concluded that less than 1% of Kv2.1 channels are conducting in smooth muscle cells [98]. This study supports the findings from an older examination of Kv2.1 in cerebral arterial smooth muscle cells, which express high levels of Kv2.1 protein but only produce a 100-200 pA of delayed rectifier current [68, 99]. Although the Kv2.1 channels were not counted in this work, the trend remains.

Given our expertise in single molecule microscopy, our lab was interested in quantifying the prevalence of the Kv2 non-conducting state with the hopes of uncovering the mechanism underlying the silencing of Kv2 conductance. In 2013, our lab published a quantitative method to count non-conducting GFP-tagged Kv2.1 channels expressed in HEK293 cells. This method relied on total internal reflectance fluorescence (TIRF) microscopy, a technique that is well suited to the study of membrane proteins because it allows the specific visualization of fluorescent proteins in the PM and those within approximately 100 nm of it [100]. In this work, Fox and coworkers used the fluorescence associated with a single GFP molecule to estimate the number of GFP-tagged channels in the PM of each HEK293 cell imaged in TIRF. The same cells were also voltage-clamped to obtain two parameters: the magnitude of the Kv2.1 current and the cell capacitance [101]. These two parameters, along with the estimate of GFP-tagged channel densities made prior were used to compare the number of conducting channels and the number of fluorescent channels in the PM. Fox et al. found that there were more fluorescent channels in the PM than those that contributed to Kv current. Furthermore, the fraction of PM channels that were non-functional was not a constant. Instead, the more channels that were expressed the larger the fraction of non-functional channels became. The same results were observed for a truncated Kv2.1 construct that lacked the ability to interact with the ER

and thus cluster. These data led to the conclusion that increasing the expression of channels in the membrane led to increased silencing of channel electrical function and that this effect was independent from the channel's localization to clusters. In other words, the non-conducting state of Kv2.1 channels was favored by increased channel density in the PM.

High density in the PM is currently our best model for a mechanism that silences Kv2.1 function. However, a true molecular mechanistic understanding of the Kv2.1 non-conducting state requires more experimentation. For example, is the density-dependent mechanism simply due to protein crowding in the membrane? Or is the non-conducting state favored at high densities because the expression or activity of some interacting partner is limiting? These questions were some of the major motivations for developing a new approach to assaying non-conducting channel behavior, as described in the first half of this dissertation.

1.4.2 Non-conducting functions of Kv2.1 channels

As discussed in section 1.3, Kv2.1 channels in the PM form junctions with the ER membrane. The stable contact site between the two membranes represents an organelle with many functions. For example, our lab showed that membrane contact sites (MCS) between the PM and ER are sites of exocytosis of both nascent and recycled membrane proteins [80, 102]. Kv2.1's role in exocytosis is linked to its interaction with SNARE proteins. Indeed, the Lotan and MacDonald groups largely pioneered our understanding of Kv2.1's effects on exocytosis in both endocrine and neuronal cells. Early on, Kv2.1 was found to interact directly with Syntaxin-1a, a member of the SNARE complex that mediates Ca^{2+}-dependent vesicle fusion [103]. In further studies, the presence of WT Kv2.1 enhanced vesicle fusion in response to depolarization in dorsal root ganglion neurons, chromaffin cells, and pancreatic islet cells as measured by cell capacitance or biochemical detection of secreted factors [103–105]. In each case mutant channels lacking the syntaxin-1a binding domain, or C1a domain, failed to facilitate exocytosis. In addition, mutant channels with

non-functional pores facilitated exocytosis to the same degree as the WT channel, suggesting that K^+ flux was not involved in Kv2.1's effects on exocytosis. The expression of soluble C1a domain in these systems completely blocks the Kv2.1-dependent facilitation of release, further supporting the requirement of Kv2.1's interaction with Syntaxin-1a for this effect [103, 105]. However, additional parts of the Kv2.1 C-terminus likely are involved as well, because Kv2.1Δ318, a truncation mutant lacking the VAP-binding domain but containing the C1a domain, also failed to facilitate exocytosis in pancreatic beta cells [65]. In any case, the recruitment of exocytotic vesicles to the PM and the facilitation of their release is an important non-conducting function of Kv2.1 channels. Current work in our lab aims to expand the investigation of Kv2.1-facilitated exocytosis to neurotransmitter release in central neurons. Preliminary data suggests that Kv2.1-induced ER-PM junctions are found at axonal presynaptic release sites. Furthermore, shRNA-mediated knock down of Kv2.1 reduces glutamatergic vesicle fusion at these sites by 50%, as measured by the signal from a pH-dependent fluorophore fused to the vesicular glutamate transporter (vGlut-SEP). Importantly, the AP waveform in these cells was not affected by Kv2.1 knock down, suggesting that Kv2.1's ability to mediate glutamate release was not related to its control of the AP waveform. Instead, these data suggest that synaptic vesicle release is an additional non-conducting function of Kv2.1 channels.

Another area of active research regarding non-conducting functions of Kv2.1 channels addresses the physiological relevance of Kv2.1 clustering to neuronal apoptosis. As discussed previously, work done primarily in the Aizenman laboratory showed that Kv2.1 mediates the pro-apoptotic K^+ current surge that triggers cell death in many cells [90,106]. Furthermore, apoptotic Kv2.1 currents could be reduced by blocking the Kv2.1-Syntaxin interaction described above [92], supporting a model in which apoptotic currents come from newly inserted channels. In accordance with our finding that Kv2.1 clusters are sites of exocytosis, recent work in the Aizenman lab revealed that interrupting Kv2.1 clustering by preventing the Kv2.1-VAP interaction was also neuroprotective under conditions

that would normally induce apoptosis, e.g. ischemia [93]. In fact, these authors showed that administering a de-clustering peptide within a few hours after ischemic neuronal injury reduced infarct volume and prevented adverse long-term behavioral deficits in mice. Although this work establishes that Kv2.1 de-clustering can be neuroprotective by preventing apoptosis, it is unclear whether injury-induced changes in Kv2.1 activation threshold also play a role in this process.

The most recently discovered non-conducting function of Kv2.1 channels is their ability to mediate interactions with glial cells, as originally predicted by Du and colleagues in 1998. Last year, Cserép et al. found that microglia make contact with neuronal somas and proximal dendrites and >90% of these contacts occur at Kv2 clusters [107]. These authors also showed that Kv2.1 was sufficient to induce these long-lived contacts by co-culturing microglia with HEK293 cells expressing a Kv2.1 cDNA construct. Under these conditions microglial processes made contact with the HEK293 cell membrane at Kv2.1 clusters, but they did not make contacts in the absence of Kv2.1. *In vivo* the microglial membrane adjacent to neuronal Kv2.1 clusters was enriched in purinergic receptors. Therefore the authors hypothesize that Kv2.1 clusters are sites of neuronal ATP release that signal neuronal states to glial cells. Whether Kv2.1 itself or one of its binding partners mediate the transcellular interaction with microglia is under current investigation. The Kv2.1 beta subunit AMIGO1 is an intriguing candidate for this mechanism due to its cell-adhesion molecule-like characteristics [108]. The interaction between Kv2.1 and the different AMIGO isoforms is the topic of Chapter 4 of this dissertation and represents a relatively young field of study.

1.4.3 On the mechanism of non-conducting Kv2.1

Non-conducting Kv2.1 channels have been observed in several systems, including heterologous expression systems such as *Xenopus oocytes* [97] and HEK293 cells [88,101], and endogenous systems including hippocampal neurons [101] and smooth muscle cells [98]. This suggests that the non-conducting phenotype is controlled by some relatively com-

mon signaling event. It is unknown whether each Kv2.1 channel's conducting phenotype is fixed during channel synthesis/trafficking or if individual channels can switch between conducting and non-conducting in the PM. To date, no stimulus has been found that removes channels from the non-conducting state, although several paradigms have been tried. These include declustering via complete dephosphorylation of the channel using alkaline phosphatase, declustering via actin depolymerization [88], declustering via C-terminal truncation [101], minutes-long exposure to extremely hyperpolarized potentials, and intracellular exposure to the reducing agent dithiothreitol (unpublished observations). Given that there are an infinite number of testable hypotheses regarding stimuli that may alter the non-conducting fraction, it is clear that alternative approaches are necessary to elucidate the mechanism of the Kv2.1 non-conducting state. To that end, I devised a new method in our lab for quantifying Kv channels residing in either conducting or non-conducting states, the details of which are contained in Chapters 2 and 3.

1.5 Methods for counting channels

1.5.1 Single channel recordings

After the voltage clamp method was invented and ion channel proteins had been discovered, there was a desire to observe the opening and closing of these membrane pores. Neher and Sakmann accomplished this feat in 1976 by modifying the voltage clamp method in a few key ways [109]. They realized that in order to resolve such small-amplitude events as single channel currents they needed to reduce the background noise of their preparations. Instead of using wire electrodes inserted into cells, Neher and Sakmann fabricated glass capillary pipettes with a small opening at one end. By gently placing the small opening onto a cell membrane and applying negative pressure, they could suck a small patch of membrane into the pipette and seal the lipid membrane to the glass. To their surprise, biological membranes formed extremely high-resistance seals, on the order of gigaohms, with the glass pipettes leading to orders of magnitude less noise in their

recordings [109,110]. The first single ion channel events were recorded from acetylcholine receptors in frog muscle cells. Two properties of the recorded events helped distinguish them from noise: the frequency of the small deflections in the current waveform were dependent on the concentration of agonist in the glass pipette and their amplitude was dependent on the membrane voltage. The single channel recording technique is extremely powerful in that it is one of the few biological techniques that can record the behavior of individual molecules in real time, *in situ*. Indeed, from a few tens of seconds of recordings one can estimate parameters related to the channel's function such as single channel conductance and open probability. The downside to single channel recordings is that only active, i.e. conducting, channels are detected. Therefore the experimenter must make an assumption about the number of channels that are present in a given patch of membrane. In general, the number of channels in a membrane patch is assumed to be equal to the maximum number of simultaneous openings observed. However, one can never be sure how many silent, or non-conducting, channels are present in the patch. Nevertheless, single channel recordings have been used to estimate the number and density of ion channels in various preparations by dividing the macroscopic conductance of the preparation by the single channel conductance obtained from single channel recordings [2].

Two examples will help impress upon the reader that estimating the number of channels in a patch from the simultaneous openings is not always accurate. First, while exploring mutations in the *Shaker* channel pore that altered C-type inactivation, López-Barneo and colleagues found that some mutations also imparted an exquisite dependence of macroscopic current magnitude on external K^+ concentration [111]. Single channel recordings from the mutants expressed in *Xenopus oocytes* revealed that the increase in macroscopic current magnitude could not be attributed to an increase in the single channel conductance. Instead, upon elevation of external K^+, the authors noted that single channel current actually decreased (due to reduced driving force for K^+) while the number of simultaneous openings increased. Therefore the authors concluded that elevated

K^+ resulted in an increase in the "number of channels that open on depolarization," i.e. an increase in channel open probability [111]. A similar result had been reported for the WT Kv1.4 channel one year prior [112]. The question remains, what were these silent channels doing in the lower, yet more physiological K^+ concentrations? What state were they in that they so rarely opened in response to depolarization?

Second, exploration of the effect of TEA on Kv2.1 led the Korn lab to identify two different conductance states of the channel, one which was sensitive to TEA and one which was not [113]. Under physiological K^+ concentrations, 15% of Kv2.1 channels reside in the low conductance, TEA-insensitive state, which is too small to resolve under common single channel recording conditions. Trapani and coworkers used modeling to detect the low conductance state in the face of only 0.3 pA of baseline noise. Trapani's identification of potassium-dependent conducting states in Kv2.1 hearkens to the experiments described in the previous paragraph. Here the authors found that raising extracellular K^+ increased the likelihood of Kv2.1 channels opening into the high conductance state. There, authors found that raising extracellular K^+ increased the open probability of channels in their patches. Could these mechanisms be equivalent? Could a low or non-conducting populations of channels be more common than previously thought? Evidence in this dissertation suggests so.

1.5.2 Noise fluctuation analysis

An alternative method for counting channels relies on inferring single channel properties from recordings of ensembles of channels. This method actually preceded single channel recording methods, because it is technically more feasible [114]. In short, the statistical variance in an ensemble of macroscopic recordings is measured at various voltages [115, 116]. In this way the experimenter builds up a sample of the noise associated with different channel open probabilities. The data can then be analyzed under the assumption that the overall noise comes from the additive noise associated with the opening and closing of individual channels in the population. Under this assumption, maximal

noise occurs at $P_o = 0.5$ and overall noise increases with the number of channels. Fitting the data to a model with these assumptions yields estimations of the single channel conductance and the number of channels in the population (see Appendix A for further details). Noise fluctuation analysis has the ability to detect unitary events smaller than the baseline noise [117]. Indeed, recently Liu and colleagues measured the notoriously small single channel conductance of HCN channels using noise fluctuation analysis and found it to be 0.5 pS [118].

1.5.3 TIRF Microscopy

As mentioned above, our lab has used TIRF microscopy to count ion channels in heterologous and primary cells [101]. In principle the method is the same as counting channels from electrophysiological measurements: a macroscopic value is divided by a unitary value to find the number of channels in the population. However, in this case the values are fluorescent intensities as opposed to charges. To measure the unitary fluorescence associated with a single fluorescently-tagged ion channel the channels must be present at low enough density in the PM to resolve fluorescence from individual channels. The density of channels in the membrane can be reasonably well-controlled by adjusting the amount of cDNA the cells are given to express. Once resolved, an average unitary fluorescence is taken from a sample of single channels. This number will be subject to error from several sources such as photobleaching, the folding efficiency of the fluorescent protein, and spatial variations in the interaction of light with the sample (either due to uneven illumination or ripples/folds in the PM). Nevertheless, reasonable estimates can be made with a large enough sample size. When coupled with electrophysiology TIRF microscopy can act as an internal control for the total number of channels in a cell. A discrepancy between the functional channels detected with electrophysiology and the total number of channels detected with microscopy would suggest that multiple populations of channels are present. Indeed this method revealed the density dependence of the Kv2.1 non-conducting state in our lab [101].

1.6 Overview of this Dissertation

This dissertation contains the results of experiments designed to further our understanding of both conducting and non-conducting functions of Kv2 channels. It builds on observations made in our lab over the past decade and attempts to push the boundaries of our understanding of Kv channels further. The results herein may prove to be useful in future neuroscientists' quest to understand and control the electrical behavior of the nervous system.

Chapter 2 details the development and validation of an updated method to count non-conducting Kv channels that improves upon the previous methods used in our lab. The three distinct advantages are 1) voltage-dependent gating and channel conductance are measured from a single population of channels simultaneously, 2) the measurements can be made under more physiological conditions than were previously used and 3) the new method is more high throughput. We use Kv2.1 to test and validate the assay in this chapter and we test the hypothesis that while only a fraction of Kv2.1 channels in the PM conduct, they all sense voltage.

Chapter 3 presents data on the prevalence of non-conducting channels from three different Kv channel types using the method developed in Chapter 2. The data in this chapter support the hypothesis that Kv2.2 also has a density-dependent non-conducting state. Furthermore, we show evidence for similar non-conducting states in two *Shaker*-related channels, Kv1.4 and Kv1.5, suggesting the mechanism controlling conductance state is somewhat common.

Chapter 4 presents experiments undertaken to characterize the role of the AMIGO family of proteins as Kv2 beta subunits. This chapter tests the hypothesis that all 3 AMIGOs effect Kv2 conducting functions, and therefore represents a departure from the direct study of non-conducting Kv channels. However, results from this chapter have implications for both conducting and non-conducting Kv2 channel functions, including the role of AMIGO in neuron/glial communication.

Chapter 5 summarizes the conclusions reached from the data in this dissertation. It also discusses the difficulties of studying non-conducting channels and my outlook for these studies in the future. It goes on to propose some future avenues of research for both determining the mechanism of Kv channel silencing and for discovering the localization and prevalence of AMIGO isoform-specific assembly with Kv2 channels *in vivo*.

Chapter 2

An improved method for counting non-conducting Kv2.1 channels

2.1 Chapter Overview

Ion channel proteins have historically been appreciated for their contribution to cell excitability. However, many ion channels play additional roles for cell biology beyond their ion conducting functions. The Kv2 channels are one family of ion channels whose non-conducting functions are of interest in mammalian physiology. Kv2 channels form stable contact sites between the endoplasmic reticulum and plasma membrane via an interaction with ER resident Vamp-associated proteins. In order to perform this structural role, Kv2 channels are expressed at extremely high levels on the plasma membranes of many cell types, including central pyramidal neurons, alpha motoneurons, smooth muscle cells, and pancreatic beta cells. Research from our lab and others suggests that the majority of plasma membrane Kv2.1 channels do not conduct potassium in response to depolarization. The mechanism of channel silencing is unknown but has been shown to be dependent on channel density in the membrane. In this work we develop an improved electrophysiological assay that can be used to test the mechanism underlying the Kv2.1 non-conducting state. We use this assay to count conducting and non-conducting Kv2.1 channels expressed in individual HEK293 cells. We reproduce the finding that the majority of Kv2.1 channels in the plasma membrane are non-conducting, and that the non-conducting fraction is favored by high channel density in the membrane. In order to validate the method, we make the quantitative measurements of gating charge from a known number of fluorescent channels. Results from this experiment directly show that all Kv2.1 channels in the PM have functional voltage-sensing domains, suggesting that the non-conducting state is not due to protein misfolding. The described assay has distinct advantages over previously used methods to detect non-conducting channels. Specifically, it detects gating transitions and ion conductance from the same

population of channels, it does not require pharmacological block of channels, and it is higher throughput. This method will be useful for identifying the molecular mechanism of Kv2.1 silencing in the future.

Hypotheses to be tested:

1. All Kv2.1 channels in the PM have functional voltage sensing domains.
2. The majority of Kv2.1 channels in the PM do not conduct potassium despite having activated voltage sensing domains.
3. The fraction of Kv2.1 channels that conduct in response to depolarization decreases with increased channel density in the PM.
4. Kv2.1 single channel conductance and open probability are insensitive to channel density in the PM.

2.2 Introduction

The Kv2.1 potassium channel is the most abundant K^+ channel in the mammalian nervous system. This delayed rectifier is expressed in several tissue types, including brain, muscle and pancreas [69, 76]. It plays a canonical role in controlling neuronal excitability, especially under conditions of high frequency firing [85]. However, it also has non-canonical functions that are intimately related to its localization. Kv2.1 channels aggregate into large clusters on the plasma membrane and interact directly with ER-resident Vamp-associated Proteins (VAPs). The interaction is regulated by the phosphorylation status of a non-canonical FFAT (two phenylalanines in an acidic tract) motif in the Kv2.1 C-terminus, which provides the cell a means to dynamically control the formation of junctions between the ER and plasma membranes (ER-PM junctions) [74, 81]. Indeed, the phosphorylation state and therefore localization of Kv2.1 channels is regulated by the balance of activity between several kinases and the Ca^{2+}-sensitive phosphatase, calcineurin [83]. Although we do not fully understand the cellular events downstream of

cluster formation, we know that Kv2-induced ER-PM junctions represent important domains for diverse processes such as endo- and exocytosis [102, 104, 119], Ca^{2+} channel localization and function [79, 98, 120, 121]), and cell-cell communication [60, 107].

Interestingly, our lab and others have shown that the majority of Kv2 channels expressed in the plasma membrane do not conduct potassium in response to depolarization. We hypothesize that the high number of channels required for ER-PM junction formation demands a concomitant silencing of channel conductance to prevent electrical paralysis of cell membranes. Indeed, high densities of Kv2.1 channels in the membrane appears to favor the non-conducting state of the channel [88, 101]. However, the molecular mechanism of Kv2.1 silencing is unknown.

Two approaches have been used to infer the presence of non-conducting Kv2.1 channels. Since non-conducting channels do not contribute to ionic current recordings, both published approaches rely on detecting a difference in the numbers of total versus conducting Kv2.1 channels in a membrane patch or whole cell. The major difference is the means by which the total number of Kv2.1 channels were estimated. Benndorf et al., O'Connell et al., and O'Dwyer et al. used the whole-cell gating charge moved by Kv2.1 channels as a readout for total channels [88, 97, 98]. O'Connell et al. and Fox et al. used optical methods to estimate the total number of Kv2.1 channels in on-cell patches [88] or whole cells [101], respectively. Each method has its drawbacks, as discussed below.

In the studies that used gating currents as a readout for total channel number, two measured gating channels and conducting channels from two different cell populations. For example, O'Connell and colleagues expressed Kv2.1 in HEK293 cells and recorded whole cell gating currents from one group of cells under conditions of total ionic current block. They estimated that on average, these cells expressed 10^6 total channels. A second group of cells was patched under physiological conditions and the ionic current at maximal open probability was used to estimate the number of conducting channels. On average, this population of cells only had $\sim$30,000 conducting channels. Therefore, it appeared

that about 97% of Kv2.1 channels expressed in HEK293 cells were non-conducting [88]. Similarly, O'Dwyer and coworkers used spider toxins to measure the Kv2 gating charge from one population of arterial myocytes in the absence of permeant ions. They estimated that each myocyte expressed between 75,000 and 180,000 total Kv2.1 channels. They then used physiological ionic solutions to measure the toxin sensitive ionic current in another population of myocytes and estimated only 60-200 channels were conducting. This suggested that more than 99% of Kv2.1 channel endogenously expressed in arterial myocytes were non-conducting [98].

The above studies are certainly informative. For example, they suggest that non-conducting Kv2.1 channels have functional voltage-sensing domains. However the clear issue with the approach is the possibility that the cells used for measuring gating current simply expressed more channels than the cells used for measuring ionic current. To date, Benndorf and coworkers are the only authors to estimate total and conducting Kv2.1 numbers from the gating and ionic currents in single cells [97]. Indeed, although it wasn't their intention, they were able to record Kv2.1 gating and ionic currents in the same voltage clamp trace in physiological solutions. The relative magnitude of the gating charge and ionic current in their recordings suggested that 99% of channels were non-conducting in their hands. It is not clear why there were so many non-conducting channels in their *Xenopus oocytes*, while other authors have not reported a large non-conducting population of Kv2.1 when expressed in the same cell type [36, 54, 122].

Unlike in the experiments described above, O'Connell et al. and Fox et al. used electrophysiology combined with optical methods to detect non-conducting channels. O'Connell targeted a patch-pipette to areas of HEK293 cell membrane that contained clusters of GFP-tagged Kv2.1 channels. Kv2.1 channels can reach densities of hundreds of channels per square micron in clusters, so the authors assumed there were hundreds of channels in each bit of patched membrane. Channel activity was exceedingly rare in these patches, even with depolarizing stimuli up to +150 mV. Although they could not

give an exact percentage of conducting channels in their patches, these qualitative data suggested that the majority of clustered Kv2.1 channels were non-conducting [88]. At the time of this work, O'Connell and colleagues did not know that Kv2.1 clusters were also sites of ER-PM junctions. That discovery led to questions regarding the use of on-cell patch clamp to study channel behavior in the plasma membrane of ER-PM junctions. Is it possible that the entire junction could have been sealed to the glass of the on-cell pipette, potentially leading to artifacts in the recordings of plasma membrane channel function? This question inspired Fox and coworkers to develop a different method of counting non-conducting Kv2.1 channels. In their work, GFP-tagged channels were again expressed in HEK cells. This time, whole-cell patch clamp was used to avoid potential on-cell artifacts. The whole-cell ionic current, along with a cited value of Kv2.1 single channel conductance, was used to estimate the number of conducting channels. The number of total channels was taken as the number of fluorescent channels in the plasma membrane, which was elegantly estimated by extrapolating the fluorescence of a single GFP-tagged channel to the whole-cell area. The two measurements yielded wildly different numbers of conducting and total Kv2.1 channels, and suggested again that up to 96% of channels were non-conducting [101]. One strength of the method developed by Fox et al. was that it allowed them to measure the percentage of non-conducting channels from HEK293 cells across a range of expression levels. The data from those experiments suggested that channel density, as opposed to clustering, led to channel silencing.

While innovative, the method developed by Fox and colleagues also had some issues. In their method, ionic currents were measured from a known number of fluorescent channels bathed in a physiological K^+ gradient. The ionic currents were extremely large under these conditions, so they also included TEA in the external solution to lower the potential for voltage error in their recordings. Thanks to work from the Korn lab, we now know that Kv2.1 has two major conducting states when bathed in physiological K^+. We also know that TEA selectively blocks Kv2.1 channels in the high conductance state, but

not the low conductance state [113]. Therefore, the cited value of Kv2.1 single channel conductance that Fox and coworkers relied on to count conducting channels was likely inaccurate for Kv2.1 bathed in TEA. This means that Fox et al. probably overestimated the number of non-conducting Kv2.1 channels in HEK293 cells in that work.

Given the drawbacks of published approaches for counting non-conducting Kv2.1 channels, we developed an improved method for making these measurements in HEK293 cells. Our method builds on the approach taken by O'Connell and O'Dwyer by measuring gating charge and ionic conductance. However, largely inspired by the work of Benndorf and colleagues, we aimed to make both of these measurements from each cell. To ensure accurate channel counts, we went to great lengths to measure both the unitary gating charge and conductance of Kv2.1 channels in our system. We relied heavily on the fluorescent channel counting approach taken by Fox et al. to do this, and so build on their work as well. In all, our approach has three major advantages to those described in the literature: 1) it detects gating and conducting channels from each cell simultaneously, as opposed to separate cell populations 2) it does not require the use of pharmacological blockers and avoids any associated artifacts and 3) it is higher throughput because all the data are contained in a single voltage-clamp trace. We use this approach to count non-conducting Kv2.1 channels expressed in HEK293 cells. We find that on average, 50% of Kv2.1 channels are non-conducting, but this percentage is a function of channel density in the membrane and at the highest expression levels 70% of channels are non-conducting. Therefore, our results largely corroborate earlier findings. This approach represents a significant improvement in our ability to detect non-conducting channels and it will be used in the following chapter to further explore mechanisms of channel silencing.

2.3 Materials and Methods

2.3.1 DNA constructs

Plasmid DNA containing the coding sequence for GFP-Kv2.1 (rat) was transiently transfected into HEK293 cells and has been described previously [72, 74, 102, 123]. The fluorescent protein is fused in frame to the N-terminus of the Kv2.1 open reading frame which minimizes effects on channel trafficking and function.

2.3.2 Cell culture and transfection

HEK293 (ATCC #1573) cells were maintained in 10 cm cell culture dishes (CellTreat #229620) at 37° C under 5% CO_2 in DMEM (Corning #10-013-CV) supplemented with 10% FBS. Cells were transfected with plasmid DNA (200 ng-2 µg) via electroporation (BioRad GenePulse Xcell) in a 0.2 cm gap cuvette (Bulldog Biosciences #12358-346; single pulse, 110 V, 25 ms) and returned to new 10-cm dishes containing DMEM+10% FBS. After 12-18 hours, transfected cells were trypsinized and plated at low density on glass-bottom dishes (MatTek #P35G-1.5-14-C) coated with Matrigel (BD Biosciences #354230) for use in electrophysiological or imaging experiments over the course of a single day.

2.3.3 Electrophysiology

For simultaneous gating and ionic current recordings, transfected HEK293 cells plated at low-density on glass-bottom dishes were bathed in High K^+ external recording solution to shift the potassium reversal potential to +40 mV (in mM: 150 KCl, 2 $CaCl_2$, 2 $MgCl_2$, 10 glucose, 10 HEPES, pH 7.37, 340 ± 3 mOsm/L). Transfected cells were identified by GFP fluorescence. Patch pipettes were fabricated from thin-walled borosilicate glass with a Sutter P-97 puller. Tip resistances were in the range of 1-3 MΩ when filled with low K^+ intracellular recording solution, resulting in a theoretical E_K=41.2 mV (in mM: 30 KCl, 115 NMDG-Cl, 1 $MgCl_2$, 0.5 EGTA, 10 HEPES, 2 ATP-Mg_2, pH 7.35, 310 ± 3 mOsm/L). The

liquid-junction potential between these Flipped K^+ solutions was measured each recording day (9.5 ± 1.3 mV, N=23) and command voltages were corrected accordingly offline.

For noise fluctuation analysis, transfected cells were bathed in either High K^+ external solution (described above) or physiological external solution containing (in mM): 140 NaCl, 5 KCl, 2 $CaCl_2$, 2 $MgCl_2$, 10 glucose and 10 HEPES, pH 7.4, 340 ± 3 mOsm/L. The internal solutions varied to facilitate measurements of unitary channel properties in different potassium concentrations. The physiological and symmetrical High K^+ internals were the same and contained (in mM): 150 KCl, 4 NaCl, 1 $MgCl_2$, 0.5 EGTA and 10 HEPES, pH 7.4, 310 ± 3 mOsm/L. The internal solution used in the Flipped K^+ condition was as described above.

Whole-cell voltage-clamp experiments were carried out at room temperature using an Axopatch200b amplifier and a Digidata1550A digitizer using pClamp10.6 software (Axon Instruments). Currents were compensated for whole-cell capacitance and series resistance (>85%), digitized at 33 kHz and low-pass filtered at 5 kHz. Online leak subtraction was applied using the P/-2 (gating assay) or P/-4 (noise fluctuations) method prior to data acquisition. Raw traces were inspected by eye to ensure data quality.

2.3.4 Simultaneous gating and ionic current recordings

Transfected cells were identified by GFP fluorescence as described below (TIRF imaging). Giga-ohm seals were formed at 0 mV with light suction. After break-in, cells were held at -90 mV until the pipette solution exchanged with cytoplasm. Full solution exchange occurred over the first 2 minutes after break-in as evidenced by a stabilization of the K^+ reversal potential near +40 mV. Leaky seals were common after break-in with these solutions and cells with more than 1 pA/mV holding current after this time were not used further. Cells were depolarized from -90 mV to E_K for 40 ms to activate all available voltage-sensors without eliciting significant ionic current. Four 5 ms, increasing voltage steps between 39 mV and 42 mV were applied before repolarizing the membrane to -90 mV (see Figure 2.2 for graphical protocol). The area under the on-gating current ob-

served at E_K was used to calculate charge moved during the depolarizing step (Q_{ON}) and the slope of the current-voltage relationship between 39-42 mV was used to calculated membrane conductance (G_{Mem}). Membrane current was ohmic in this small voltage window. This "miniature" IV relationship was also used to confirm that the reversal potential of each cell was near the theoretical E_K. All cells had E_K within ±5 mV of the theoretical E_K, ensuring voltage control in cells with membrane conductance up to 1400 nS.

2.3.5 Mitigation of electrophysiological errors

Non-ideal voltage-clamp conditions can lead to inaccurate measurements of membrane conductance, and it is of paramount importance that these potential errors are taken into consideration when making quantitative electrophysiological measurements. We made several accommodations to ensure the best possible clamping conditions in this work. First, we minimized the tip resistance of our electrodes to between 1-2 MΩ and we only recorded from cells with less than 7 MΩ series resistance after break in. In addition, we used at least 85% series resistance compensation for every recording so that our effective resistances were at most 1 MΩ. Because we measured ionic currents near the reversal potential, their magnitudes were relatively small (<3 nA) and should not have caused significant voltage error in our experiments. Nonetheless, we monitored the reversal potential of each cell to ensure we had maintained voltage control and cells with observed E_K more than 5 mV away from the theoretical E_K were discarded. We applied this cutoff despite the fact that we believe the major source of error in E_K was due to slight deviations in the liquid junction potential from recording-to-recording, as opposed to voltage error. We believe this for two reasons. First, liquid junction potential often differed by up to ±3 mV on different recording days, differences that were of similar magnitude to observed differences in reversal potential. Second, there was no relationship between reversal potential and current magnitude, as would be expected if voltage error were the major determinant of the measured value of reversal potential.

2.3.6 Non-stationary noise fluctuation analysis

In order to obtain data on the unitary properties of Kv2.1 under the Flipped K^+ conditions, we repeatedly depolarized cells to +40 mV then repolarized to -60 mV. We analyzed the noise fluctuations in the deactivating tail currents as described in the Results section and Figure 2.6. In the symmetrical High K^+ and physiological solutions we depolarized cells to +80 mV and repolarized them at -80 mV. We analyzed noise fluctuations in both the activating step currents and deactivating tail currents, as shown in Figure 2.7.We collected between 56 and 200 consecutive sweeps from each cell. Data was inspected by eye for quality and traces with sources of noise not due to channel gating were discarded (i.e. sudden changes in leak, oscillations, seal deterioration, etc). The remaining traces were analyzed offline following the method of Liu *et. al.* 2016 and as described below. The average current, $\overline{I}(t)$, during either the activation or deactivation phase of each experiment was calculated from M number of sweeps:

$$\overline{I}(t) = \frac{1}{M}\sum_{m=1}^{M} I_m(t) \tag{2.1}$$

We obtained the difference records, $y_m(t)$, by subtracting subsequent sweeps from one another (see [116]):

$$y_m(t) = \frac{I_m - I_{m-1}}{2} \tag{2.2}$$

Nonstationary noise was calculated as the variance in the difference records according to:

$$\sigma_y^2 = \frac{2}{M-1}\sum_{m=1}^{M}(y_m(t) - \overline{Y_m}(t))^2 \tag{2.3}$$

The variance was plotted as a function of the average current and fit with a second order polynomial with offset, k:

$$\sigma_y^2(I) = i * \overline{I} - \frac{1}{N} * \overline{I}^2 + k \tag{2.4}$$

The single channel current was obtained directly from this fit and converted to single channel conductance using:

$$i = g * (V_M - E_K) \tag{2.5}$$

where E_K is the theoretical reversal potential in each solution pair (Physiological = -87 mV, symmetrical High K^+ = 0 mV, Flipped K^+ = 41.2 mV). In experiments using the Flipped K^+ solutions the single channel conductance obtained from noise analysis of tail currents was adjusted by a rectification index (see Figure 2.6A) to estimate the single channel conductance near +40 mV.

2.3.7 TIRF microscopy

Images were acquired on a Nikon Eclipse Ti fluorescence microscope equipped with Nikon Perfect Focus and 100mW diode lasers at 405, 488, 561, and 640 nm. Light was collected using a 100x PlanApo 1.49 NA TIRF objective in conjunction with appropriate band pass filters housed in a Sutter Lambda 10-3 filter wheel. Images were acquired with an Andor iXon DU-897 EMCCD camera (512x512). Cells expressing Kv alpha subunits were identified by GFP fluorescence.

2.3.8 Fluorescent channel counting

HEK293 cells were transfected with either 200 ng or 2 µg of plasmid DNA encoding GFP-Kv2.1. Cells expressing the two amounts of DNA were mixed after transfection and plated on glass bottom dishes and bathed in external solution. First, each dish was searched for cells expressing low enough levels of transfected protein to resolve single channels. These cells were imaged at 20 Hz for 10 s with 15% 488 laser power for offline analysis of single-channel fluorescence. Offline, single channels were identified by their mobility [102, 124] and selected by hand with 3x3 pixel ROIs. The fluorescence intensity of each ROI was measured from the first frame of the time series to reduce effects of photobleaching. The average single channel fluorescence in each dish was calculated

from the distribution of single channel fluorescence values from 3-10 cells per dish. This value was used to estimate the number of fluorescent channels from brighter cells in the same dish (those yielding gating currents) as outlined below.

In the same dish, brighter cells were identified that were likely to contain enough channels to resolve gating currents from electrophysiological noise. Static images of these cells were acquired with 2% 488 laser power under the same TIRF illumination conditions used to acquire movies of single channels. The background-subtracted fluorescence from the entire cell footprint was multiplied by a conversion factor (7.8 ± 0.5) to account for the decreased laser power used to image bright cells. We determined this conversion factor from a separate experiment in which we acquired TIRF images of GFP-expressing cells at several laser powers. The response from our system was linear and cells imaged at 15% laser were 7.8 ± 0.5 times brighter than those imaged at 2% laser, on average. After this conversion, the corrected footprint fluorescence was divided by the average fluorescence of the single channels measured from that dish to obtain the number of channels in the TIRF footprint. This value was divided by the area (in square microns) of the cell footprint to estimate the fluorescent channel density in the footprint. Finally, the overall channel density on the basal surface was multiplied by the total cell area determined from cell capacitance (1.11 $\mu F/cm^2$ [125]) to estimate the total number of fluorescent channels in each patched cell.

2.3.9 Measuring the percent of channels in clusters

Kv2.1 TIRF images were analyzed offline to determine the percent of footprint fluorescence represented by clusters. Images underwent two separate thresholding events in order to select pixels representing either the entire cell footprint or clusters. Thresholding was applied by eye to capture pixels represented by each area without including background noise. Binary images were created from the thresholded images. The binary image of clusters underwent further Watershed analysis (built-in ImageJ algorithm) to prevent artifactual merging of bright clusters into single ROIs. The binary images were

used to create ROIs around the entire cell footprint and each individual cluster. The sum of GFP fluorescence in the footprint ROI and each cluster ROI was measured. Areas in the field of view devoid of cells were used to measure the background fluorescence associated with each ROI. The background-subtracted sum of fluorescence from all cluster ROIs was divided by the background-subtracted fluorescence in the entire footprint to obtain the percent of fluorescence in clusters, which we took to represent the percent of channels residing in clusters.

2.3.10 Analysis and statistics

Error bars represent standard error. Fitting was performed in Origin2018b using least-squares methods. Statistical significance was defined as $p<0.05$ in T-tests comparing sample means.

2.4 Results

2.4.1 Resolving gating and ionic currents simultaneously from the same channels

As discussed in the introduction, we sought an improved method of counting Kv channels that could detect the fraction of non-conducting channels in individual cells. Given previous work cited above, we expected that all Kv2.1 channels would have functional gating machinery, even those that do not conduct. If true, we reasoned that we could count all the channels in the PM from the whole-cell gating current while relying on the whole-cell ionic current to report the number of conducting channels, as we have done in the past [101]. However, measuring these two parameters from the same population of channels is non-trivial because gating currents are several orders of magnitude smaller than ionic currents. Furthermore, because they are so small, gating current magnitudes are most easily measured from extremely large populations of channels. At the same time, this requirement for high expression compromises the ability to accurately measure the large ionic currents from that population due to inherent limitations of sin-

gle electrode voltage clamp. Compounded with these limitations, we wanted to avoid the use of pharmacological blockers so that we could study several different channel types with the same method. Our methodological solution to the above problems is described in detail below. In short, we shifted the potassium equilibrium potential by altering the potassium gradients in our electrophysiological solutions. The new equilibrium potential was at a voltage where Kv channels were maximally activated. The definition of equilibrium potential is the voltage at which the net flow of ions into and out of the cell is zero. Therefore, gating currents measured at the new equilibrium potential for potassium would be free of contamination from large ionic currents. Similarly, ionic currents measured within a small window near the K^+ equilibrium potential would be small, even from populations of hundreds of thousands of channels.

Like most Kv family members, Kv2.1 channels are activated by depolarization. The threshold of Kv2.1 activation is near -20 mV, a potential much higher than the physiological equilibrium potential for potassium, which is near -80 mV. Figure 2.1A shows typical ionic currents recorded from Kv2.1 channels expressed in a HEK293 cell bathed in a physiological K^+ gradient. Upon increasing step depolarizations, ionic currents are first observed at a command potential of -20 mV and are outward. Increasing the membrane potential leads to an increase in the current magnitude in the outward direction via 1) increased channel activation and 2) increased driving force on the K^+ ions. These two phenomena are evident from the filled symbols in Figure 2.1C, which shows the steady-state IV relationship (left) and the activation curve (right) for the Kv2.1 currents in Figure 2.1A. The reversal potential for K^+ in the physiological conditions is not obvious from the IV curve because channels are closed below -20 mV. We knew we could not measure gating currents from Kv2.1 at the physiological equilibrium potential because channels are not active there. However, the reversal potential for K^+ can be shifted to a potential where channels are active simply by altering the potassium concentrations on either side of the membrane. Figure 2.1B shows whole-cell currents from Kv2.1 expressed in a HEK293

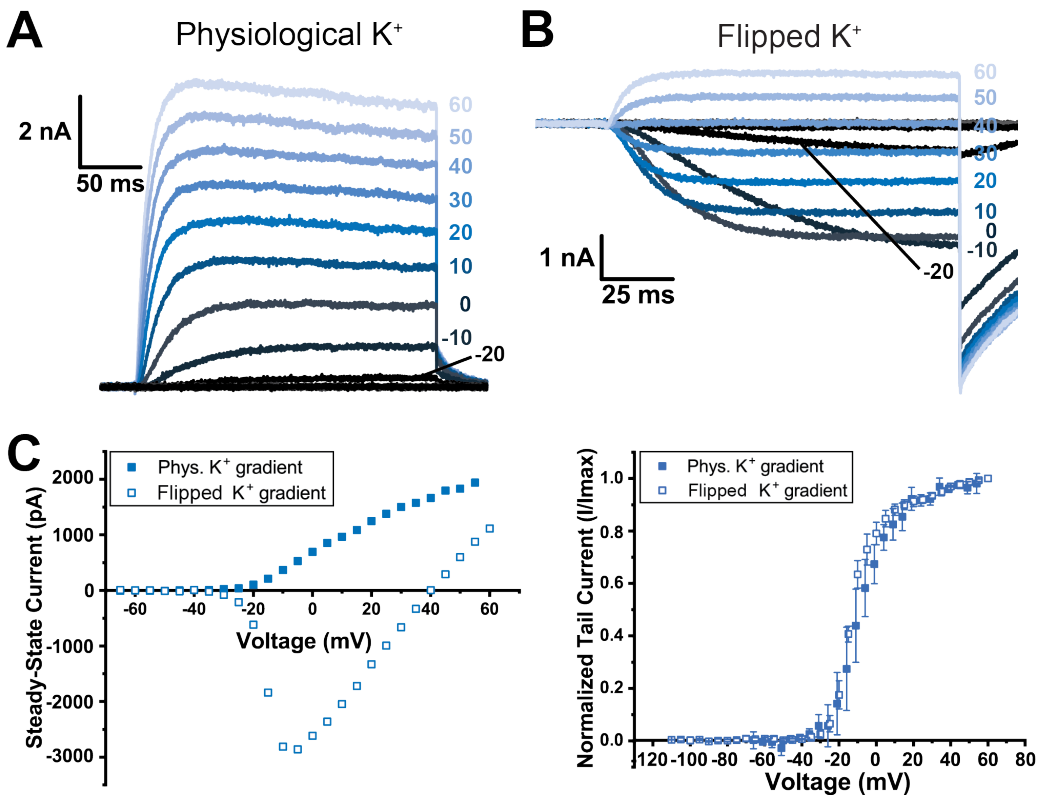

Figure 2.1: **A)** Representative whole-cell currents from HEK293 cell expressing GFP-Kv2.1 bathed in physiological K^+ gradient (5 mM K^+out / 150 mM K^+in) in response to 250 ms depolarizing steps to the voltages listed on the right. Tail currents were recorded at -40 mV and are seen at the end of the current traces. **B)** Representative currents from HEK293 cell expressing GFP-Kv2.1 bathed in Flipped K^+ conditions (150 mM K^+out / 30 mM K^+in) in response to the same 250 ms steps as in A. Tail currents were again recorded at -40 mV and are large due to the increased driving force at negative potentials in these ionic conditions. **C)** *Left* - Steady-state current-voltage plots from recordings like that in A and B. Filled symbols are from GFP-Kv2.1 in a physiological K^+ gradient and open symbols are from GFP-Kv2.1 in Flipped K^+. *Right* – activation curves generated from normalized tail currents like those recorded in A and B. Filled symbols represent the activation of Kv2.1 in physiological K^+ (N=4) while open symbols represent channel activation in Flipped K^+ (N=3).

cell that was bathed in 150 mM extracellular K^+ while the K^+ concentration in the pipette was 30 mM. The theoretical potassium equilibrium potential in these conditions was 41.2 mV, as estimated from the Nernst equation. We called these ionic conditions "Flipped K^+" because the direction of gradient is opposite to that in physiological systems. As in physiological conditions, no ionic currents were observed from Kv2.1 channels at potentials below -20 mV, as seen in Figure 2.1B. Kv2.1 currents began to activate at -20 mV, however, between -20 mV and +40 mV Kv2.1 currents in Flipped K^+ were inward due to

the opposite driving force on the potassium ions at these voltages. The open symbols in Figure 2.1C show the steady-state IV and activation curve of Kv2.1 measured in Flipped K^+. The IV relationship clearly shows that ionic currents are inward below a command potential of about +40 mV, the predicted K^+ equilibrium potential, while above +40 mV the direction of the current switches to outward. The activation curve on the right shows that despite the dramatic change in the polarity of Kv2.1 ionic currents, the voltage dependence of Kv2.1 activation was not different from that measured in a physiological K^+ gradient (Two sample T-test for midpoints, p=0.26). Note that in both ionic conditions the activation curves are almost completely saturated at +40 mV (Figure 2.1C, right) suggesting that at this voltage all activatable Kv2.1 channels were activated. The Flipped K^+ conditions represent an ideal system to record gating and ionic currents from Kv2 channels because gating currents can be recorded at the new equilibrium potential where channel activation is maximal, yet ionic currents are absent. Similarly, ionic currents are small in a window near the new E_K and thus accurate ionic recordings can be made from a large population of maximally activated channels.

We designed a relatively simple voltage-clamp protocol to capture gating and ionic currents simultaneously from individual HEK293 cells as shown in Figure 2.2. We held the membrane at a strongly hyperpolarized potential (-90 mV) for 2 minutes to ensure all channels were removed from the active state. We then stepped the membrane directly to the new potassium equilibrium potential (+40 mV) for 40 ms to activate the channels without inducing time-dependent inactivation. We then stepped the membrane to voltages between +39 and +42 mV in 1 mV increments, then finally repolarized the membrane to the holding potential. As seen in the black trace in Figure 2.2, we saw no evidence of either gating or ionic currents when we applied this voltage-clamp protocol to untransfected HEK293 cells bathed in Flipped K^+, because these cells have very few endogenous Kv channels. However, in HEK293 cells transfected with Kv2.1 channels we saw both gating and ionic currents as shown in the blue trace in Figure 2.2. The step to +40 mV elicited

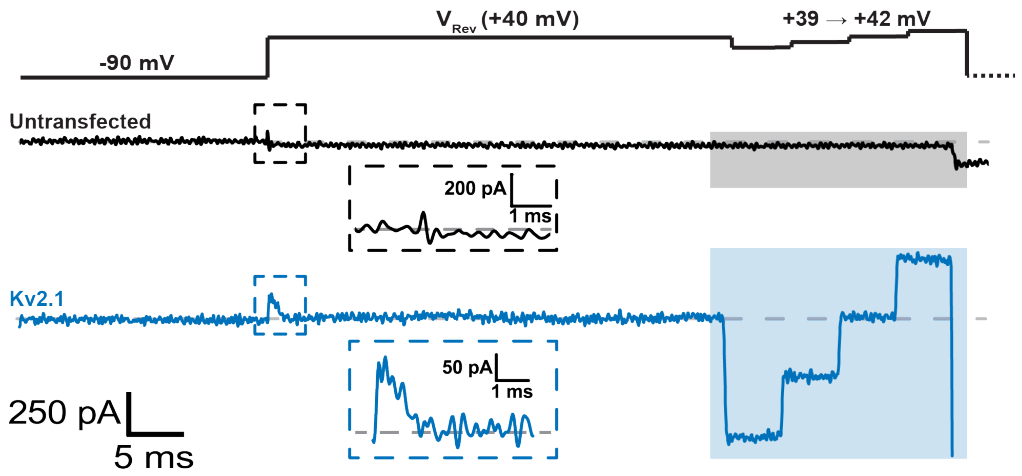

Figure 2.2: Resolving Kv2.1 gating and ionic currents simultaneously. *Top* – Voltage-clamp protocol used to elicit gating and ionic current in Flipped K^+. Black trace – response from an untransfected HEK293 cell to the protocol. No currents were elicited by the protocol in these cells. Blue trace – representative current response to the protocol from a HEK293 cell expressing GFP-Kv2.1 bathed in Flipped K^+. ON gating current was evident at the onset of the step to +40 mV (dashed box) and square ionic currents were seen in response to the 1 mV steps at the end of the protocol (shaded box).

a transient outward current that resembled ON gating current (dashed inset) but did not elicit a sustained current component, as expected at the K^+ equilibrium potential. The four 1 mV steps at the end of the protocol elicited square shaped ionic currents that reversed at the theoretical K^+ equilibrium potential (shaded box). Three pieces of evidence suggest that the transient current at the start of the +40 mV step is indeed gating current. First, these putative gating currents were not observed in recordings from untransfected HEK293 cells. Second, the magnitude of the charge moved in the putative gating current increased linearly with GFP-Kv2.1 expression (see Figure 2.5B). Third, the time constant of the decay of these currents was consistent with previous recordings of Kv2.1 gating currents (τ=1.6±0.5 ms, N=7, data not shown, [54,55]).

2.4.2 Quantification of macroscopic gating charge and ionic conductance

Figure 2.3 illustrates the way we calculated values of macroscopic gating charge and membrane conductance from each cell in the Flipped K^+ assay. We patch-clamped HEK293 cells expressing variable levels of GFP-Kv2.1 in Flipped K^+ using the protocol described in

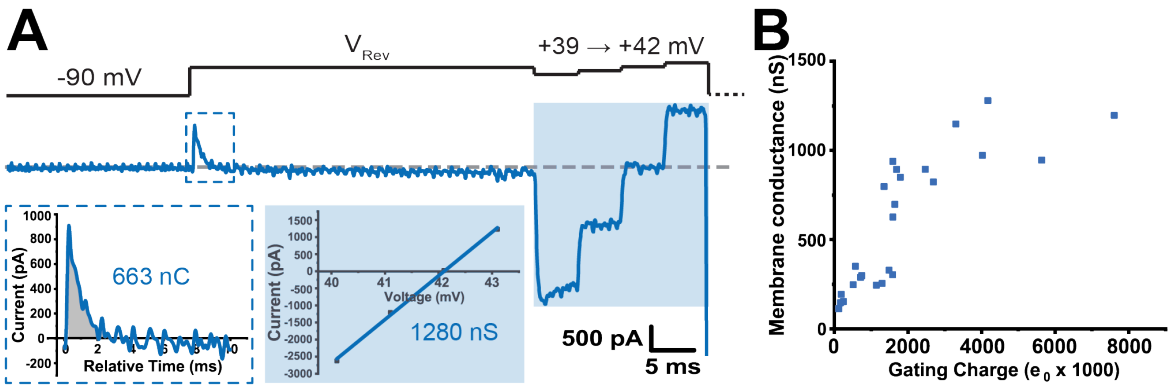

Figure 2.3: Quantification of macroscopic gating charge and ionic conductance **A)** Representative current response to the voltage-clamp protocol from a HEK293 cell expressing GFP-Kv2.1 bathed in Flipped K^+. ON gating current was evident at the onset of the step to +40 mV (dashed box) and square ionic currents were seen in response to the 1 mV steps at the end of the protocol (shaded box). Whole cell gating charge was measured as the mathematical area under the curve of the ON gating current (dashed inset). In this cell, 663 nC were moved at the onset of depolarization. Membrane conductance was calculated as the slope of the current response from the four voltage steps at the end of the protocol (shaded inset). In this cell, membrane conductance was 1280 nS. The observed reversal potential was 42.1 mV. **B)** Cross plot of Kv2.1 membrane conductance and whole-cell gating charge acquired from 25 cells as described in A. Note that at the highest expression levels the relationship begins to plateau.

Figure 2.2. Again, a step to the reversal potential from -90 mV elicited ON gating current (dashed box) and the 1 mV steps at the end of the protocol elicited ionic currents (shaded region). We measured the whole cell gating charge from the mathematical area under the first 3 ms of the ON gating current, as shown by the gray shaded area in the inset of Figure 2.3A. The area under the ON gating current had units of $pA * ms$, which is equivalent to fC. For brevity, we converted this value to nC, and in this cell we determined that 663 nC were moved at the onset of depolarization. From the same trace, we measured the average current during each of the four 1 mV steps at the end of the protocol. We plotted these currents against their respective command voltages to yield the IV relationship of the membrane, which is shown in the blue shaded inset in Figure 2.3A. Note that the IV relationship is linear in this small voltage window near the reversal potential. We fit the IV relationship with a line whose slope is equal to the membrane conductance, according to $I = G(V_M - E_K)$. The cell in this figure had a membrane conductance of 1280 nS. We made these measurements in 25 HEK293 cells expressing a wide range of GFP-Kv2.1 lev-

els. Figure 2.3B shows a cross plot of membrane conductance and gating charge where each data point represents the two quantities measured from a single cell. In general, the relationship between the two parameters was positive as expected if membrane conductance comes from the same channels that gate. However, at the highest expression levels, the relationship between membrane conductance and gating charge appeared to plateau. This result is in accordance with our previous work which showed that the fraction of conducting channels depends on Kv2.1 density in the PM.

2.4.3 Measuring Kv2.1 unitary charge

To get a sense of the numbers of conducting and non-conducting channels represented by the data in Figure 2.3, we needed to convert the macroscopic charge and conductance measurements to channel numbers. To this end, we performed two independent experiments to estimate unitary gating charge and channel conductance in Flipped K^+ conditions.

In the literature, the Kv2.1 unitary charge has been estimated to be 12.5 elementary charges [54]. However, a recent study of Kv2.1 gating suggested that only half of that charge moves in a concerted manner within the first 10 ms after depolarization, such that ON gating currents under-report the unitary charge per channel [126]. Therefore, we felt it necessary to directly measure the unitary charge that moves within the first 3 ms after a depolarizing stimulus. To do this, we needed an independent measure of the total number of channels in the PM. We took advantage of the sensitivity of TIRF microscopy to count the GFP-Kv2.1 channels in a subset of the cells from which we had recorded gating currents. In short, we measured the fluorescence associated with a single GFP-Kv2.1 channel (the "unitary fluorescence") and used that value to estimate the number of fluorescent channels in cells from which we had recorded gating currents.

We plated a mixture of HEK293 cells expressing high and low amounts of GFP-Kv2.1 protein in the same dish as illustrated in the cartoon in Figure 2.4A. We searched the dish for cells expressing low densities of GFP-tagged channels. Once identified, we imaged

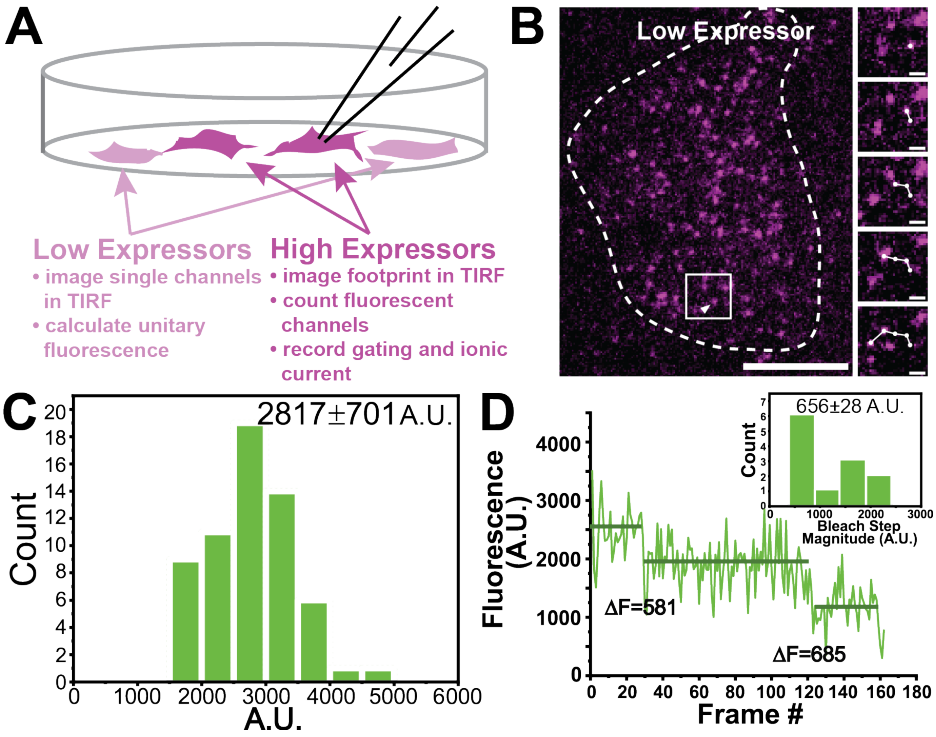

Figure 2.4: The unitary fluorescence associated with GFP-Kv2.1 **A)** Experimental set-up to allow quantification of gating and fluorescent channels from the same cell. A mixed population of transfected HEK293 cells was plated in the same dish. Single GFP-Kv2.1 channels could be resolved in low expressors while gating current and macroscopic fluorescence could be measured in high expressors. **B)** Still image from a movie of single, diffusing GFP-Kv2.1 channels expressed in a HEK293 cell. The right panels show a 3 sec time series of the boxed region and illustrate diffusive behavior of a single channel in this cell. Scale bar = 10 µm. **C)** Histogram of fluorescence intensities measured from putative single GFP-Kv2.1 channels as identified in B. The average fluorescence from the mobile single Kv2.1 channels in this dish was 2817±701 A.U. **D)** A plot of fluorescence vs. time showing two GFP bleach events taken from a time lapse movie like that in B. The inset shows a histogram of all GFP-Kv2.1 bleach events we analyzed. The average fluorescence of the smallest bin was 656±28 A.U. and corresponds to the fluorescence of a single GFP molecule.

these cells in TIRF continuously for at least 10 s at 20 Hz with high enough laser power to resolve single GFP-Kv2.1 channels. Figure 2.4B shows still images from one of these movies. Each fluorescent spot in the TIRF image likely represents 1-2 Kv2.1 channels. Some of these spots were mobile and some were immobile over the course of the time lapse imaging. The boxed region is enlarged on the right to show the mobility of a putative single GFP-Kv2.1 channel. Each panel is from a different frame of the movie and in total the panels span 3 sec. The white track overlaid onto the panels emphasizes the path of this particular channel in the membrane over those 3 sec. This characteristic diffusion

behavior of individual Kv channels has been studied extensively in our lab [102,124]. We used this diffusion behavior to identify individual mobile channels offline and measured the fluorescence intensity associated with these mobile channels. Figure 2.4C shows a histogram of the fluorescence intensities of individual mobile channels measured from several cells in a single dish. The mean unitary fluorescence of GFP-Kv2.1 channels in the dish was taken as the average from this distribution, and was equal to 2817±701 fluorescence units for this dish. The variability in the measurements is likely due to uneven adhesion of the basal cell membrane to the glass or the less-than-perfect folding efficiency of GFP proteins [101]. In order to further convince ourselves that this value was reasonable for a single GFP-tagged channel, we measured GFP bleaching events from immobile channels in the time lapse movies. Figure 2.4D shows an example of two bleach events recorded from an immobile spot of GFP fluorescence. We measured the magnitudes of several bleach events and the histogram of values is shown in the inset of Figure 2.4D. The magnitudes of all bleach events we measured fell into four bins which represent the bleaching of 1, 2, 3 or 4 GFP molecules at once. The average fluorescence from the smallest bin was 656±28 fluorescence units and represents the fluorescence of a single GFP molecule under our imaging conditions. Therefore, a channel with four GFP molecules would have a total fluorescence of approximately 2624 A.U. This value was similar to the average fluorescence associated with the mobile channels we identified by diffusion (Figure 2.4C), supporting the idea that these mobile spots represent single GFP-tagged Kv2.1 channels.

After imaging single channels from 3-5 cells per dish, we then searched the dish for cells expressing higher amounts of Kv2.1. Figure 2.5A shows a TIRF image of a HEK293 cell expressing a high level of GFP-Kv2.1 and clearly shows the characteristic large clusters of Kv2.1 that represent ER-PM junctions. We voltage-clamped these "high expressors" in Flipped K^+ to determine the macroscopic gating charge as described in Figures 1 and 2. Offline, we used the unitary fluorescence measured from low expressors in the

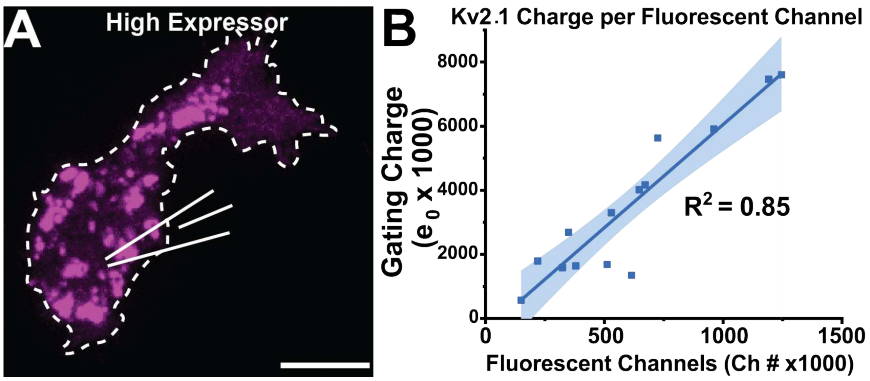

Figure 2.5: Kv2.1 unitary charge **A)** TIRF image of a "high expressor" from the same dish as the cell in Figure 2.4B. The density of GFP-tagged channels in this image was calculated from the average unitary fluorescence found in Figure 2.4C. High expressors were also voltage-clamped in Flipped K^+ to measure the macroscopic gating charge and the cell capacitance. Scale bar = 10 µm. **B)** The relationship between whole cell gating charge and fluorescent channel number for cells like that in A. The relationship is linear with a slope equivalent to the unitary charge of the channel. The shaded area represents the 95% confidence interval of the linear regression. Slope = 6.4 ± 0.75 e_0. N=14.

same dish to measure the density of channels in the cell membrane of the high expressors. We then estimated the number of channels in the entire cell using the whole cell membrane capacitance, which we also recorded during voltage clamp. We now had an independent estimate of total fluorescent channels from a subset of cells whose macroscopic gating charge was known. We plotted the gating charge against the number of fluorescent channels and found the relationship to be linear across the entire expression range as shown in Figure 2.5B. The relationship had a slope of 6.4 ± 0.75 elementary charges per channel, which we take to be the unitary charge per Kv2.1 channel that moves within the first few milliseconds after depolarization. This result is consistent with the report that about half of all Kv2.1 gating charge moves in the first 10 milliseconds after depolarization [126] and so we conclude that all fluorescent Kv2.1 channels in the membrane have functional voltage-sensing machinery.

2.4.4 Measuring Kv2.1 unitary conductance

We next needed to determine the single channel conductance of Kv2.1 at +40 mV in the Flipped K^+ conditions. Kv2.1 conductance is sensitive to external potassium concentra-

tion [113]. Indeed, at physiological potassium concentrations, Kv2.1 can open into either a high or low conductance state, while at extracellular K^+ concentrations above 60 mM all channels open into the high conductance state [113]. Given our bath concentration of 150 mM K^+, we expected that all Kv2.1 channels would open into a single, high conductance state. However, because some Kv channel pores are not saturated in solutions <600 mM K^+ [127] we could not predict the value of Kv2.1 single channel conductance under our exact ionic conditions. Therefore, we used non-stationary noise fluctuation analysis of macroscopic GFP-Kv2.1 currents to measure single channel conductance in the Flipped K^+ conditions.

We performed non-stationary noise fluctuation analysis on Kv2.1 tail currents from transfected HEK293 cells bathed in Flipped K^+. We chose to measure channel noise from tail currents instead of activating currents because single channel currents would be larger and easier to distinguish from baseline noise at hyperpolarized potentials due to the strong inward potassium gradient [5, 128]. Figure 2.6A shows the open channel IV curve averaged from 6 HEK293 cells expressing Kv2.1 in Flipped K^+. Indeed, there was significant inward rectification in the IV, especially at negative potentials where tail currents would be measured. To perform noise fluctuation analysis, we activated and deactivated Kv2.1 channels repeatedly between 56 and 200 times and collected the tail current sweeps. Figure 2.6B shows every tenth sweep from 60 consecutive recordings of Kv2.1 tail currents at -60 mV and illustrates that tail currents were relatively stable over multiple recordings. However, some cells did show variability in the tail current magnitudes due to channel run down over time, and therefore we analyzed the variance from the difference between adjacent sweeps to minimize errors (see [116, 118] and Methods). We plotted the variance from the set of difference traces for each cell as a function of the mean current during channel deactivation as shown in Figure 2.6C. As expected, the relationship was fit well by a parabola whose coefficients correspond to the single channel current and number of channels in the membrane. We converted the single channel

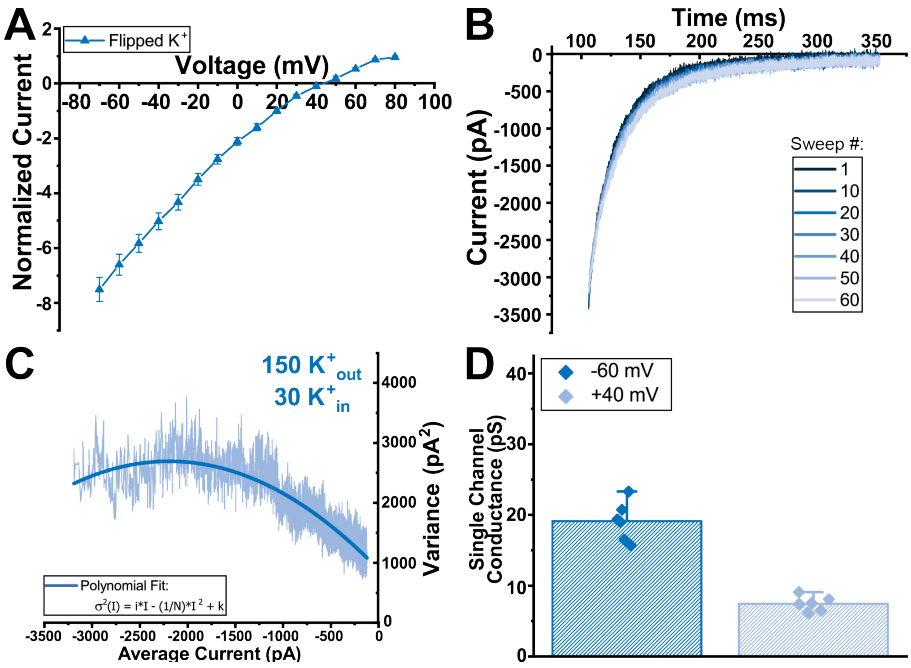

Figure 2.6: Kv2.1 unitary conductance in Flipped K^+ **A)** Open channel IV curve from GFP-Kv2.1 expressed in HEK293 cells bathed in Flipped $^+$ revealed inward rectification due to the strong inward gradient on potassium. The plotted current is the normalized instantaneous current at the given voltage after activating channels at +50 mV for 100 ms. Values were normalized to the current at +80 mV to allow for averaging (N=6). The slope of the IV at +40 mV is 39% that of the slope at -60 mV. **B)** Example tail current traces used for noise fluctuation analysis in Flipped K^+. Channels were opened at +40 mV (not shown) and tails were recorded at -60 mV. **C)** Current variance vs. average current plot for the data shown in B. The data were fit with a 2nd order polynomial (see legend) with offset. Single channel current is given by the coefficient of the first term of the polynomial and was -1.6 ± 0.01 pA for this cell. **D)** Absolute values of Kv2.1 single channel conductance obtained from parabolas like that in C by converting single channel current to conductance. At -60 mV the average single channel conductance was 19.1 ± 1.1 pS (dark blue). After correcting for rectification the average single channel conductance at +40 mV was 7.5 ± 0.44 pS (light blue) N=6.

current to conductance according to Equation 2.5, and a summary of the single channel conductance values are given in Figure 2.6D. From 7 cells, we found the average single channel conductance at -60 mV to be 19.1±1.1 pS (Figure 2.6D, dark blue). In order to estimate the single channel conductance at +40 mV, where our macroscopic conductance measurements were taken, we scaled the single channel conductance values at -60 mV by a rectification index. The index was simply the ratio of the slope of the open channel IV at +40 mV over the slope at -60 mV, which was 0.39 as measured from Figure 2.6A. We multiplied the single channel conductance values measured at -60 mV by 0.39 to obtain

the single channel conductance of Kv2.1 at +40 mV, which was 7.5±0.44 pS (Figure 2.6D, light blue).

In order to convince ourselves that the noise fluctuation analysis measurements were accurate, we performed two control experiments. First, we wanted to make sure that measuring noise from deactivating tail currents was just as valid as measuring noise from activating step currents. We reasoned that in symmetrical K^+ solutions, the conductance values obtained in either way should be identical. Figure 2.7A shows the variance-current parabola obtained from Kv2.1 bathed in symmetrical 150 mM K^+ after repeated activating sweeps to +80 mV. Figure 2.7B shows the variance-current parabola obtained from the same recording used in A, but this time noise was analyzed from tail currents recorded at -80 mV. We measured single channel currents from three cells in this way and converted them to single channel conductance, and the values from the fluctuations in the activating steps or deactivating tails are compared in Figure 2.7D (red). On average, the single channel conductance of Kv2.1 was the same when measured from the tails or the step when bathed in symmetrical 150 mM K^+ (Tails = 18.2±3.2 pS, Step = 17.9±0.9 pS). Second, given that Kv2.1 single channel conductance is sensitive to potassium concentrations [113], we wanted to make sure noise fluctuation analysis would detect K^+-dependent changes in Kv2.1 single channel conductance. Therefore, we repeated noise fluctuation analysis on Kv2.1 channels bath in physiological K^+ concentrations. Figure 2.7C shows a variance-current parabola from repeated activating steps to +80 mV in a cell exposed to 5 mM extracellular and 150 mM intracellular potassium. We collected data from three such cells and calculated the single channel conductance of these channels at +80 mV, as shown in Figure 2.7D (grey). The average single channel conductance was 6.6±0.4 pS at +80 mV in physiological K^+ which is a value similar to that of the large conductance state reported by Korn and colleagues [113] and from previous experiments in our own lab [88]. Importantly, this value is lower than the single channel conductance measured in symmetrical High K^+, as expected. Together these results suggest that either activating step currents

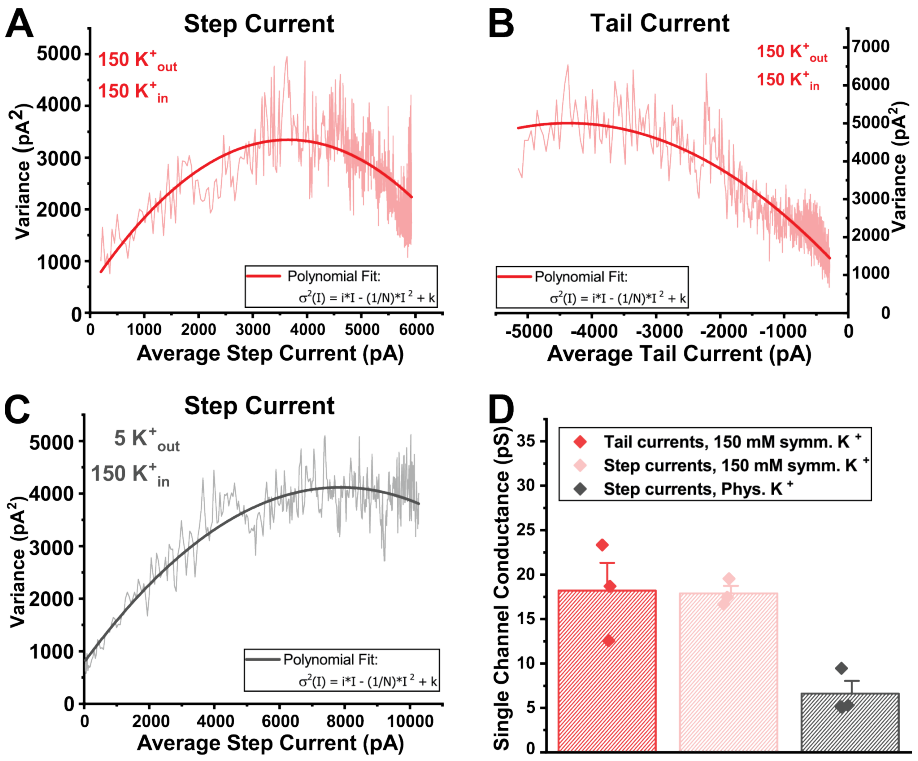

Figure 2.7: Kv2.1 unitary conductance in other ionic conditions **A)** Variance vs. current plot from step current measured at +80 mV in HEK293 cell expressing Kv2.1. Extracellular solution contained 150 mM K^+ and intracellular solution contained 150 mM K^+. Variance was measured from the activation phase during a step to +80 mV. The unitary current obtained from the fit of the parabola was 1.56 ± 0.07 pA. **B)** Variance vs current plot from tail currents measured at -80 mV from the same HEK293 cell in A. The unitary current obtained from the fit of the parabola was -1.87 ± 0.05 pA. **C)** Variance vs current plot from step current measured at +80 mV in HEK293 cell expressing Kv2.1. Extracellular solution contained 5 mM K^+ and intracellular solution contained 150 mM K^+. Variance was measured from the activation phase during a step to +80 mV. The unitary current obtained from the fit of the parabola was 0.84 ± 0.03 pA. **D)** Absolute values of single channel conductance calculated from the single channel currents as obtained in A, B and C using Equation (2.5). In symmetrical High K^+, the single channel conductance at -80 mV was 18.2±3.2 pS and at +80 mV it was 17.9±0.9 pS (N=3). In physiological K^+, the single channel conductance at +80 mV was 6.6 ± 1.4 pS (N=3).

or deactivating tail currents can be used to measure single channel conductance and that noise fluctuation analysis in our hands can detect potassium-dependent changes in single channel conductance.

2.4.5 The number and density dependence of non-conducting Kv2.1 channels in HEK cells

The macroscopic gating charge is a function of the unitary charge and the number of channels in the membrane. Therefore, we divided each cell's macroscopic charge from Figure 2.3B by the unitary charge obtained in Figure 2.5B (6.4 e_0) to estimate the number of gating channels. Similarly, macroscopic membrane conductance is a function of the unitary conductance, the number of channels and the channel open probability. We divided each cell's membrane conductance from Figure 2.3B by the single channel conductance obtained from noise analysis and the open probability, which we also measured from our noise analysis experiments (Kv2.1 P_o = 0.75 ± 0.03). Figure 2.8A shows a summary of the number of conducting and gating channels from each cell. As we expected,

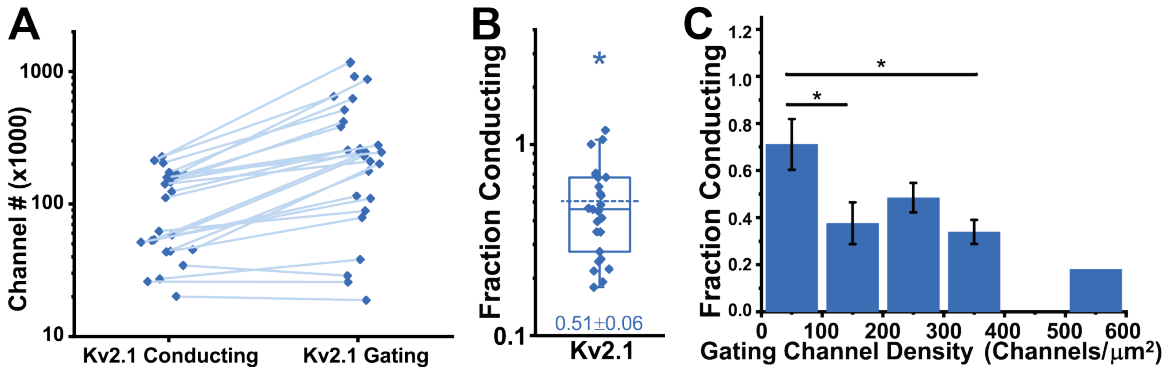

Figure 2.8: Counting non-conducting Kv2.1 channels expressed in HEK293 cells **A)** Comparison of the number of conducting and gating channels in individual HEK293 cells expressing GFP-Kv2.1. These values were obtained from the macroscopic gating charge, membrane conductance, unitary charge, unitary conductance and open probability as described in the text. The number of conducting channels was consistently lower than the number of gating channels in individual cells. Note the logarithmic scale. **B)** The same data in A shown as the fraction of gating channels that were conducting. On average, about 51% of Kv2.1 channels were conducting (dashed horizontal line). Asterisk indicates that the sample mean was significantly different from a mean of 1. The box indicates the middle 50% of the data and the median. **C)** The fraction of conducting Kv2.1 channels plotted as a function of the overall density of gating channels. Data from all cells were binned into 100 channels/μm^2 bins. Bins without error bars only contain one data point. The conducting fraction decreased as more channels were expressed in the membrane, suggesting a density dependent mechanism that silences some channels. Asterisks indicate p<0.05 between bin means using two-sample T-tests.

most cells had fewer conducting channels than gating channels. We divided the number of conducting channels by the number of gating channels to determine the conducting fraction in each cell. Figure 2.8B shows that the average fraction of conducting channels was 0.51±0.06, which was significantly different from 1. Therefore, on average, about half of the gating Kv2.1 channels conducted potassium.

In our previous investigation of the Kv2.1 nonconducting state, it appeared that the fraction of nonconducting channels in HEK293 cells was not a constant. Instead, increased channel expression in the membrane was associated with higher fractions of nonconducting channels [101], suggesting that the non-conducting state of the channel was somehow dependent on channel density in the membrane. As seen in Figure 2.8B, the fraction of nonconducting Kv2.1 channels measured in this work was quite variable. We were curious whether this variability came from a density dependent mechanism, therefore, we plotted the fraction of conducting channels as a function of the density of gating channels in each cell. Figure 2.8C shows a summary of the Kv2.1 conducting fraction as a function of the density of gating channels in the cell, split into bins of 100 channels/μm^2. As channel density in the membrane increases the fraction of conducting channels decreases, as evidenced by the decreasing conducting fraction in the larger bins. These data support the earlier suggestion of a density-dependent mechanism regulating the Kv2.1 non-conducting state.

2.4.6 Kv2.1 single channel conductance and open probability are not density dependent

The non-conducting state is evidenced by a mismatch in the number of channels that sense voltage and the number that conduct. The number of channels that conduct is a function of single channel conductance and open probability. Therefore, a reduction in single channel conductance, open probability, or both at high expression levels could underlie the non-conducting state. We again used noise fluctuation analysis to look for evidence of expression dependence in these two Kv2.1 parameters. Figure 2.9 shows single channel conductance and open probability detected from noise fluctuation experiments

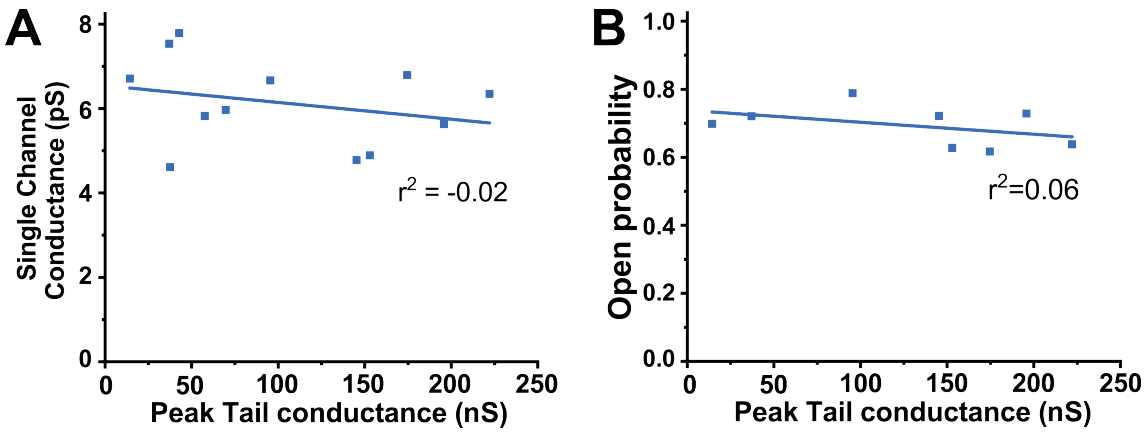

Figure 2.9: Kv2.1 unitary conductance and open probability are constant with increasing expression. **A)** Plot of Kv2.1 single channel conductance measured using noise fluctuation analysis in cells expressing a range of Kv2.1 expression levels. In this figure, the X-axis shows the maximal membrane conductance measured during tail currents, which is a proxy for expression level. Each data point represents one cell. A line fit to the data had an R^2 value of -0.02, indicating that there was no relationship between the two parameters. **B)** Plot of Kv2.1 open probability from the same cells in A as a function of the peak conductance. There was no relationship between these parameters across the expression range tested.

of Kv2.1 in Flipped K^+ as a function of the maximum membrane conductance, which is a proxy for channel expression. Neither single channel conductance, nor open probability was a function of channel expression, as evidenced by the low R^2 values of the fits to the data in Figure 2.9. This suggests that the reduction in conducting fraction at high densities seen in Figure 2.8C is not due to a graded decrease in either of these parameters. Instead channel silencing is likely due to uncoupling of channel gating from pore opening, suggesting that these channels are in a specialized non-conducting state with an open probability near zero.

2.5 Discussion

2.5.1 Summary

We developed an improved method for counting non-conducting Kv2.1 channels expressed in HEK293 cells. This method uses a simple voltage clamp protocol to capture Kv channel gating transitions and ionic currents in the same trace. This was made possible by altering the potassium gradient of our recording solutions to shift the potassium rever-

sal potential to a value where Kv2.1 channel activation was maximal. These conditions allowed us to measure both the macroscopic charge associated with channel activation as well as the membrane conductance associated with pore opening from the same population of channels. We used this method to count conducting and non-conducting channels in HEK293 cells expressing a range of protein levels. We found that on average, about 50% of channels were non-conducting, but at the highest expression levels approximately 70% of channels were non-conducting. The results largely reproduce the findings of Fox et al. that the fraction of Kv2.1 channels that conduct is a function of the density of channels in the membrane. We also reproduce the findings of O'Connell et al., O'Dwyer et al. and Benndorf et al. which suggested that non-conducting Kv2.1 still have functional voltage sensing domains. Our approach provides several improvements over previous attempts to count non-conducting channels, as discussed below. Therefore, the method we developed will be useful in uncovering the molecular mechanism of Kv2.1 channel silencing.

2.5.2 A more direct approach

We set out to develop an approach to detect non-conducting Kv2.1 channels in HEK293 cells that improved on some of the short comings of earlier methods. One major disadvantage of previous methods was that estimates of non-conducting channels were made by comparing the activity of channels in different populations of cells. For example, O'Connell et al. compared the average macroscopic gating charge and the average ionic current in two populations of transfected HEK293 cells [88]. A similar approach was taken by O'Dwyer et al. to estimate the number of non-conducting Kv2 channels in arterial smooth muscle cells [98]. In each of these studies, macroscopic gating charge was measured from one population of cells, and ionic current was measured from another. The indirect nature of these comparisons made us wonder whether the cells from which they measured gating charge simply expressed more channels than the cells from which they measured ionic currents. Our method removed this shortcoming by recording gating

charge and ionic currents from the same cells. Furthermore, we collect these two parameters in a single voltage-clamp protocol and therefore we detected both pore opening and the gating rearrangements that precede it in each cell.

2.5.3 Minimal voltage error

Another disadvantage of earlier methods of counting non-conducting Kv2.1 channels was the potential for voltage error. In the assay described by Fox et al., ionic currents were measured from a known number of fluorescent channels. They used physiological K^+ gradients and measured potassium currents at maximal activation. The ionic currents were extremely large under these conditions, so they used TEA to lower the potential for voltage error in their recordings. We now know that TEA selectively blocks Kv2.1 channels in a high conductance state and is completely without effect on the remaining channels in the low conductance state [113]. Indeed, the cited value of Kv2.1 single channel conductance that Fox and coworkers relied on was likely inaccurate for channels bathed in TEA. Therefore, the percentages of non-conducting channels found in that work, which ranged from 50-96%, probably overestimated the non-conducting fraction of Kv2.1 channels in HEK293 cells. We mitigated voltage error in this work by recording ionic currents near the reversal potential, preventing the need for pharmacological agents. Furthermore, we directly measured Kv2.1 single channel conductance under our experimental conditions. Therefore, we believe the percentages of non-conducting channels found in this work, which ranged from 0-70% are more realistic than those published by Fox et al.

2.5.4 Measuring unitary Kv2.1 properties

Another distinct improvement in the current work was the empirical measurement of unitary gating charge and conductance of Kv2.1 channels in our system. We were able to measure the Kv2.1 unitary charge by relying on the fluorescent counting method described by Fox et al. to make an independent estimate the number of channels in each cell. We found that macroscopic charge scaled linearly with our estimate of fluorescent

channels with a slope equal to the unitary gating charge. The value we obtained was reasonable considering recently published evidence that only half of the total Kv2.1 gating charge moves in a concerted manner in the first few milliseconds after depolarization. Therefore, we believe our estimate of total channel number from macroscopic gating charge is not in error.

As previously mentioned, the incorrect assumption that Kv2.1 single channel conductance was unaffected by TEA was a major drawback to earlier methods. Interestingly, the switch from the TEA-sensitive to insensitive conformation is partially controlled by the effective potassium concentration at the outer mouth of the channel (see below and [113, 129]). Given our non-physiological potassium gradient, we felt it especially important to measure Kv2.1 single channel conductance in our solutions, which we did with noise fluctuation analysis. We further validated our use of noise fluctuation analysis by showing that we could detect potassium dependent changes in the Kv2.1 single channel conductance as predicted by the literature. Therefore we believe our estimation of conducting channel numbers is accurate.

2.5.5 Is the non-conducting state a low-conducting state?

Two major conducting conformations have been described in Kv2.1 channels, one high and one low. The two conformations are associated with the positions of two lysine residues in the outer pore which are sensitive to K^+ concentration. With physiological internal K^+, the external K^+ site that determines the outer pore conformation has a K_D of 10 mM, and higher external K^+ favors the high conductance state [113, 129]. This phenomenon is thought to allow Kv2.1 to maintain strong K^+ efflux in the face of rising extracellular K^+ conditions, such as occur during high frequency neuronal activity or pathological conditions. Interestingly, the ability of the outer vestibule to change conformations is governed by K^+ occupancy of the channel central cavity, internal to the selectivity filter [130]. When K^+ occupies this site (i.e. during channel conduction) the outer vestibule conformation is fixed. When the central cavity is empty (i.e. when the channel is

closed or blocked from the inside) the outer vestibule is free to change conformation. Is it possible that the detection of non-conducting channels in this work and others is instead a detection of Kv2.1 channels in the low conductance state?

In our study, intracellular K^+ was lower than the predicted K_D of the central cavity (60 mM, [130]). Furthermore, we held the channels at -90 mV for at least 2 minutes before opening which should promote an empty central cavity. Therefore, the outer vestibule should be free to take on the high conductance conformation that is favored by our extremely high K^+_{out}. This was confirmed by our detection of the high conductance state with noise fluctuation analysis. Therefore we suggest that the non-conducting Kv2.1 channels are in a state that is different from the previously described low conductance conformation.

2.5.6 The relationship between clustering and conducting state

Kv2.1 clustering is linked to its function. Indeed, our lab showed that almost all conducting channels reside outside of clusters [88]. This suggested that clustering led to channel silencing, however, subsequent work showed that non-clustering Kv2.1 mutants also had a non-conducting population that was regulated by channel density in the membrane [101]. We decided to analyze the dependence of the Kv2.1 non-conducting state observed in this work as it related to channel localization. Figure 2.10 shows the fraction of conducting Kv2.1 channels as a function of the percent of channels that were clustered, binned into 10% bins. The data suggest that as more channels partition into clusters, fewer channels conduct. This may seem to suggest that clustering itself favors the non-conducting state. However, as the percentage of channels in clusters increases, there will be an overall increase in the average density that each channel experiences in the membrane. Therefore these data does not necessarily suggest that that non-conducting state is associated with a channel's localization to clusters. It would be interesting to repeat the quantification of conducting fraction in a non-clustering mutant, as Fox et al. did, using

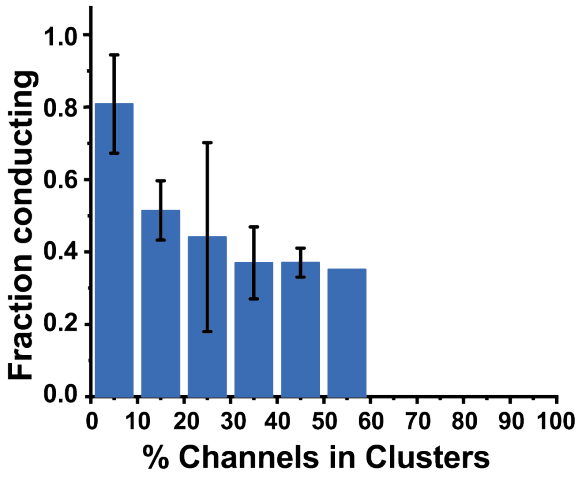

Figure 2.10: Kv2.1 non-conducting state is associated with increased clustering. The same data in Figure 2.8C plotted as a function of the percent of channels found in clusters. The percent of channels in clusters was defined as the percent of total footprint fluorescence associated with clusters. The data was binned into 10% increments. The conducting fraction of Kv2.1 decreased as more channels were found in clusters. Error bars are standard error. Bins without error bars only had one data point.

the updated approach. In general, the dependence of Kv2.1 non-conducting fraction on density and clustering is consistent with our previous work.

2.5.7 Non-conducting channels are *not* non-functional channels

Earlier studies of Kv2.1 in HEK293 cells and arterial myocytes suggested that all of these channels had functional voltage sensing domains, but did not directly test this hypothesis since channel protein numbers were not measured. In the current work we measured the gating charge from fluorescent Kv2.1 channels expressed in HEK293 cells. To our knowledge, this is the first quantitative measurement of gating transitions from a known number of fluorescently-tagged Kv2.1 channels. The data revealed that only half of the full charge associated with Kv2.1 gating moved in the first few milliseconds after depolarization. However, this charge appeared to move in every fluorescent channel, not only the conducting channels. Therefore, non-conducting channels are not simply non-functional channels. Indeed, it may seem plausible that at high expression levels some proteins would be synthesized incorrectly or be subject to misfolding. However, the detection of functional voltage-sensing machinery from non-conducting channels makes

this scenario unlikely. Since Kv2.1 gating charge is uncoupled from pore opening in non-conducting channels, is it possible that this charge is coupled to some other cellular process? Kv2.1 induced ER-PM junctions are thought to be specialized Ca^{2+} signaling domains. For example, voltage-gated Ca^{2+} channels are localized near these membrane contact sites [79, 121]. Furthermore, Kv2-dependent clustering of Cav channels in this domain appears to increase Cav channel open probability after depolarization [98]. The idea that gating charge movement from non-conducting Kv2.1 channels could be coupled to the gating of nearby calcium channels is an intriguing hypothesis. However, HEK293 cells do not express an apparent calcium current, therefore this type of direct functional coupling between Kv2.1 and calcium channels is not likely occurring under our experimental conditions. If Kv2.1 gating charge is somehow coupled to calcium channel gating, we expect the mechanism to require an intermediary protein. Alternatively, the gating charge movement from non-conducting Kv2.1 channels could be coupled to a completely different cellular process.

2.5.8 Limitations

Although the approach we took improves on earlier methods in several ways, it is not perfect. One issue we encountered was that many cells could only be recorded from once. After recording gating and ionic currents, we repolarized the membrane to the holding potential. Inevitably, at this point in the recordings a large influx of potassium flowed through the open Kv2.1 channels, then decayed as the channels underwent voltage-dependent closing. For many cells at the higher expression levels, this K^+ influx either destroyed the patch or was fatal. For those cells that survived, we found that E_K was not stable in subsequent recordings. Indeed, several minutes of recovery time were needed before the K^+ reversal potential returned to the theoretical E_K. We attributed this problem to changes in the local K^+ concentration at the plasma membrane, although we did not rigorously test it. Perhaps including a few millimoles of Na^+ in the recording so-

lutions could alleviate these issues by supporting the function of the endogenous Na^+/K^+ ATPase. Future studies could address this.

Another downside to our assay is that the large liquid junction potential coupled with high membrane conductances made it difficult to clamp cells to the exact zero-current potential on the first recording attempt. This meant that some cells had small amounts of ionic current contamination in the gating current waveform. For other cells, there was so much ionic current that we could not resolve enough of the gating current to confidently estimate the total charge moved, and these cells were not analyzed. Indeed in some of the highest expressing cells, sub-millivolt changes in the command potential could mean a difference of a few hundred picoamps of ionic current (see the recording in Figure 2.3 for an example). We believe that reducing the junction potential between internal and external solutions could improve this problem in future iterations by removing some of the variability in the measured E_K. Perhaps using choline instead of NMDG as the replacement cation in the internal solution would solve this problem.

2.5.9 Future directions

The mechanism underlying the silencing of Kv2.1 conductance is not clear. Although expression level seems to modulate the non-conducting fraction, this could be due to multiple molecular mechanisms. For example, perhaps a binding partner required for Kv2.1 conductance is expressed at low enough levels to be limiting. Conversely, the expression of a silencing factor may be coupled to the expression of Kv2.1 channels. Alternatively, perhaps tight packing of the channels in the membrane leads to channel interactions that favor non-conducting states. Understanding how specific the non-conducting state is to Kv2.1 would be an important clue in the underlying mechanism of channel silencing. One additional advantage of the assay developed in this chapter is its general utility for any potassium-selective channel. Therefore we decided to investigate whether the second Kv2 isoform, Kv2.2, as well as two *Shaker*-related channels would show evidence of the density-dependent non-conducting state. The results from these studies are given in

Chapter 3 and suggest that the mechanism of channel silencing is likely more common than we originally thought.

Chapter 3

Channel density is a common regulator of Kv channel function

3.1 Chapter Overview

In this chapter we take advantage of the assay developed in Chapter 2 to quantify conducting and non-conducting channels from three other Kv channels. First, we apply the assay to the second Kv2 family member, Kv2.2. Next we apply it to Kv1.4, a *Shaker*-type channel which we have studied before in the context of the non-conducting state [101]. Lastly we apply the assay to another *Shaker*-type channel, Kv1.5. Each of these studies was differently motivated, as discussed in the introduction below. We show evidence for significant non-conducting populations in Kv2.2 and Kv1.5, but not Kv1.4. However, all three channels show density-dependent regulation of the number of non-conducting channels we counted, suggesting that channel silencing may be subject to a common mechanism across Kv channel families.

Hypotheses to be tested:

1. Gating rearrangements and ionic conductance from three additional Kv channels can be detected under the conditions set out in Chapter 2.

2. Kv2.2 has a similar fraction of non-conducting channels as Kv2.1 and that fraction is density-dependent.

3. Kv1.4 and Kv1.5 do not have non-conducting states nor density-dependent conductance.

3.2 Introduction

The Kv2 family has an additional member, Kv2.2, which is less-well studied than Kv2.1. Kv2.2 expression overlaps extensively with Kv2.1 and the two channels can form heterotetramers, although it is not uncommon to find cells that express one or the other

isoform exclusively [62, 70, 71]. Kv2.2 also aggregates into clusters on the plasma membranes at sites where it forms ER-PM junctions via interaction with ER VAPs [74]. However, Kv2.2 is less sensitive to stimuli that induce dephosphorylation-dependent changes in Kv2.1 function [62]. Kv2.1 and Kv2.2 are highly homologous in their N-terminal and transmembrane regions and diverge significantly in their distal C-termini, as shown in Figure 3.1. However, as indicated with the orange bar in Figure 3.1, the C-terminal VAP-binding motif is highly conserved between the two channels, consistent with their conserved ability to form ER-PM junctions. Despite the similarity between Kv2.1 and Kv2.2 function *in vivo* and their highly conserved sequence, a non-conducting population has not been reported for Kv2.2. Given our earlier work that suggested that the Kv2.1 C-terminus is not required for the non-conducting state [101], we expected that Kv2.2 would also have a significant non-conducting population of channels. Indeed the work herein shows a density-dependent non-conducting state of Kv2.2 for the first time.

Although we went to great lengths to convince ourselves that the assay developed in Chapter 2 was accurate, we sought an additional biological control. The previous quantitative assay published by our lab was tested on Kv1.4, a member of the *Shaker*-related channel family whose *in vivo* function is unrelated to that of Kv2 channels. In that work, Fox and coworkers found no evidence for a non-conducting population of Kv1.4 channels, nor density-dependent regulation of the Kv1.4 macroscopic current [101]. We were able to reproduce the finding that on average, nearly 100% of Kv1.4 channels were conducting. However, we did observe density dependence in the fraction of conducting Kv1.4 channels on a cell-by-cell basis.

We were curious whether another *Shaker*-related channel would behave similarly to Kv1.4. To that end, we applied the gating assay from Chapter 2 to Kv1.5, another delayed rectifier highly expressed in cardiac myocytes where it controls the cardiac AP [67]. Surprisingly, Kv1.5 had a more prominent non-conducting population than Kv2.2 and also showed density-dependent regulation. Together these results support the idea that

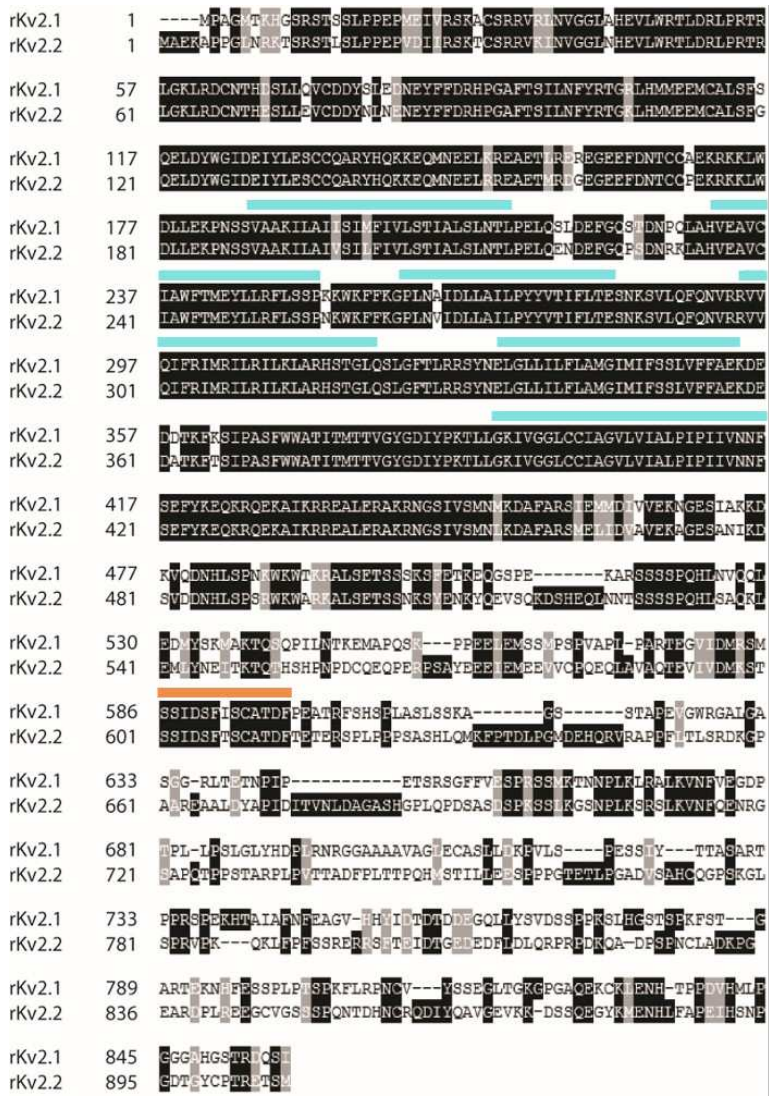

Figure 3.1: Alignment of Kv2.1 and Kv2.2. Amino acid sequence alignment for rat Kv2.1 and rat Kv2.2. Black residues are identical between the two sequences and grey residues are similar. Teal bars represent the location of the 6 transmembrane segments. The orange bar denotes the conserved VAP-binding motif. Note the divergence in the C-terminal end of the two proteins.

diverse Kv channels are sensitive to their density in the membrane. This finding has implications for the function of cells that express high densities of channels or that localize channels to dense microdomains.

3.3 Materials and Methods

In general the methods were very similar to the methods described in Section 2.3. Pertinent details relating to this chapter specifically have been added below. Otherwise, the reader is directed to the appropriate subsection of Section 2.3.

3.3.1 DNA constructs

Plasmid DNA containing the coding sequence for GFP-Kv2.2 (rat), GFP-Kv1.4-BAD (rat) or YFP-Kv1.5 (human) was transiently transfected into HEK293 cells and have been described previously [72,74,102,123]. The fluorescent proteins are fused in frame to the N-terminus of each channel's open reading frame to minimize effects on channel trafficking and function. The N-terminal GFP fusion to Kv1.4 interferes with N-type inactivation resulting in a slowly-inactivating current [90]. The Kv1.4 construct differs further from the wild-type channel in that it contains a biotin acceptor domain (BAD) encoded in the first extracellular loop, which does not alter channel activation or inactivation [102, 123].

3.3.2 Cell culture and transfection

See Section 2.3.2.

3.3.3 Electrophysiology

See Section 2.3.3.

3.3.4 Simultaneous gating and ionic current recordings

See Section 2.3.4.

3.3.5 Non-stationary noise fluctuation analysis

See Section 2.3.6. In this chapter, noise fluctuations were measured from each channel in Flipped K^+ ionic conditions only. Tail currents were collected at -70 mV for Kv1.4 and Kv1.5 and -60 mV for Kv2.2 because of their different voltage dependencies. Single

channel conductances estimated from tail currents were scaled by the same rectification index used in Chapter 2.

3.3.6 TIRF microscopy

See Section 2.3.7.

3.3.7 Fluorescent channel counting

See Section 2.3.8.

3.3.8 Analysis and statistics

Error bars represent standard error. Fitting was performed in Origin2018b using least-squares methods. Statistical significance was defined as $p<0.05$ in T-tests comparing sample means.

3.4 Results

3.4.1 Macroscopic gating charge and ionic conductance from Kv2.2, Kv1.4, and Kv1.5 in Flipped K^+

As shown in Figure 3.2, Kv2.2, Kv1.4 and Kv1.5 were all amenable to the gating assay described in Chapter 2. Figure 3.2A shows representative TIRF images of HEK293 cells expressing high amounts of each of the three Kv alpha subunits. Kv2.2 had a punctate localization in the HEK293 cell membrane, in accordance with its ability to bind to ER VAPs and form ER-PM junctions. Micron sized clusters of Kv2.2 channels are readily visible in the top panel of Figure 3.2A. In contrast, Kv1.4 and Kv1.5 channels were uniformly distributed across the HEK293 cell plasma membrane, as seen in the middle and bottom panels in Figure 3.2A. We voltage-clamped cells expressing high levels of each Kv subunit in the Flipped K^+ solution set described in Chapter 2. As expected, we observed small, transient currents resembling ON gating currents from all three channel types when we stepped the membrane to the new reversal potential for potassium (+40 mV). These gat-

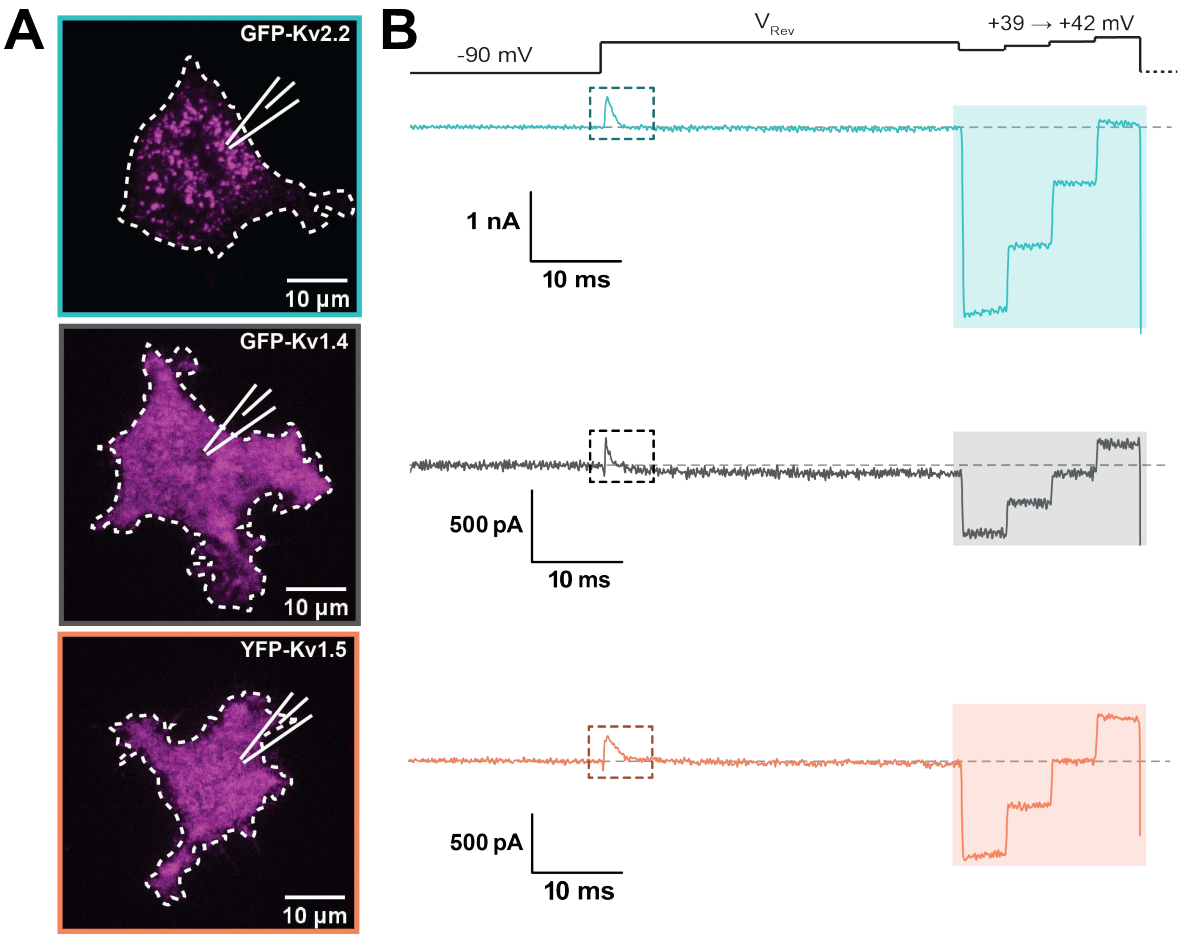

Figure 3.2: Macroscopic gating charge and ionic conductance from Kv2.2, Kv1.4, and Kv1.5. **A)** TIRF images of HEK293 cells expressing GFP-Kv2.2 *(top)*, GFP-Kv1.4 *(middle)* or YFP-Kv1.5 *(bottom)*. Note the difference in Kv2.2 localization compared to the other two channels. Scale bars = 10 µm. **B)** Examples recordings of gating (dashed boxes) and ionic currents (shaded boxes) from Kv2.2 *(Top)*, Kv1.4 *(Middle)*, or Kv1.5 *(Bottom)*.

ing currents are indicated by the dashed boxes in Figure 3.2B for Kv2.2 *(teal)*, Kv1.4 *(grey)*, and Kv1.5 *(orange)*. We also observed ionic currents in the same voltage-clamp traces when we stepped the membrane to voltages near the K^+ reversal potential, as seen in the shaded boxes in Figure 3.2B.

We patched at least 18 cells expressing each Kv alpha subunit and measured the macroscopic gating charge and membrane conductance from each as described in Section 2.4.2. We plotted membrane conductance as a function of macroscopic gating charge for each channel type as shown in Figure 3.3. In general, the relationships between conductance and gating charge were positive, suggesting that the measured membrane con-

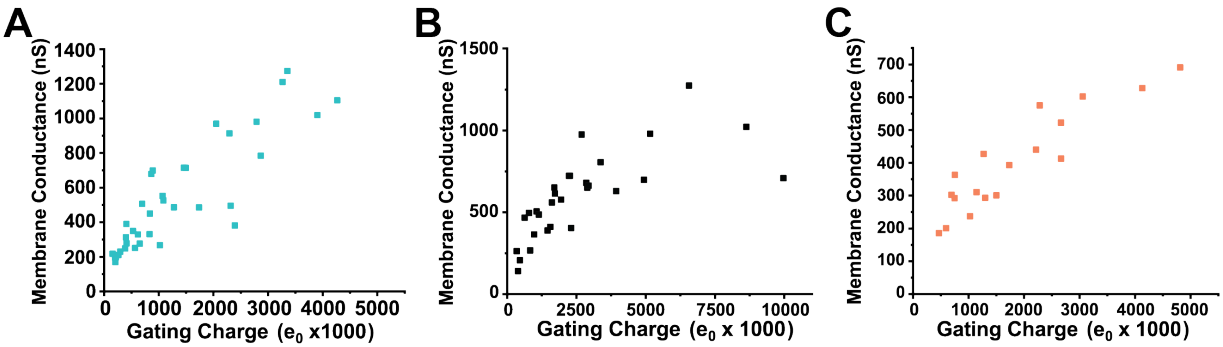

Figure 3.3: Relationship between membrane conductance and gating charge in three Kv channels. The macroscopic conductance as a function of macroscopic gating charge from HEK293 cells expressing **A)** Kv2.2 **B)** Kv1.4 or **C)** Kv1.5.

ductance came from the activity of the expressed subunits. The relationship between membrane conductance and gating charge appeared mostly linear for the three channels. However, as channel expression increased a plateauing effect could be seen for each of the three channels, although it was most prominent for Kv1.4.

3.4.2 Unitary properties of Kv2.2, Kv1.4, and Kv1.5 in Flipped K^+

In order to convert the raw values in Figure 3.3 to channel numbers, we needed to measure the unitary properties of each channel. We again turned to TIRF microscopy to measure the unitary fluorescence of the GFP- and YFP-tagged channels expressed in HEK293 cells. Figure 3.4 shows results from our observations from HEK293 cells expressing low amounts of Kv channel subunits such that single channels could be resolved. Figure 3.4A, B and C shows still images from movies taken of HEK293 cells expressing each of the three channel subunits. The punctate pattern seen in these images is due to the low expression of fluorescent proteins in the cells, which are not dense enough to cover the entire plasma membrane. The arrowheads in Figure 3.4A, B and C indicate single channels identified from time lapse series of GFP-Kv2.2, GFP-Kv1.4 and YFP-Kv1.5, respectively. We selected putative singles from multiple cells per dish by their diffusion behavior and measured their intensities to obtain the average unitary fluorescence of each Kv subunit. Figure 3.4D shows histograms of the measured fluorescence intensity of pu-

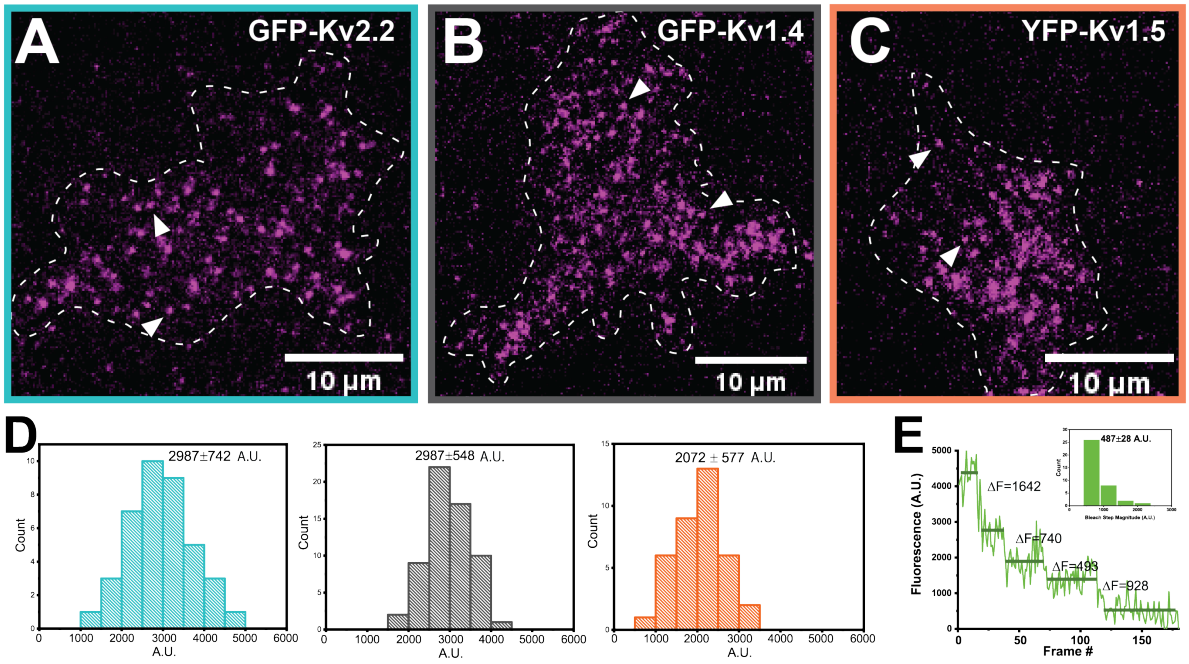

Figure 3.4: Unitary fluorescence of Kv2.2, Kv1.4 and Kv1.5 **A)**TIRF image of a HEK293 cell expressing a low amount of GFP-Kv2.2. This image is the first frame of a 10s time series. Arrowheads indicate putative single channels as identified by their diffusion behavior. **B)** TIRF image from a time series of GFP-Kv1.4 expressed in HEK293 cell at low enough amount to resolve diffusing channels. Arrowheads indicate two single channels. **C)** First frame of a time series taken using TIRF of a HEK293 cell expressing a low density of YFP-Kv1.5. Arrowheads are single channels. **D)** Histograms of the fluorescence intensities associated with putative single channels from TIRF images like those in A, B and C. Each histogram is from a single dish. The average unitary fluorescence values were: Kv2.2=2987±742 A.U. (teal), Kv1.4=2987±548 A.U. (grey), and Kv1.5=2072±577 A.U. (orange). **E)** Plot of fluorescence vs time illustrating sequential bleaching of several YFP molecules. *Inset* - histogram of all bleach events we measured from YFP. The average fluorescence associated with a single YFP bleach event was 487±28 A.U.

tative single channels from individual dishes of GFP-Kv2.2 *(teal)*, GFP-Kv1.4 *(grey)* and YFP-Kv1.5 *(orange)*. The average intensity of the two GFP-tagged channels was similar (Kv2.2 = 2987±742 A.U. and Kv1.4 = 2987±548 A.U.), while the average intensity of the YFP-tagged Kv1.5 channels was significantly lower (2072±577 A.U.). We suspected this was because our emission filter set was more optimal for collecting light from GFP, as opposed to YFP molecules. To ensure that our estimation of YFP-Kv1.5 unitary fluorescence was accurate, we measured bleach steps from immobile YFP-Kv1.5 puncta. An example of sequential bleaching of several YFP molecules is shown in Figure 3.4E. A histogram of all events measured in this way is shown in the inset of this panel, and revealed that the

smallest bin of YFP bleach events had an average fluorescence of 487±28 A.U. This value likely corresponds to the fluorescence of a single YFP molecule. Therefore, a Kv1.5 channel made of four YFP-tagged subunits would have a unitary fluorescence near 1948±112 A.U. This value was in good agreement with the averages obtained from histograms like that in Figure 3.4D *(orange)*. Therefore, we accurately measured the unitary fluorescence of all three alpha subunits.

The unitary fluorescence values determined above allowed us to estimate the number of fluorescent channels from TIRF images of the brighter cells that we had patched in Flipped K^+. We simply divided the footprint fluorescence of bright cells by the unitary fluorescence and then again by the footprint area, to obtain the density of fluorescent channels in the membrane. Because we had patched these cells using whole-cell voltage clamp, we also had a measurement of the total cell area from the cell capacitance. By assuming the density of channels on the basal surface is representative of the entire cell, we were able to estimate the number of channels in the entire cell membrane. The panels along the top of Figure 3.5 show crossplots of macroscopic gating charge and the number of fluorescent channels from HEK293 cells expressing each of the Kv channel types. The relationship between macroscopic charge and fluorescent channels was linear for all

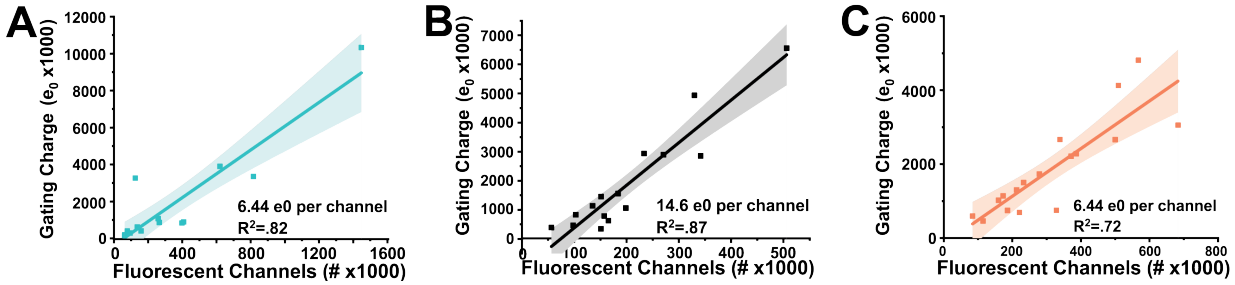

Figure 3.5: Unitary charge of three Kv channels **A)** Macroscopic gating charge as a function of the number of fluorescent channels in individual Kv2.2-expressing cells. The slope of the line is the unitary charge and is equal to 6.44±0.84 elementary charges (N=13). The shaded region around the fitted line represents the 95% confidence interval of the fit. **B)** Plot of macroscopic Kv1.4 gating charge vs. number of fluorescent channels in each cell. The unitary charge of Kv1.4 was 14.6±1.5 elementary charges (N=15). **C)** Kv1.5 macroscopic gating charge as a function of fluorescent Kv1.5 channels in the same cells. The unitary charge of Kv1.5 was 6.4±1.0 elementary charges (N=17).

three channels, as shown by the fits of the crossplots in Figure 3.5. The slope of each line represents the charge per fluorescent channel that is moved in the first 3 ms after depolarization. Kv2.2 and Kv1.5 both moved approximately 6.4 elementary charges per channel, while Kv1.4 moved 14.6 elementary charges. The number of elementary charges moved by Kv1.4 was approximately double that moved by Kv2.2 and Kv1.5, and Kv2.1 which was shown in the previous chapter. The value of the Kv1.4 unitary charge is actually more consistent with what we expected to measure for all the channels studied here, as it matches closely with other estimates of unitary charge for *Shaker*, *Shab*, Kv2.1 and Kv1.2 gating charge per channel [54, 131, 132]. As discussed in Chapter 2, we believe only half of Kv2.1 charge moves in a concerted manner in the first few milliseconds after depolarization. Our data suggest the same is true for Kv2.2 and Kv1.5, but not Kv1.4. We believe the detection of $\sim$14 elementary charges from Kv1.4 validates our measurements further, by proving that the underestimation of Kv2.1, Kv2.2 and Kv1.5 unitary charge is not due to an inherent lack of sensitivity in our recording system, but likely due to differences in these channels' gating rearrangements.

In order to estimate the unitary conductance of Kv2.2, Kv1.4 and Kv1.5 we performed noise fluctuation analysis on tail currents from each channel bathed in Flipped K^+. The results of these experiments are summarized in Figure 3.6. We voltage-clamped HEK293 cells expressing each channel type and made repetitive recordings of channel activation and deactivation. We activated channels at +40 mV for 40 ms and then recorded deactivating tail currents at hyperpolarized potentials. We repeated this protocol up to 200x per cell to build an ensemble of ionic recordings for each cell. We analyzed the statistical variance in ensembles of tail current recordings and obtained the single channel conductance as described in Section 2.3.6. As shown in the lower panels of Figure 3.5, the three channels had very similar single channel conductances in these ionic conditions. Indeed, the single channel conductances were 16.7±1.5 pS for Kv2.2 at -60 mV *(teal)*, 15.5±1.9 pS for Kv1.4 at -70 mV *(grey)* and 16.9±2.3 pS for Kv1.5 at -70 mV *(orange)*. After correction

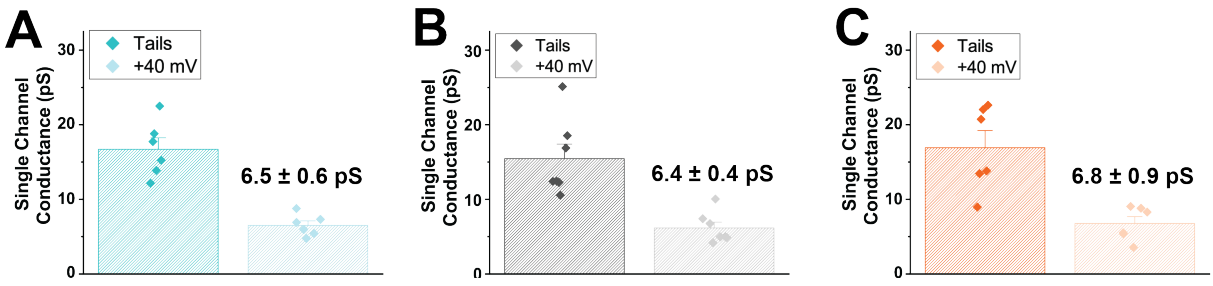

Figure 3.6: Unitary conductance of three Kv channels **A)** Summary of Kv2.2 single channel conductance measured using non-stationary noise fluctuation analysis on HEK293 cells bathed in Flipped K^+. Tail currents were recorded at -60 mV and revealed an average single channel conductance of 16.7±1.5 pS. After correction for rectification Kv2.2 single channel conductance at +40 mV was 6.5±0.6 pS (N=6). **B)** Kv1.4 single channel conductance measured from noise fluctuations was estimated to be 15.5±1.9 pS at -70 mV and 6.4±0.4 pS at +40 mV (N=6). **C)** Kv1.5 single channel conductance was estimated using noise fluctuation analysis in HEK293 cells and was 16.9±2.3 pS at -70 mV and 6.8±0.9 pS at +40 mV (N=6).

for rectification, the single channel conductances were 6.5±0.6 pS, 6.4±0.4 pS, and 6.8±0.9 pS, respectively.

3.4.3 Counting non-conducting Kv2.2, Kv1.4 and Kv1.5 channels

With the unitary charge and conductance values in hand for the three channels, we converted the macroscopic charge and membrane conductance values from Figure 3.3 to channel numbers. Figure 3.7A contains a comparison of the number of conducting and gating channels obtained from individual cells expressing each channel isoform. These paired measurements show that in some cells the estimates of the number of conducting and gating channels were quite different. Panel B of Figure 3.7 shows the same data as the fraction of gating channels that were conducting in HEK293 cells expressing each channel type. Kv2.2-expressing HEK293 cells had an average conducting fraction of 0.79±0.06, Kv1.4-expressing cells had an average conducting fraction of 0.91±0.08 and Kv1.5 had an average conducting fraction of 0.51±0.04. One sample T-tests revealed that the average conducting fraction of Kv1.4 was not significantly different from a test mean of 1, supporting our previously published finding that Kv1.4 does not have a significant population of non-conducting channels. However, the conducting fractions of Kv2.2 and Kv1.5 were significantly different from 1, indicating that these two channels had significant non-

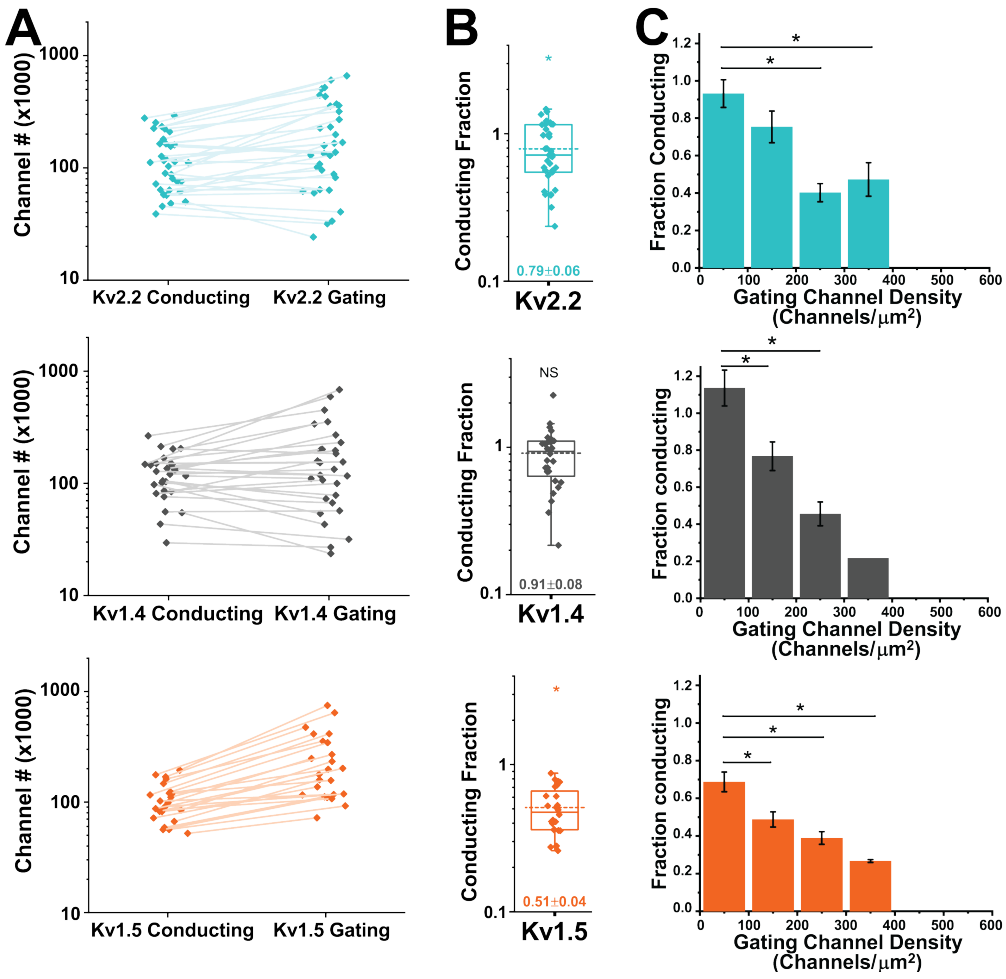

Figure 3.7: Density-dependence in Kv2.2, Kv1.4 and Kv1.5 **A)** Summary of the number of conducting vs gating channels for Kv2.2 *(Top)*, Kv1.4 *(Middle)*, and Kv1.5 *(Bottom)*. **B)** The same data in A shown as the fraction of conducting channels in each cell. On average, 79±6% of Kv2.2 channels, 91±8% of Kv1.4 channels and 51±4% of Kv1.5 channels were conducting. The fraction of conducting Kv2.2 and Kv1.5 channels were significantly different from 1 (One-sample T-test, $p<0.05$ and $p<0.0005$, respectively). Boxes represent the middle 50% of data and the median. The dashed horizontal lines represent the means. **C)** Conducting fraction plotted as a function of the density of gating channels in the membrane for Kv2.2 *(Top)*, Kv1.4 *(Middle)*, and Kv1.5 *(Bottom)*. Data from all cells were binned into 100 channels/μm^2 bins. Bins without error bars only contain one data point. Asterisks indicate $p<0.05$ between bin means from two-sample T-tests. The conducting fraction decreased as more channels were expressed in the membrane, suggesting a density dependent mechanism for each of the three channels types shown.

conducting populations. These are the first results to suggest that Kv2.2 and Kv1.5 exhibit non-conducting states.

Similar to our measurements from Kv2.1-expressing HEK293 cells in Chapter 2, the three channels studied here showed significant variability in the fraction of conducting

channels from cell-to-cell. This variability is evidenced by the spread of the data in Figure 3.7B. In Chapter 2 we attributed this variability to a density-dependent mechanism regulating the number of conducting channels in Kv2.1. We wondered if similar regulation was occurring for the three new channels studied in this chapter. Figure 3.7C shows the conducting fractions from Figure 3.7B as a function of the density of total channels in the membrane. We binned the data into 100 channels/μm^2 bins for ease of comparison between channel types. Much like we saw for Kv2.1 in Chapter 2, all three channels shown in Figure 3.7C appear to have conducting fractions that decrease with increasing channel density in the membrane. This phenomenon is apparent even for Kv1.4, which on average did not have a non-conducting state, but upon increased expression appeared to develop one.

3.5 Discussion

3.5.1 Summary

In this chapter we used the assay developed in Chapter 2 of this dissertation to explore the prevalence of non-conducting states in Kv channels of three different types. First we applied the assay to Kv2.2, the second member of the Kv2 family. We found that on average, only about 80% of Kv2.2 expressed in HEK293 cells were conducting. This is the first evidence of a non-conducting state for the second Kv2 family member and suggests that Kv2.1 and Kv2.2 are regulated similarly. Furthermore, as we showed for Kv2.1 in Chapter 2, the Kv2.2 conducting fraction was a function of the density of Kv2.2 channels in the membrane.

We next studied Kv1.4 using the gating and conducting channel assay. On average, 90% of the Kv1.4 channels were functional when expressed in HEK293 cells, indicating that this channel did not have a non-conducting population. This finding is consistent with our lab's earlier quantification of functional Kv1.4 channels in HEK293 cells [101]. However, unlike in the earlier investigation, in the current work we noticed density de-

pendence in the percentage of conducting Kv1.4 channels. The discrepancy between these results can be attributed to the different expression ranges explored in each study. In this work we recorded from cells expressing up to 300 channels/μm^2, while the highest Kv1.4 density achieved by Fox et al. was 120 channels/μm^2. Indeed, the lack of a non-conducting Kv1.4 population on average is likely related to its overall lower expression in the membrane as opposed to its complete resistance to a silencing mechanism.

The last channel we studied was Kv1.5. We chose to investigate Kv1.5 after the interesting results we saw from Kv1.4. We were surprised to find that on average, only 51% of Kv1.5 channels were conducting. The conducting fraction of Kv1.5 was also influenced by density in the membrane, with higher expressing cells having a smaller conducting fraction.

3.5.2 Density-dependent silencing is common among Kv channels

In the current and previous chapter, we found that the activity of four Kv channels is sensitive to those channels' expression level in HEK293 cells. We suggest that expression-dependent Kv channel silencing is prevalent phenomenon, even though Kv2.1 is the only channel in this work for which a non-conducting population has been observed before. If density-dependent silencing is common among Kv channels, why haven't there been more reports of Kv channel silencing in the literature? We think this is can be explained by two properties of Kv2 channels that make them unique. First, Kv2 channels are expressed at high levels in many cell types. Indeed, cultured rat hippocampal neurons and arterial myocytes express between 100,000 and 200,000 Kv2 channels endogenously [98, 101]. Therefore inconsistencies between the magnitudes of delayed rectifier currents generated by these cells and the number of channels are easy to detect. Second, Kv2 channels form clusters that are readily visible using light microscopy and therefore, relatively easy to study. The specialized localization of Kv2 channels was detected relatively early in the field of ion channel biology and likely contributed to the plethora of research attempting to relate Kv2 channel localization to its function.

Over the past several years, ion channel field has begun to focus on the subcellular organization of these membrane proteins. Super-resolution techniques have aided greatly in this work because most ion channel species are localized at the nanoscale [133–136]. Importantly, nanoscale clustering has been associated with changes in ion channel gating. Recent studies of the KcsA channel in lipid bilayers using atomic force microscopy and solid state NMR suggested that channel clustering is exquisitely linked to channel gating [137, 138]. Additionally, super-resolution light microscopy coupled with patch-clamp electrophysiology has revealed that voltage-gated calcium channels cluster in multiple cell types and clustering appears to facilitate their cooperative gating [139, 140]. Cooperative gating has also been recorded from sodium-activated potassium channels and appears to be favored by close proximity of the channels [141]. Therefore it is not entirely surprising that high expression levels modulate the function of Kv channels from multiple families.

3.5.3 The Kv non-conducting state exists at physiologically relevant channel densities

Kv2 channels are found at relatively high densities in many cell types *in vivo*. Fox et al. measured densities of Kv2.1 in rat hippocampal neurons using quantitative immunolabeling and found that the density of Kv2.1 channels in clusters was about 62 channels/μm^2, while channels outside of clusters had an average density of about 10 channels/μm^2 [101]. O'Dwyer and colleagues counted the number of gating Kv2 channels in mesenteric arterial smooth muscle cells and although they did not distinguish between clustered and non-clustered channels, they found overall densities of about 36 channels/μm^2 for males and 85 channels/μm^2 for females. Figure 3.8 shows the conducting fraction of the four Kv channels measured in this dissertation as a function of gating channel density, zoomed in to the range of physiological Kv2 densities. This figure contains the same data as that in Figure 2.8C and Figure 3.7C but is shown as the moving average of all data points, instead of as binned data. It is clear that significant silencing of

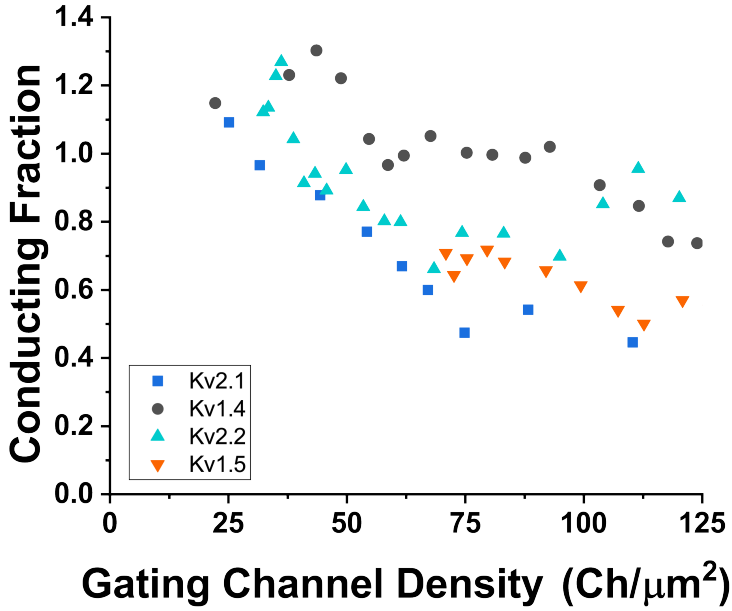

Figure 3.8: The conducting fraction in the physiological range of channel densities. A plot of the conducting fraction for each channel type as a function of the density of gating channels, zoomed to the range between 0 and 125 channels/μm^2. The data shown represents a moving average (window = 4) of the data from all cells. Note that the all Kv1.4 channels are conducting up to a density of 100 channels/μm^2.

Kv2.1 and Kv2.2 channels occurs in the range of 50-100 channels/μm^2, consistent with the aforementioned detection of non-conducting Kv2 channels in this density range *in situ*.

In contrast, as seen in Figure 3.8, Kv1.4 largely lacks a non-conducting population at densities up to 100 channels/μm^2. Therefore, the Kv1.4 non-conducting state is only likely to be physiologically relevant at extremely high densities, which to our knowledge have not been reported for Kv1.4 in any endogenous system. The physiological relevance of the Kv1.5 non-conducting state is somewhat difficult to predict. We did not acquire data from cells at the lowest expression levels, but as seen in Figure 3.8, 35% of Kv1.5 channels were non-conducting at a density of $\sim$75 channels/μm^2.

Do Kv1.5 channels ever reach this density in physiological systems? Kv1.5 is known to be enriched at the intercalated disc of cardiac myocytes, but quantitative measurements of the numbers of channels there are lacking [142, 143]. Interestingly, the function of Kv1.5 channels at the intercalated disk is equally mysterious. The ultra rapid potassium current (IK_{UR}) carried by Kv1.5 channels in the heart is undetectable in ventricular myocytes

where these clusters of Kv1.5 have been observed by immunolocalization [142]. Might these channels be largely non-conducting?

3.5.4 A potential molecular mechanism

Membrane lipids are thought to be integral to ion channel behavior. Indeed, crystallization of a mammalian Kv channel required the presence of phospholipids, and the X-ray structure of Kv1.2 revealed multiple contacts between membrane lipids and channel transmembrane domains [30]. Kv7.1 channels are probably the most well-known lipid-regulated Kv channels to date. Indeed, phosphatidylinositol 4,5,-bisphosphate (PIP2), an anionic membrane lipid, is thought to be required for coupling Kv7 voltage sensor activation to pore opening [144]. There are mixed reports on the effects of PIP2 on other Kv channels' function [37, 145, 146]. However, even if PIP2 does not control the gating of the channels studied in this work, other membrane lipids could be involved. This hypothesis is attractive because individual cell types have different lipid compositions which could modulate pore opening among Kv channel families to different extents. A lipid composition that favors the Kv2.1 non-conducting state might be less effective at silencing Kv1.4 channels, and vice versa. Furthermore, plasma membrane lipid composition is dynamic and this mechanism could allow the cell to silence or activate Kv channels under variable conditions. Perhaps, as suggested by Hilgemann [145], all Kv channels require some type of anionic lipid for proper function and the non-conducting states seen here arise as the available lipids specific to HEK293 cells become saturated.

3.5.5 Limitations

It is evident in Figure 3.7B that in some cells we measured conducting fractions higher than 1, a result that is theoretically impossible. We believe this phenomenon is mostly due to error in the measurement of macroscopic gating charge from cells at the lower end of expression. Indeed, as fewer channels are expressed, it is more difficult to resolve gating currents from the baseline electrophysiological noise. Ideally we could have used averag-

ing to improve measurements in this range, but as discussed in Chapter 2, the ionic conditions were not conducive to making multiple recordings from each cell. Other sources of noise likely contributed to this phenomenon as well. For example, we used average values of single channel conductance and unitary fluorescence to quantify numbers of conducting and fluorescent channels, which each had their own measurement variability. Therefore, even if we could measure gating currents with 100% accuracy at all expression levels, we may still have obtained some conducting fractions >1.

One criticism of the present work is the sole use of fluorescently-tagged channels in heterologous systems. Indeed, it would be more convincing to show non-conducting states in wild-type channels, or better yet, wild-type channels endogenously expressed in physiological systems. This could theoretically be accomplished in the same way that Fox et al. counted non-conducting channels endogenous to rat hippocampal neurons. Those authors performed quantitative immunolabeling in conjunction with whole-cell patch clamp, where they measured delayed rectifier current magnitudes. This approach has its own limitations. For example, Fox and coworkers had to assume that immunolabeling was uniform across the entire cell and that antibodies interacted with antigens in a fixed ratio. Alternatively, we could have used O'Dwyer's approach, using channel-specific gating modifiers and blockers to extract gating charge and ionic currents from endogenous channel populations. This approach comes with its own challenges, including finding isoform-specific pharmacological agents and dealing with the potential presence of heterotetrameric channels expressed endogenously. Indeed, the best approach would be a combination of the current work done in a heterologous system and studies in physiological systems. This has already been done for Kv2.1, but should be pursued for the others channels described in this chapter.

Another potential limitation of this work is the use of HEK293 cells for channel expression. Is this a good model system for the channels studied herein? Certainly a mammalian cell line is the best option for recapitulating regulatory mechanisms of mammalian pro-

teins. However, the results obtained in HEK293 cells should not be taken to represent the behavior of these channels in every mammalian cellular context. For example, neurons are thought to contain a higher mole fraction of cholesterol in their plasma membranes than other mammalian cell types [147]. If lipids play a role in the regulation of the non-conducting fraction, this fraction would likely be different if studied in central neurons. Another confounding factor present in HEK293 cells but absent in neurons might be cell cycle-dependent kinases, which are known to phosphorylate Kv2.1 in Cos cells [148], and could modulate additional Kv channels' function as well.

3.5.6 Future Directions

Non-conducting ion channels are difficult to study. Ideally we could use single channel recordings to measure the open probability of ion channels at different plasma membrane densities. Unfortunately, non-conducting channels do not contribute ionic currents to electrophysiological recordings. Since the gating charge of a single channel cannot be detected electrically with patch-clamp, it is impossible to know the number of channels in patch that contains non-conducting channels. Perhaps optical methods could be coupled to single channel recordings to somehow visualize the gating of individual channels in the patch while recording the ionic currents from the same patch. This would yield a true measurement of the open probability of non-conducting channels. The data presented in this dissertation suggest than the non-conducting state we detected is uncoupled from channel activation, and that if the non-conducting channels' true open probabilities could be measured they would be nominally zero. If single fluorescently-tagged channels could be resolved on the apical cell membrane, perhaps using spinning disk confocal microscopy, then one could estimate the number of fluorescent channels in an area of membrane and subsequently perform on-cell patch clamp of that membrane area to record single channel currents. This task is made difficult by the lower signal-to-noise ratio in confocal vs. TIRF microscopy. However, reasonable estimates would likely be possible with bright enough fluorophores.

It would be intriguing to test the hypothesis that lipid composition regulates the non-conducting state observed in this work. One simple approach would be to compare the prevalence of non-conducting states in various cell-types with different lipid profiles. For example, one study found that mammalian HEK293T cells and insect SF9 cells had reciprocal amounts of phophatidylcholine (PC) and phosphatidylethanolamine (PE). Further, HEK293T cells had an almost 5-fold higher cholesterol-to-total phospholipid ratio than SF9 cells [149]. A comparison of non-conducting fractions in each of these cell types could be a starting point for determining which lipids might be important, if any.

Alternatively, studies could focus on correlating the presence of various types of lipids with the Kv channel isoforms shown here to have non-conducting states. The localization of different lipid species in cell plasma membranes *in situ* is not trivial. Current methods for localizing particular lipids include immunocytochemistry, expression of fluorescent lipid-binding protein domains, or imaging of incorporated synthetic fluorescently-tagged lipids, among others [150]. Each of these approaches has its drawbacks, and it is difficult to imagine building up a comprehensive picture of a cell's total lipid profile using optical methods. Mass spectrometry is still the best method to investigate cell-type specific lipid composition, but of course applying this method to subcellular lipid localization is extremely challenging. It would be especially interesting to map the lipid composition of certain subcellular compartments known to contain high densities of ion channels in this work *in situ*, such as the intercalated disc.

3.5.7 Conclusion

We have developed an improved quantitative assay to detect gating transitions and ionic conductance from Kv channels transfected into heterologous cells. We used this assay to corroborate ours and others observations of a non-conducting population of Kv2.1 channels in Chapter 2. In the current chapter we went on to show potentially physiologically relevant non-conducting states in Kv2.2 and Kv1.5 for the first time. An additional unexpected finding in this chapter was the sensitivity of all channels to density in the

plasma membrane, including Kv1.4, a channel whose density dependence was not observed in past studies. We suggest that density in the PM is a common regulator of Kv channel activity. Our results suggest that increased channel densities favor an extremely low open probability state of the channels, although the mechanism of this effect remains elusive.

Chapter 4

Interaction of Kv2 channels with all three AMIGO β-subunits modulates both channel electrical properties and cell adhesion molecule surface trafficking

4.1 Chapter Overview

The Kv2 channels encode delayed rectifier currents in excitable cells that maintain membrane polarization under conditions of high excitability. They also form stable junctions between the endoplasmic reticulum and plasma membranes in many different cell types, creating membrane contact sites that mediate functions distinct from membrane excitability. Therefore, proteins that interact with Kv2 channels can alter conducting and/or non-conducting channel functions. One member of the AMIGO family of proteins is an auxiliary Kv2 subunit and modulates Kv2.1 electrical activity. However, the AMIGO family has two additional members of approximately 50% similarity that have not yet been characterized as Kv2 β-subunits. In this work we show that the surface trafficking and localization of all three AMIGOs are controlled by their interaction with both Kv2 channels. Additionally, assembly of each AMIGO with either Kv2 shifts the channel activation midpoint in the hyperpolarizing direction. However, only AMIGO2 significantly slowed inactivation and deactivation, leading to a prolonged open state of Kv2 channels. The co-regulatory effects of Kv2s and AMIGOs likely help tune both electrical and non-electrical properties of cells in which they are expressed.

Hypotheses to be tested:

1. AMIGO1, 2 and 3 co-localize with both Kv2.1 and Kv2.2 when co-expressed in HEK293 cells.

2. Co-expression with either Kv2 channel will enhance AMIGO1, 2 and 3 trafficking to the HEK293 cell surface.

3. AMIGO1, 2 and 3 each alter voltage-dependent and kinetic properties of both Kv2.1 and Kv2.2 current when co-expressed in HEK293 cells.

4. Co-expression of two AMIGO isoforms simultaneously with Kv2.1 will result in electrophysiological phenotypes in between those imparted by each AMIGO alone.

4.2 Introduction

β-subunits of the Kv superfamily are important regulators of nervous system function. Indeed, this diverse class of proteins can modulate almost every aspect of Kv channel physiology including subunit assembly, trafficking, protein stability, conduction, localization and pharmacology [151–153]. The classical Kv auxiliary subunits, Kvβ1, 2 and 3, are soluble proteins that interact with the cytoplasmic domains of Kv1 channels. They confer dramatic effects on channel gating, in some cases inducing fast inactivation in otherwise non-inactivating channels [154, 155]. There are several additional classes of Kv β subunits that alter the properties of other Kv families, such as the KChIPs (potassium channel interacting proteins) which modulate Kv4 channel gating and trafficking and the KCNEs that have been shown to assemble with Kv1, Kv2, Kv7 and others [152]. The importance of modulation of Kv channel function by auxiliary subunits is evidenced by the fact that mutations in KCNE genes can confer susceptibility to cardiac arrhythmias even upon coassembly with wild-type alpha subunits [156].

Recently, AMIGO1 (amphotericin-induced gene and ORF 1) was identified as a novel β-subunit of Kv2 channels [71,108]. That work showed that AMIGO1 assembles with both Kv2 isoforms in neurons *in vivo* and *in vitro*, and when co-expressed in HEK293 cells, and induces a 10 mV hyperpolarizing shift in the voltage-dependence of Kv2.1. Furthermore, while trafficking and localization of Kv2.1 and Kv2.2 were unchanged by assembly with AMIGO1, both Kv2s increased the surface expression of AMIGO1 and redistributed it to large clusters which are characteristic of Kv2 channel localization [71].

The clustered pattern of Kv2s is due to a phosphorylation-regulated interaction with an endoplasmic reticulum (ER) protein, VAP [74, 81]. This interaction between Kv2s and VAP brings the ER into close apposition with the PM, forming an increasingly appreciated organelle, called the ER-PM junction [74, 79]. ER-PM junctions represent approximately 12% of the total neuronal surface [157] and regulate many cellular processes, including endo- and exocytosis [65, 79, 102], Ca^{2+} signaling and store refilling [79, 98, 121], and cell-cell interactions [60, 157]. The consequences of AMIGO localization to Kv2-induced ER-PM junctions for each of these functions are not well understood. However, it is hypothesized that AMIGOs mediate transcellular interactions via their cell adhesion molecule-like extracellular domains, which could underlie cell-cell communication events at ER-PM junctions [107].

In addition to their non-conducting functions mentioned above, Kv2 channels are important regulators of neuronal excitability. They underlie the majority of the delayed rectifier current in central neurons and control neuronal excitability under conditions of high frequency firing [85, 158, 159]. Perhaps more importantly, periods of prolonged neuronal activity lead to calcium-dependent dephosphorylation of Kv2 channels, which in turn lowers their threshold of activation [87, 89, 158]. In addition to its effects on voltage-dependent gating, dephosphorylation of Kv2 channels also disrupts their interaction with ER VAPs, leading to dispersal of channels from clusters. Therefore, neuronal calcium load influences both Kv2 function and localization, albeit by distinct phosphorylation sites [89]. The physiological repercussions of Kv2 cluster dispersal is currently being investigated, but a recent study showed that blocking Kv2 clustering was neuroprotective after ischemic injury and this effect was independent of channel activation threshold [93]. The effects of AMIGO assembly on Kv2 electrical function under pathophysiological conditions have not been studied. Furthermore, because AMIGO - Kv2.1 assembly is maintained during Kv2.1 declustering [108], there are likely downstream effects on cell-cell interactions due to changing AMIGO localization on the cell surface.

While the assembly of Kv2 channels and AMIGO1 is well-documented, nothing is known about the assembly of Kv2s with other members of the AMIGO family. The AMIGO family consists of 3 members (AMIGO1, AMIGO2 and AMIGO3), all of which are type-I single-pass transmembrane proteins [160]. All 3 AMIGOs have an extracellular N-terminus that contains 6 leucine rich repeat (LRR) domains and an immunoglobulin (Ig) domain, regions which allow them to act as homophilic and heterophilic cell adhesion molecules [160, 161]. AMIGO1 is almost exclusively expressed in the brain, while AMIGO2 and AMIGO3 are more widespread, but also enriched in the brain [160]. Functionally, AMIGOs have been implicated in regulating neuronal morphology, as well as cell growth and survival. For example, neurons grown on plates coated with the AMIGO1 extracellular domain showed an increased number of neurites, suggesting a role for AMIGO1 in early axon guidance [160, 162]. Conversely, following the axotomy of adult rat dorsal root ganglion neurons, AMIGO3 expression increases and participates in the acute inhibition of axonal regeneration [163]. Although AMIGO2 has yet to be implicated in axon regulation, adult AMIGO2 knockout mice show larger dendrites in starburst amacrine cells and retinal bipolar cells [164]. Taken together, these studies suggest a role for AMIGOs in neurite outgrowth in early development and neurite inhibition in adulthood. Interestingly, AMIGO2 has also been implicated in enhanced growth and survival in a variety of cells, including cerebellar granule neurons [165], vascular endothelial cells [166], gastric adenocarcinoma cells [167], and melanoma cells [168]. This increase in cell viability may be due to an interaction between AMIGO2 and PDK1, a kinase that activates Akt in cell survival pathways [169]. While the residues involved in AMIGO1 - Kv2.1 interaction are unknown, electrophysiology studies with chimeras between AMIGO1 and neuronal cell adhesion molecule (NCAM) suggest that the AMIGO1 transmembrane domain is required for interaction with Kv2.1 [108]. The transmembrane domain of the AMIGO family is 48% conserved, supporting the possibility that the other AMIGO family members could also act as β-subunits for the Kv2 family.

Given the lack of detailed information regarding the structural basis of the AMIGO1 - Kv2 interaction it is difficult to predict whether AMIGO2 and AMIGO3 will interact with and exert similar functional effects on the Kv2 channels. The aim of the present study was to investigate whether AMIGO2 and AMIGO3 also act as auxiliary β-subunits for Kv2.1 and Kv2.2 and to further characterize the effects of interaction on the AMIGOs and the Kv2 channels. The results of this work suggest that all three AMIGOs assemble with both Kv2 channels. The interaction of Kv2 channels with the AMIGOs appears to have isoform-specific effects on AMIGO trafficking but minimal effects on Kv2 trafficking and localization. Furthermore, while all three AMIGOs modulate Kv2 channel activation, the association of AMIGO2 also specifically alters channel inactivation and deactivation. These results indicate that the three AMIGOs interact with both Kv2.1 and Kv2.2 and alter both channel conducting functions and the composition of Kv2 surface clusters.

4.3 Materials and methods

4.3.1 DNA constructs

The original AMIGO1, AMIGO2 and AMIGO3 constructs were obtained from the DNASU plasmid repository (plasmid IDs HsCD00-29615, HsCD00-513136, and HsCD00-512989, respectively). Fluorescent protein fusion constructs were generated by PCR-based addition of restriction sites to the ends of each AMIGO family insert. Fluorescent protein vectors were cut with the same enzymes and each insert was ligated into the recipient vector, such that the fluorescent protein (GFP-N1 or Ruby2-N1) was fused to the C-terminus of AMIGO. The full length, codon optimized Kv2.2 coding sequence (accession number NM_054000) was synthesized by GeneWiz and inserted into a pEGFP-C1 expression vector (Clontech) via EcoRI and SalI restriction sites. GFP-Kv2.1 and Kv2.1-loopBAD have been described previously [72, 78]. hBirA was a gift from Alice Ting [170]. Pleckstrin homology domain (PH)-GFP was obtained from Colin Clay. For additional details, see Table 4.1.

Table 4.1: DNA constructs used in this chapter.

Construct Name	Insert Origin	Vector Backbone	Cloning Method	Restriction Enzymes
AMIGO1-GFP	AMIGO1 from DNASU plasmid repository (plasmid ID HsCD0029615)	pEGFP-N1 from Clontech	Restriction Digest	ApaI and XhoI
AMIGO1-Ruby2	AMIGO1-GFP (see above)	mRuby2-N1 from Michael Davidson (Addgene plasmid #54614)	Restriction Digest	ApaI and XhoI
AMIGO2-GFP	AMIGO2-Ruby2 (see below)	pEGFP-N1 from Clontech	Restriction Digest	NotI and AgeI
AMIGO2-Ruby2	AMIGO2 from DNASU plasmid repository (plasmid ID HsCD00513136)	mRuby2-N1 from Michael Davidson (Addgene plasmid #54614)	PCR and Restriction Digest	NheI and BamHI
AMIGO3-GFP	AMIGO3-Ruby2 (see below)	pEGFP-N1 from Clontech	Restriction Digest	NotI and AgeI
AMIGO3-Ruby2	AMIGO3 from DNASU plasmid repository (plasmid ID HsCD00512989)	mRuby2-N1 from Michael Davidson (Addgene plasmid #54614)	PCR and Restriction Digest	NheI and AgeI
GFP-Kv2.1	Gift from the late Rolf Joho	pEGFP-C1 from Clontech	Restriction Digest	EcoRI and XbaI
GFP-Kv2.2	GeneWiz codon-optimized fragment	pEGFP-C1 from Clontech	Restriction digest	EcoRI and SalI
Kv2.1-loopBAD	GFP-Kv2.1 (see above), GFP removed	pEGFP-C1 from Clontech	PCR and Restriction Digest	EcoRI and NheI to remove GFP, BglII sites to insert BAD into S1-S2 loop
BirA	Gift from Alice Ting			
PH-GFP	Gift from Colin Clay			

4.3.2 Cell culture and transfection

HEK293 cells were maintained in 10 cm dishes (CellTreat #229620) at 37°C under 5% CO_2 in DMEM (Corning #10-013-CV) supplemented with 10% FBS. For transfections, cells were trypsinized and electroporated (BioRad GenePulse Xcell) with either Kv2 alpha subunits (500 ng per dish), AMIGO subunits (300 ng per dish) or a combination of both. In some experiments a GFP-tagged pleckstrin-homology domain construct was used as a marker to facilitate measurements of fluorescence associated with the PM. For electrophysiology competition experiments, Kv2.1-loopBAD (500 ng) was transfected along with AMIGO2-GFP (300 ng) and either AMIGO1-Ruby2 (300 ng) or AMIGO3-Ruby2 (300 ng) simultaneously along with the biotin ligase hBirA. (1µg per dish). In these experiments, Kv2.1-LB was labeled with streptavidin-conjugated fluorophores to facilitate iden-

tification of transfected cells. Fluorescent labeling at this site does not alter Kv2.1 localization or function [77].

4.3.3 Microscopy

Spinning disk confocal microscopy was used for all imaging experiments where electrophysiology was not conducted. HEK293 cells were electroporated as described above and plated at a low density on glass-bottom dishes (MatTek #P35G-1.5-14-C) coated with Matrigel (BD Biosciences #354230) in a maintenance medium for 18-24 hours. Cells were briefly removed from incubation for medium exchange to HEK293 Imaging Saline (HIS), which contains the following: 146 mM NaCl, 4.7 mM KCl, 2.5 mM $CaCl_2$, 0.6 mM $MgSO_4$, 1.6 mM $NaHCO_3$, 0.15 mM NaH_2PO_4, 0.1 mM ascorbic acid, 8 mM glucose, and 20 mM HEPES, pH 7.4. After medium exchange, cells were immediately placed on the heated microscope stage and allowed to equilibrate for 10 minutes before imaging. Spinning disk confocal microscopy was performed on a Yokogawa-based CSUX1 system with an Olympus IX83 inverted stand, and coupled to an Andor laser launch containing 405, 488, 568, and 637 nm diode lasers, 100-150 mW each. Images were collected using an Andor iXon EMCCD camera (DU-897) and 100X Plan Apo, 1.4 NA objective. This system is equipped with the ZDC constant focus system and a Tokai Hit chamber and objective heater. Images were collected using MetaMorph software (version 7.8.13.0). Total Internal Fluorescence (TIRF) microscopy was used to identify transfected cells for electrophysiological experiments. TIRF microscopy was performed on a Nikon Eclipse Ti microscope equipped with 100 mW diode lasers at 405, 488, 561 and 640 nm. Cells were imaged using a Plan Apo TIRF 100x 1.49 NA objective and captured by an Andor iXon EMCCD DU-897 camera using appropriate band pass filters.

4.3.4 Electrophysiology

Transfected HEK293 cells were plated at low density on Matrigel-coated glass-bottom dishes. The next day, cells were bathed in extracellular solution containing (in mM): 140

NaCl, 5 KCl, 2 $CaCl_2$, 2 $MgCl_2$, 10 Glucose, 10 HEPES, pH=7.4, 340 mOsm/L. Transfected cells were identified by fluorescence using TIRF microscopy. Pipettes were pulled from thin-walled borosilicate glass and had tip resistances of 1-3 MΩ when filled with internal solution: 4 NaCl, 150 KCl, 1 $MgCl_2$, 0.5 EGTA, 10 HEPES, pH = 7.4, 310 mOsm/L. Whole-cell voltage-clamp experiments were performed at room temperature with an Axopatch200b amplifier and Digidata 1550A using Clampex 10.6 software (Axon Instruments). Data was acquired at 20 kHz and low pass filtered at 5 kHz. At least 80% series resistance prediction and compensation were used to mitigate voltage error and all recordings were leak subtracted using the P/-4 method. To investigate channel activation, cells were depolarized from a holding potential of -80 mV to between -80 and +70 mV for 250 ms in 10 mV increments (every other step is shown in figures for clarity). After each depolarizing pulse the membrane was stepped to -40 mV for 250 ms to probe channel deactivation before repolarizing to -80 mV. Tail currents at -40 mV were fit with a single exponential function and extrapolated backwards to obtain the instantaneous current at the end of the variable voltage pulse. These currents were normalized (I/I_{Max}) and fit with a Boltzmann function to estimate channel activation parameters. The time constants of single exponential fits of tail currents were used as a measure of channel deactivation. Channel inactivation was probed using a standard three-pulse protocol: a 100 ms pre-pulse to +40 mV was used to activate all channels followed by a 2500 ms pulse to potentials between -80 mV and +60 mV to elicit inactivation, followed by a 100 ms test pulse to +40 mV. The amount of channel inactivation was taken as the fraction of current in the test pulse compared to the pre-pulse for each variable voltage. Single Boltzmann functions were fit to the data between -80 mV and +10 mV to avoid fitting errors due to U-shaped inactivation. U-shaped inactivation is a characteristic of steady-state Kv2 inactivation curves thought to arise from either preferential closed state inactivation at intermediate voltages or voltage-clamp protocols that do not allow sufficient time for channels to reach steady-state [171, 172]. We also probed the kinetics of activation and

inactivation. The current traces associated with channel activation were fit with a single exponential function from the inflection point to the end of the trace. The current traces associated with channel inactivation were fit from 250 ms after the end of the pre-pulse to the end of the 2500 ms variable pulse. To estimate the voltage dependence of activation kinetics, we fit the τ-V plots with the exponential equation:

$$\tau = Ae^{-zFT/RT} + B \tag{4.1}$$

Where z is the charge associated with forward transitions underlying the activation kinetics [55].

4.3.5 Analysis and Statistics

Images were processed and analyzed using ImageJ (v1.52p). All images are single z-planes, unless otherwise noted.

Surface trafficking was measured from single z-planes at the center of each cell. A region of interest (ROI) was hand drawn around each cell and total fluorescence was measured for each channel. Seven pixels were then subtracted from the perimeter of the cell ROI (to account for the width of the membrane) to measure total fluorescence which was not on the PM. By subtracting the internal fluorescence from the total fluorescence, the fluorescence on the surface was determined. In the case of AMIGO3, where little fluorescence was on the surface, PH-GFP was co-expressed to determine the location of the plasma membrane. These measurements were performed in ImageJ.

Density in arbitrary fluorescence units per square micron (AU/μm^2) was calculated by dividing the sum of fluorescence in each ROI by the area of the ROI in microns. A surface trafficking index was determined by dividing the surface density by total density. This measure indicates the preference of a protein for surface expression (if greater than 1) or intracellular expression (if less than 1). The surface trafficking index was compared to a test mean of 1 using a one-sample t-test to determine whether the protein significantly

preferred to localize to the surface or intracellularly. To determine if co-expression with Kv2s significantly increased the AMIGO surface trafficking index, one-way ANOVAs with post-hoc Tukey tests were used.

To assess competition between 2 AMIGOs for Kv2.1 binding sites, cells were cotransfected with Kv2.1-loopBAD, AMIGO2-Ruby2 and either AMIGO1-GFP or AMIGO3-GFP. For measurements of relative abundance in Kv2.1 clusters, the summed fluorescence of each AMIGO was measured in each cluster, and total expression of each protein was determined using an ROI drawn around the perimeter of the cell. Percent cluster expression was measured by using the summed cluster fluorescence over the total cell fluorescence for each protein. Competition ratios were calculated by dividing the percent cluster expression of AMIGO1 or AMIGO3 over the percent cluster expression of AMIGO2. A ratio of 1 indicates equal representation in clusters, while a ratio greater than 1 indicates a preference for either AMIGO1 or AMIGO3. One sample t-tests were used to compare ratio means to a test mean of 1.

Electrophysiological data were analyzed using MatLab and plotted using Origin2018b software. Data shown are mean and standard error. Data points with no error bars have standard error smaller than the symbol size. One-way ANOVA was used to test for significance between multiple groups, alpha = 0.05. Post-hoc Tukey's tests were performed to determine significance between each group, alpha = 0.05. Sample sizes are included in figure legends and represent data from at least 2 biological replicates.

4.4 Results

4.4.1 Kv2s increase AMIGO surface expression

While previous work demonstrated that AMIGO1 is a β-subunit for Kv2s [71, 108], it is unknown whether other members of the AMIGO family also act as β-subunits. The relative localization of the Kv2s and each AMIGO could yield insight into this question. We first expressed each fluorescently-tagged AMIGO subunit alone in HEK293 cells. The left

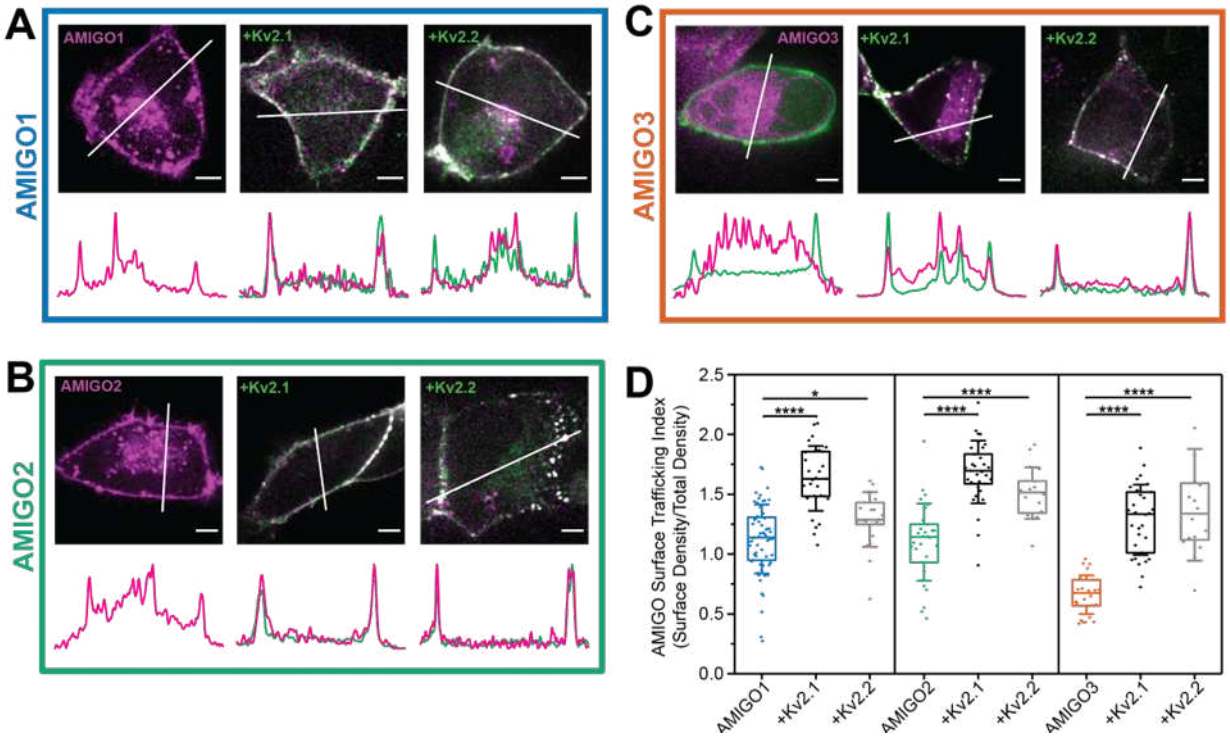

Figure 4.1: Kv2s colocalize with AMIGOs and increase their surface trafficking. Representative images of **A)** AMIGO1, **B)** AMIGO2, or **C)** AMIGO3 alone (left images), with Kv2.1 (middle images) and with Kv2.2 (right images). Line scans through the center of the cells are indicated by the white lines on the images and plotted below. Images are single z-planes at the middle of the cell. Scale bars = 5 µm. **D)** AMIGO surface trafficking index for each condition. A ratio >1 indicates a preference for surface trafficking. AMIGO1 surface trafficking was significantly increased with co-expression of Kv2.1 (median=1.63, N=29, $p<0.0005$) and Kv2.2 (median=1.29, N =21, $p<0.05$) compared to AMIGO1 alone (median=1.14, N=65 cells, F=34.37, $p<0.0005$). AMIGO2 surface trafficking was significantly increased with co-expression of Kv2.1 (median=1.70, N=33 cells, $p<0.0005$) and Kv2.2 (median=1.51, N=18 cells, $p<0.0005$) compared to AMIGO2 alone (median=1.14, N=30 cells, F=35.99, $p<0.0005$). AMIGO3 surface trafficking was significantly increased with co-expression of Kv2.1 (median=1.33, N=30 cells, $p<0.0005$) and Kv2.2 (median=1.34, N=16 cells, $p<0.005$) compared to AMIGO3 alone (median=0.67, N=27 cells, F=35.99, $p<0.0005$), which was largely internal. * = $p<0.05$, ****= $p<0.0005$.

panels in Figure 4.1A, B and C show optical slices of HEK293 cells expressing AMIGO1, AMIGO2 or AMIGO3 in the absence of Kv2 subunits, respectively. When expressed alone, AMIGO1 and AMIGO2 largely localized to the PM, as indicated by the peaks of fluorescence in the line scans that are associated with each cell's perimeter. However, AMIGO1 and AMIGO2 were also found in intracellular vesicles, as seen by the punctate pattern of fluorescence within the cells in Figure 4.1A and B and their corresponding line scans. In contrast, AMIGO3 was almost exclusively localized to intracellular membranes with very

minimal fluorescence associated with the PM, as seen in the left panel of Figure 4.1C. In these cells, a PH-GFP construct was co-expressed with AMIGO3 to act as a membrane marker. It is clear from the linescan in the left panel of Figure 4.1C that there was no AMIGO3 fluorescence corresponding to the PH-GFP peaks at the perimeter of the cell.

The remaining panels in Figure 4.1A, B and C show representative images of HEK293 cells co-expressing each AMIGO isoform with each Kv2 alpha subunit. Co-expression with the Kv2s dramatically reduced the intracellular, vesicular fluorescence of AMIGO1 and AMIGO2 and appeared to increase their localization to the PM as seen in the dual-color linescans in Figure 4.1A and B. Likewise, co-expression of each Kv2 subunit with AMIGO3 also increased AMIGO3's localization to the PM, as evidenced by the correspondence of AMIGO3 and Kv2 fluorescence peaks in the dual-color linescans in Figure 4.1C.

Figure 4.1D shows a summary of the changes in AMIGO surface expression conferred by co-expression with Kv2 subunits. The data are given as a trafficking index, which is a ratio of AMIGO fluorescence associated with the PM to total AMIGO fluorescence on a cell-by-cell basis. For this measure, a value >1 indicates preferential targeting to the PM and a value <1 indicates preferential targeting to intracellular membranes. Consistent with the images from panels A, B and C, AMIGO1 and AMIGO2 had trafficking indices slightly higher than 1 when expressed alone, indicating a small preference for PM localization. In contrast, AMIGO3 had a trafficking index of 0.67 when expressed alone, in accordance with its preference for intracellular membranes. Co-expression of each AMIGO isoform with either Kv2.1 or Kv2.2 significantly increased the AMIGO trafficking indices, as indicated by the asterisks in Figure 4.1D. This data suggests that all three AMIGO isoforms interact with both Kv2 subunits, and that assembly with Kv2 channels alters AMIGO expression on the PM.

4.4.2 The three AMIGOs enhance the voltage-sensitivity of Kv2 activation

After finding that Kv2s alter AMIGO surface expression we decided to characterize the effects of each AMIGO on Kv2 channel electrical function. We voltage-clamped trans-

fected HEK293 cells and recorded whole-cell currents in response to 250 ms depolarizing steps between -80 mV and +70 mV from a holding potential of -80 mV. Currents carried by Kv2 subunits alone or Kv2 subunits plus each AMIGO were qualitatively similar and resembled classic delayed rectifier currents as shown in Figure 4.2A and B. Differences in current magnitude in this figure, and throughout, are due to variable expression of

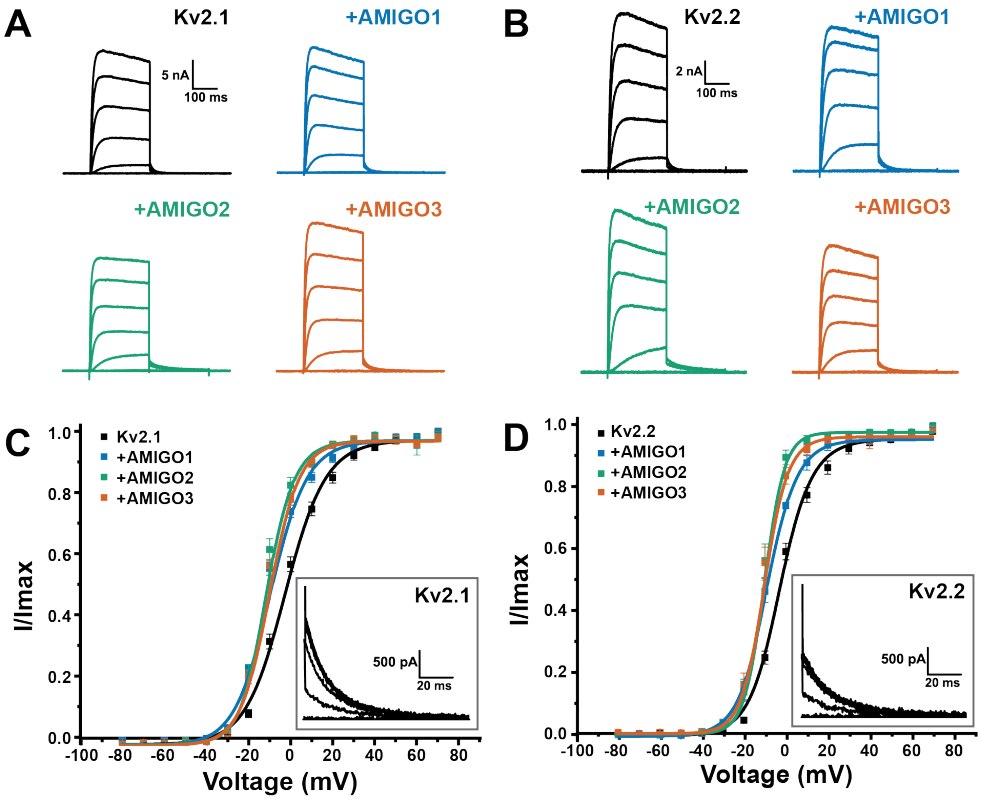

Figure 4.2: AMIGOs shift Kv2 activation. **A)** Representative activation traces from HEK293 cells expressing Kv2.1 alone (black) Kv2.1+AMIGO1 (blue), Kv2.1 + AMIGO2 (green), or Kv2.1 + AMIGO3 (orange). Every other depolarizing step between -70 and +70 mV is shown for clarity. Scale bar applies to all traces. **B)** Representative activation traces from HEK293 cells expressing Kv2.2 alone or with each of the three AMIGOs. Colors are the same as in A. Scale bar applies to all traces. **C)** Voltage dependence of Kv2.1 activation measured from normalized tail current magnitudes (inset). Coexpression with each of the three AMIGOs shifted the Kv2.1 activation midpoint to more hyperpolarized potentials (One-way ANOVA, $F=31.7$, $p<0.0005$). The midpoint of Kv2.1 alone was -2.4±1.1 mV (N=9 cells). AMIGO1 shifted the Kv2.1 activation midpoint to -8.5±1.2 mV (N=7 cells, $p<0.0005$), AMIGO2 shifted it to -10.3±1.2 mV (N=8 cells, $p<0.0005$), and AMIGO3 shifted it to -9.1±1.2 mV (N=9 cells, $p<0.0005$). **D)** Voltage dependence of Kv2.2 activation measured from normalized tail current magnitudes (inset). Coexpression with each of the three AMIGOs also shifted the Kv2.2 activation midpoint to more hyperpolarized potentials (One-way ANOVA, $F=17.0$, $p<0.0005$). The activation midpoint of Kv2.2 alone was -2.2±0.9 mV (N=12 cells). AMIGO1 shifted the Kv2.2 activation midpoint to -7.8±1.4 mV (N=9 cells, $p<0.0005$), AMIGO2 shifted it to -9.2±1.4 mV (N=8 cells, $p<0.0005$), and AMIGO3 shifted it to -9.0±1.4 mV (N=9 cells, $p<0.0005$).

the Kv channels in individual HEK293 cells as opposed to population level differences between conditions. Our voltage-clamp protocol to assay channel activation included a tail current step to -40 mV to facilitate the measurement of open probability as a function of prepulse voltage. Example tail currents from Kv2.1 and Kv2.2 alone are shown in the insets in Figure 4.2C and D. The tail currents were fit with an exponential function which was extrapolated back to the time corresponding to the end of the depolarizing pulse to obtain the maximal tail current magnitudes at each voltage. Plots of normalized tail current magnitudes for Kv2.1 and Kv2.2 with and without each AMIGO are shown in Figure 4.2C and D, respectively. We fit each data set with a single Boltzmann function in order to estimate the midpoint of the activation curves. The midpoint of Kv2.1 activation (-2.4 ± 1.1 mV) was shifted to more hyperpolarized potentials by AMIGO1 (-8.5 ± 1.2 mV, $p<0.0005$), AMIGO2 (-10.3 ± 1.2, $p<0.0005$) and AMIGO3 (-9.2 ± 1.2 mV, $p<0.0005$), consistent with the effect of AMIGO1 on Kv2.1 activation midpoint shown previously [108]. We also analyzed voltage dependent activation of Kv2.2, the second Kv2 isoform whose interactions with any AMIGO have not yet been characterized. The midpoint of Kv2.2 activation alone was -2.2 ± 0.9 mV. As we saw for Kv2.1, AMIGO1 (-7.8 ± 1.4 mV, $p<0.0005$), AMIGO2 (-9.2 ± 1.4 mV, $p<0.0005$), and AMIGO3 (-9.0 ± 1.4 mV, $p<0.0005$) each shifted Kv2.2 activation to more hyperpolarized potentials. Together these results suggest that each of the three AMIGO isoforms assembles with and modulates both Kv2.1 and Kv2.2 activation gating.

4.4.3 The AMIGOs alter Kv2 activation kinetics

To explore the mechanisms underlying the observed effects of AMIGOs on Kv2 voltage dependent activation we analyzed the time dependence of the each current trace from Figure 4.2. A comparison of normalized current traces during a step to +30 mV is shown in Figure 4.3A and reveals differences between Kv2.1 activation kinetics when expressed alone or with each AMIGO isoform. Each of the three AMIGOs sped up activation of Kv2.1 such that maximum current was reached earlier. We fit the late portion of the Kv2.1

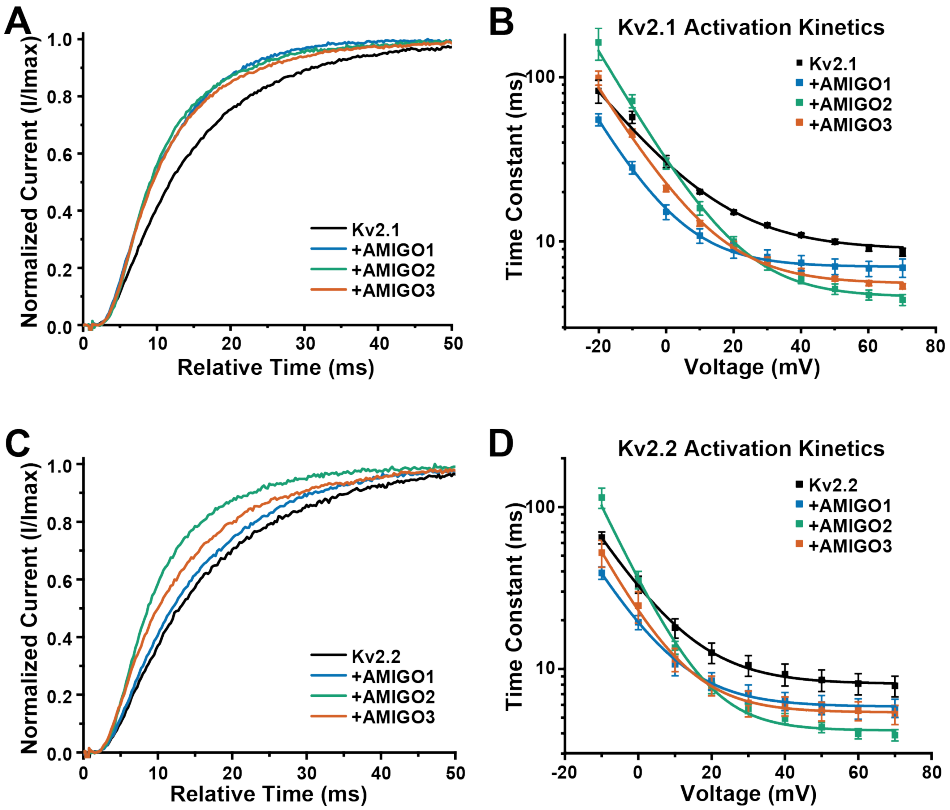

Figure 4.3: AMIGOs speed Kv2 activation. **A)** Comparison of Kv2.1 current time courses upon a depolarizing step to +30 mV. Currents were normalized to the maximum current during the step. **B)** Voltage dependence of Kv2.1 activation kinetics obtained from single exponential fits to the late phase of activation. Curves are exponential fits to the data points. At +30 mV, Kv2.1 τ=11.9±0.7 ms (N=9); one way ANOVA, F=12.5, p<0.0005 with post hoc pairwise Tukey Tests: +AMIGO1=8.0±0.9 ms, N=7, p<0.005; +AMIGO2= 7.2±0.5 ms, N=8, p<0.0005; +AMIGO3=7.7±0.3 ms, N=9, p<0.0005. **C)** Comparison of Kv2.2 current time courses at +30 mV with and without each AMIGO. Currents were normalized to the maximum current during the step. **D)** Voltage dependence of Kv2.2 activation kinetics obtained from single exponential fits to the late phase of current activation. Curves are exponential fits to the data points. At +30 mV Kv2.2 τ=10.5±1.5 ms (N=12); one way ANOVA, F=3.7, p<0.05 with post hoc pairwise Tukey tests: +AMIGO1=7.1±0.9 ms, N=9, p=0.2; +AMIGO2=5.7±0.4 ms, N=8, p<0.05; +AMIGO3=6.2±1.1 ms, N=9, p=0.06.

activating currents with a single exponential function and plotted the resulting time constants as a function of voltage as shown in Figure 4.3B. The time constants of Kv2.1 late activation were faster when co-expressed with each of the AMIGOs at most voltages. For example, at +30 mV, the time constant of Kv2.1 activation was 11.9±0.7 ms. Co-expression with AMIGO1 increased this rate to 8.0±0.9 ms (p<0.005), AMIGO2 increased it to 7.2±0.5 ms (p<0.0005) and AMIGO3 increased it to 7.7±0.3 ms (p<0.0005). Results from the same experiment with Kv2.2 are shown in Figure 4.3C and D. The normalized current traces

in Figure 4.3C show that each of the three AMIGOs also tended to increase the rate of Kv2.2 activation. However, the extent of the increase on Kv2.2 kinetics was more dramatic for AMIGO2 than the other two isoforms. Indeed, Kv2.2 activation at +30 mV proceeded with a time constant of 10.5±1.5 ms, and this rate was sped up significantly by AMIGO2 (5.7±0.4 ms, $p<0.05$), but not AMIGO1 (7.1±0.9 ms, $p=0.2$) or AMIGO3 (6.2±1.1 ms, $p=0.06$).

The AMIGOs sped up the activation time course of both Kv2.1 and Kv2.2 channels, as seen in Figure 4.3. However, since the speeding effects were observed at voltages where voltage dependent gating is near maximal, this observation cannot explain the shifts in voltage dependent activation observed in Figure 4.2. We noticed that the voltage-dependence of Kv2 activation kinetics appeared to be increased by each of the AMIGOs, as evidenced by the shape of the data in Figure 4.3B and D. Therefore, following the method of Scholle et al. [55], we fit the plots in Figure 4.3B and D with an exponential function (Equation (4.1)) and compared the equivalent charge (z) contributing to activation kinetics between conditions. By eye, the fits in Figure 4.3B and D appeared steeper when Kv2.1 or Kv2.2 was co-expressed with each AMIGO. This was especially evident when either Kv2 was expressed with AMIGO2, which slowed activation kinetics below 0 mV but sped activation kinetics above 0 mV, causing the fits to intersect (Figure 4.3B and D, green vs black curves). Indeed, the equivalent charge associated with Kv2.2 activation kinetics ($z=1.55 \pm 0.18$) was increased significantly by AMIGO2 ($z=3.23 \pm 0.71$, $p<0.05$), suggesting that AMIGO2 did increase the voltage-dependence of Kv2.2 activation kinetics. Although all three AMIGOs tended to increase this voltage-dependent parameter for both Kv2.1 and Kv2.2, most of the comparisons did not reach the level of statistical significance. Table 4.2 includes a summary of the values reported for each parameter we analyzed in this work and is given at the end of this results section.

4.4.4 AMIGO2 specifically reduces Kv2 inactivation

Previous studies on AMIGO1 and Kv2.1 have not addressed the modulatory effects of AMIGO on Kv2 inactivation. We assayed voltage-dependent inactivation using a three-pulse protocol. Pulse 1 and 3 were 100 ms steps to +40 mV, and pulse 2 contained 2.5 s steps to variable voltages to elicit channel inactivation. Currents from cells transfected with Kv2.1 with and without each AMIGO isoform are shown in Figure 4.4A. In each case, the currents showed slow inactivation over the 2.5 s step as expected for currents carried by Kv2.1. Representative currents from the analogous experiment with Kv2.2 are shown in Figure 4.4B. In order to estimate parameters of voltage-dependent inactivation we measured the fraction of current remaining after 2.5 s at each variable voltage by taking the ratio of the current in pulse 3 over the current in pulse 1. We plotted the fraction of current remaining against the pulse 2 voltage for Kv2.1 plus/minus each AMIGO in Figure 4.4C and for Kv2.2 plus/minus each AMIGO in Figure 4.4D. Both Kv2.1 and Kv2.2 alone showed U-shaped inactivation that is characteristic of Kv2.1 channels (Figure 4.4C and D, black symbols) [171]. To minimize our analysis of the U-shaped inactivation we restricted Boltzmann fits of the inactivation plots to cover voltages between -80 and +10 mV (Figure 4.4C and D, smooth curves). The midpoints of Kv2 channel inactivation did not change by more than 5 mV with the addition of any single AMIGO isoform. While some of the small differences between inactivation midpoints reached statistical significance, others did not. Furthermore, we found that the midpoint of inactivation was sensitive to the voltage range used for the fit due to the U-shape of the data. Therefore, we did not deem changes in inactivation midpoint meaningful in this figure, and do not mention them further. Interested readers will find the values from the fits in Table 2.

Although the shifts conferred by the AMIGOs on Kv2 inactivation midpoint were difficult to interpret, we were immediately struck by the absolute reduction in inactivation conferred by AMIGO2, as is evident in the plots in Figure 4.4C and D (green symbols). In order to quantify this change in inactivation we compared the fraction of current re-

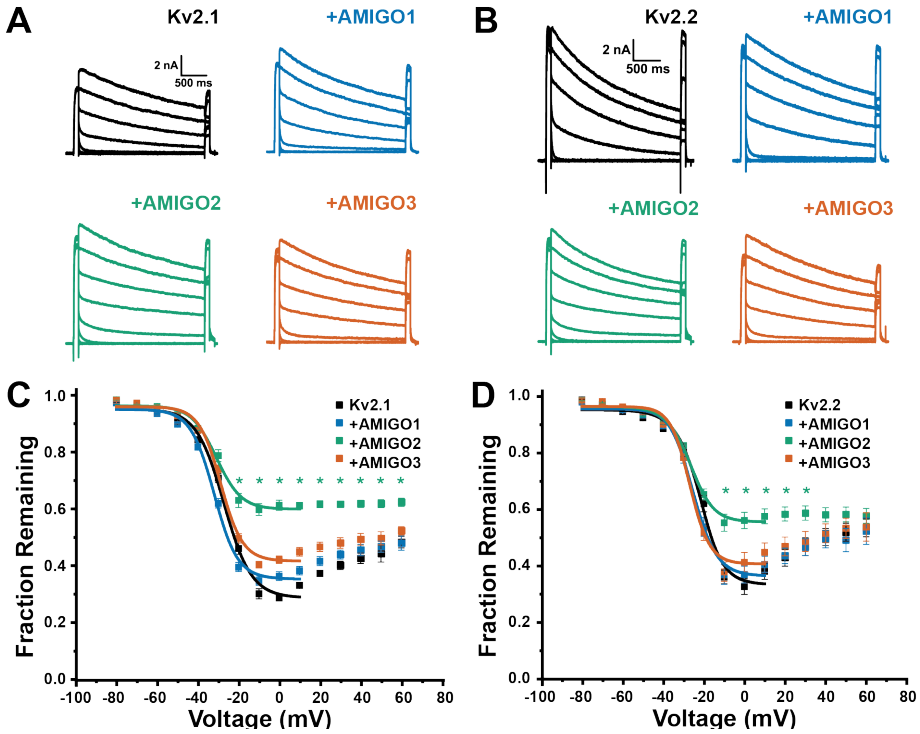

Figure 4.4: AMIGO2 reduces Kv2 inactivation. **A)** Representative currents illustrating the three-pulse protocol used to measure voltage dependent inactivation from Kv2.1. Colors are the same as in A. Pre- and test pulses were to +40 mV. Every other sweep between -80 and +60 mV is shown for clarity. Scale bar applies to all traces. **B)** Representative currents illustrating voltage dependent inactivation of Kv2.2 with and without each AMIGO. The protocol was the same as in E. Every other sweep between -80 and +60 mV is shown for clarity. Scale bar applies to all traces. **C)** Voltage dependence of Kv2.1 inactivation determined from the fraction of the pre-pulse current remaining in the test pulse after 2.5 s of inactivation. AMIGO2 reduced inactivation at voltages between -20 and + 60 mV as indicated by the asterisks ($p<0.05$). For example, at +40 mV: Kv2.1=0.43±0.02 (N=10), +AMIGO1=0.46±0.02 (N=9), +AMIGO2=0.62±0.01 (N=8), +AMIGO3=0.49±0.02 (N=9); one way ANOVA, F=20.9, $p<0.0005$ with post hoc pairwise Tukey tests: p=0.7, $p<0.0005$, p=0.05, respectively for each AMIGO as compared to Kv2.1 alone. **D)** Voltage dependence of Kv2.2 inactivation with and without each AMIGO. AMIGO2 reduced inactivation between -10 mV and +30 mV, as indicated by the asterisks on the graph ($p<0.05$). At +30 mV, the inactivated fractions were: Kv2.2=0.47±0.03 (N=10), +AMIGO1=0.47±0.03 (N=8), +AMIGO2=0.59±0.03 (N=8), +AMIGO3=0.49±0.04 (N=9); one way ANOVA, F=3.2, $p<0.05$ with pairwise post hoc Tukey tests: p=.99, $p<0.05$, p=0.97 as compared to Kv2.2 alone, respectively.

maining in the test pulse for each Kv2 isoform alone, or with each AMIGO at individual voltages. For example, after a 2.5 s step to +40 mV, Kv2.1 had 0.43 ± 0.02 of its maximal current remaining (Figure 4.4C, black symbols). Assembly with either AMIGO1 (0.46 ± 0.02, p=0.7) or AMIGO3 (0.49 ± 0.02, p=0.05) did not change the available fraction of Kv2.1 current. However, assembly of Kv2.1 with AMIGO2 increased the available frac-

tion to 0.62 ± 0.01 (Figure 4.4C, green symbols, p<0.0005). In fact, AMIGO2 increased the available fraction of Kv2.1 channels at all voltages between -20 mV and +60 mV. AMIGO2 also conferred reduced inactivation to Kv2.2 (Figure 4.4D). Expressed alone, 0.47 ± 0.03 of Kv2.2 remained after a 2.5 s step to +30 mV (Figure 4.4D, black symbols). When co-expressed with AMIGO2, the fraction of Kv2.2 current remaining was increased to 0.59 ± 0.03 (Figure 4.4D, green symbols, p<0.05). AMIGO2 reduced Kv2.2 inactivation at voltages between -10 and +30 mV. The available fraction of Kv2.2 current after the +30 mV step did not change when co-expressed with AMIGO1 (0.47 ± 0.03, p=0.99) or AMIGO3 (0.49 ± 0.04, p=0.97), and so the reduction of inactivation was specific to AMIGO2.

4.4.5 AMIGO2 slows inactivation and deactivation

To further explore the mechanism underlying AMIGO2's effect on inactivation, we compared the kinetics of Kv2 channel inactivation in the presence and absence of each AMIGO isoform. Normalized traces of Kv2.1 and Kv2.2 current decay over 2.5 s at +40 mV are shown on the left in Figure 4.5A and B, respectively. From these normalized current traces it is clear that AMIGO2 slowed the decay of both Kv2 channels' inactivation kinetics (green traces). We quantified the time course of inactivation at each voltage by fitting a single exponential function to the decay of the Kv2 current over 2.5 s at various voltages. A summary of the time constants of inactivation for Kv2.1 and Kv2.2 are shown on the right side of Figure 4.5A and B, respectively. These plots reinforce the conclusion that AMIGO2 slowed inactivation for both Kv2.1 and Kv2.2. Indeed, at +40 mV, Kv2.1 alone inactivated with a time constant of 3.2±0.1 s. AMIGO2 (5.7±0.28 s, p<0.0005) but not AMIGO1 (3.2±0.2 s, p=0.99) or AMIGO3 (3.9±0.2 s, p=0.11) significantly increased this parameter. The results for Kv2.2 were similar, although at extremely depolarized potentials the differences disappeared. At +30 mV, Kv2.2 had an inactivation time constant of 3.6±0.3 s. AMIGO2 significantly increased Kv2.2's inactivation time constant to 5.4±0.4 s (p<0.005) while AMIGO1 (3.6±0.3 s, p=0.99) and AMIGO3 (3.9±0.4 s, p=0.86) did not.

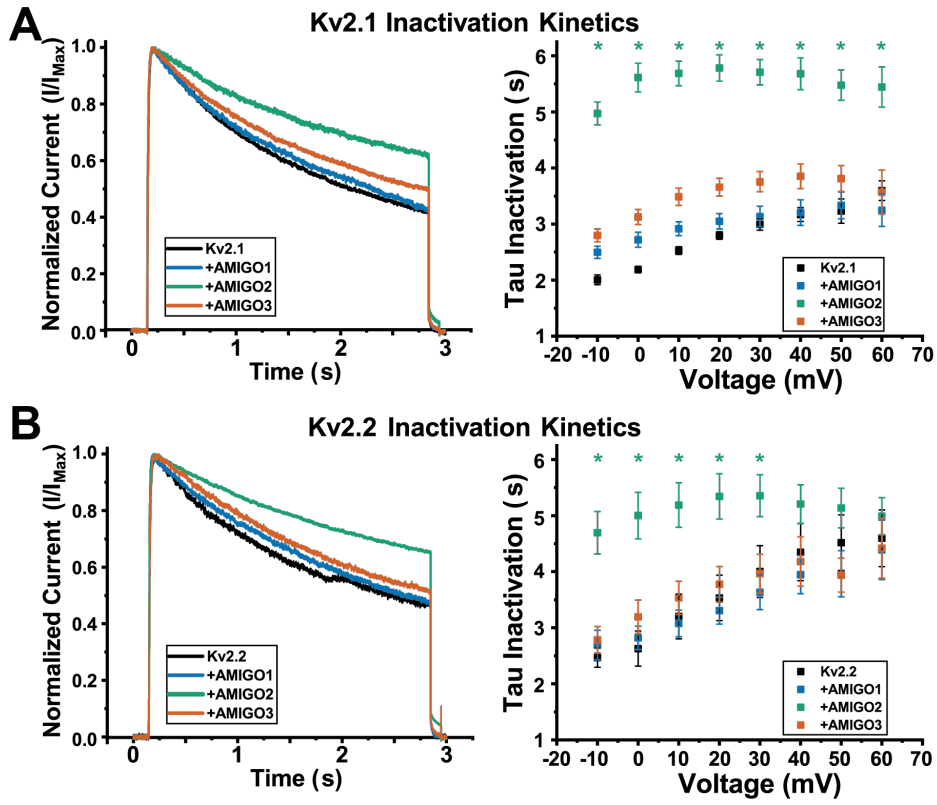

Figure 4.5: AMIGO2 slows Kv2 inactivation. **A)** *Left* - Normalized Kv2.1 currents during a 2.5 s step to +40 mV with and without AMIGO co-expression. Traces were normalized to their max values. *Right* - Summary of Kv2.1 inactivation kinetics with and without three AMIGOs. Time constants are from single exponential fits to 2.5 s current decay traces. At +40 mV, Kv2.1 τ=3.2±0.1 s (N=10); one way ANOVA, F=28.6, p<0.0005 with post hoc Tukey tests: +AMIGO1=3.2±0.2 s, N=9, p=0.99; +AMIGO2=5.7±0.28 s, N=8, p<0.0005; +AMIGO3=3.9±0.2 s, N=9, p=0.11. AMIGO2 slowed Kv2.1 inactivation at all voltages between -10 mV and +60 mV as indicated by the asterisks on the graph (p<0.05). **B)** *Left* - Comparison of normalized Kv2.2 currents during a 2.5 s step to +40 mV with and without AMIGO co-expression. Traces were normalized to their maximum values. *Right* - Voltage dependence of Kv2.2 inactivation kinetics obtained from single exponential fits to 2.5 s current decay in the presence and absence of each AMIGO. At +30 mV Kv2.2 τ=3.6±0.3 s (N=10); one way ANOVA, F=6.03, p<0.005 with post hoc Tukey tests: +AMIGO1=3.6±0.3 s, N=8, p=0.99; +AMIGO2=5.4±0.4 s, N=8, p<0.005; +AMIGO3=3.9±0.4 s, N=9, p=0.86. AMIGO2 slowed Kv2.2 inactivation at voltages between -10 mV and +30 mV as indicated by the asterisks (p<0.05).

Channel function can also be altered via changes in channel closing times. Therefore, we analyzed the kinetics of the tail currents from the recordings in Figure 4.2 to discern effects of AMIGOs on channel closing. Normalized tail currents at -40 mV are shown on the left in Figure 4.6A for Kv2.1 with and without each AMIGO isoform. AMIGO2 slowed the decay of Kv2.1 tail current, as seen in the green trace. We fit the tail currents and compared the decay time constants (Figure 4.6A, right) and found that Kv2.1 alone

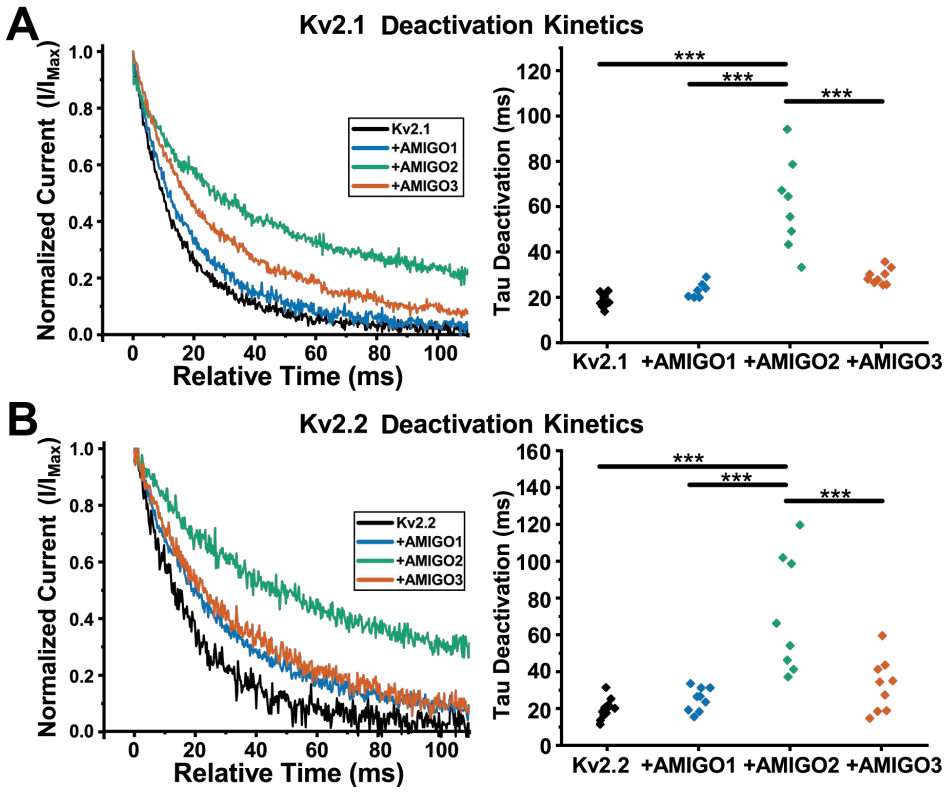

Figure 4.6: AMIGO2 slows Kv2 deactivation. **A)** *Left* - Representative traces of Kv2.1 deactivation time course at -40 mV after a depolarizing step to +30 mV in the presence and absence of each AMIGO. Currents were normalized to the current at the beginning of the -40 mV step. *Right* - Summary of deactivation kinetics at -40 mV under the four conditions. Kv2.1 deactivation at -40 mV (18.6±1.0 ms, N=9 cells) was slowed by co-expression of AMIGO2 (60.7±7.0 ms, p<0.0005, N=8 cells) but not AMIGO1 (23.2±1.3 ms, p=0.8, N=7 cells) or AMIGO3 (29.2±1.2 ms, p=0.14, N=9 cells) (One-way ANOVA, F=28.8, p<0.0005). **B)** *Left* - Representative traces of Kv2.2 deactivation time course at -40 mV after a depolarizing step to +30 mV in the presence and absence of each AMIGO. Currents were normalized as in A. *Right* - Summary of Kv2.2 deactivation kinetics at -40 mV under the four conditions. Kv2.2 deactivation at -40 mV (19.5±1.5 ms, N=12 cells) was slowed by co-expression of AMIGO2 (70.7±11.2 ms, p<0.0005, N=8 cells) but not AMIGO1 (25.1±2.1 ms, p=0.99, N=9 cells) or AMIGO3 (32.6±4.8 ms, p=0.49, N=9 cells) (One-way ANOVA, F=17, p<0.0005). *** indicates p<0.0005.

had a time constant of 18.6±1.0 ms. AMIGO2 slowed this time constant significantly to 60.7±7.0 ms (p<0.0005). Although AMIGO1 (23.2±1.3 ms, p=0.8) and AMIGO3 (29.2±1.2 ms, p=0.14) tended to increase the time constant of tail current decay, they did not confer statistically difference values compared to Kv2.1 alone. Comparable results were seen when we analyzed Kv2.2 tail currents in the presence and absence of each AMIGO. Normalized traces illustrating Kv2.2 deactivation are shown on the left of Figure 4.6B and the summary of deactivating time constants is shown to the right. Kv2.2 tail currents

had an average time constant of 19.5±1.5 ms at -40 mV. AMIGO2 slowed this parameter to 70.7±11.2 ms ($p<0.0005$), while AMIGO1 (25.1±2.1 ms, $p=0.99$) and AMIGO3 (32.6±4.8 ms, $p=0.49$) did not.

4.4.6 Multiple AMIGOs can bind to a single Kv2.1 channel

The stoichiometry of the AMIGO/Kv2 complex is not known. While AMIGO1 was suggested to interact with Kv2.1 via their transmembrane domains, the residues involved in this interaction are also unknown [160]. Electrophysiological analysis of Kv2 channel behavior in the presence of multiple AMIGO isoforms simultaneously could help address the question of stoichiometry. Therefore, we undertook experiments of Kv2.1 channels expressed alone, with only AMIGO2, or with a combination of AMIGO2/AMIGO1, or AMIGO2/AMIGO3. We expected that if only one AMIGO binds to each Kv2 channel at a time, the inactivation and deactivation kinetic phenotypes would be in between those measured in the presence of each subunit individually.

We used the same voltage clamp protocols as described above to investigate Kv2.1 activation and inactivation. Figure 4.7A shows a comparison of the Kv2.1 activation curve when expressed alone (black), co-expressed with AMIGO2 only (green), co-expressed with both AMIGO2 + AMIGO1 (blue) or co-expressed with both AMIGO2 + AMIGO3 (orange). As before, co-expression with AMIGO2 shifted the Kv2.1 midpoint of activation in the hyperpolarizing direction (Kv2.1 alone = 2.4±1.3 mV, +AMIGO2 = -11.2±0.7 mV, $p<0.05$). Interestingly, simultaneous co-expression with two AMIGOs did not confer an additional effect on the midpoint of activation. The midpoint of Kv2.1 activation in the presence of AMIGO2 + AMIGO1 together was -13.0±2.6 mV, which was not significantly different from the midpoint of Kv2.1 in the presence of AMIGO2 only ($p=.94$). The same was true for Kv2.1 expressed with both AMIGO2 + AMIGO3 simultaneously (-11.6±2.2 mV, $p=0.99$ compared to +AMIGO2 only).

Kv2.1 inactivation under each condition is shown in Figure 4.7B. As before, AMIGO2 conferred a reduction in inactivation as evidenced by a larger fraction of current remain-

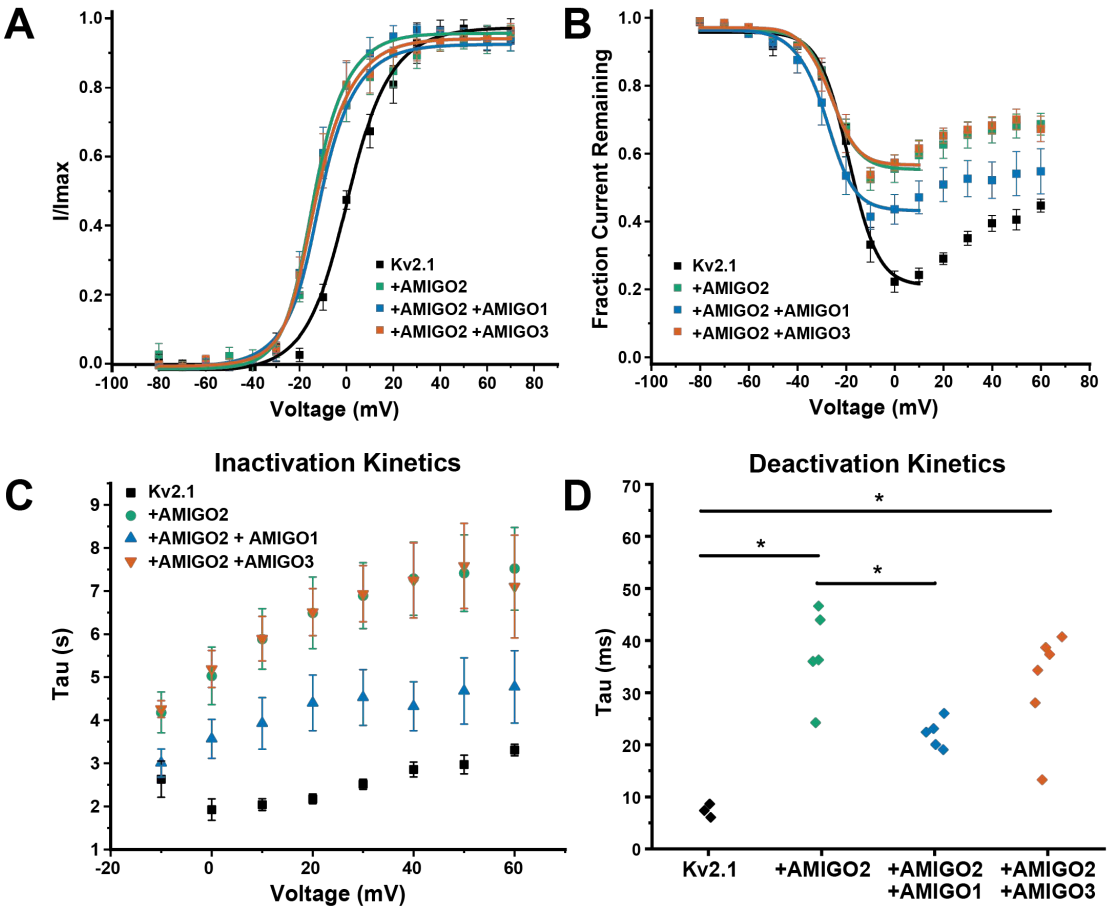

Figure 4.7: AMIGO1 competes with AMIGO2 electrical effects. **A)** Voltage dependence of Kv2.1 activation alone (black), +AMIGO2 (green), +AMIGO2/+AMIGO1 (blue) or +AMIGO2/+AMIGO3 (orange). AMIGO2 shifted the Kv2.1 midpoint from 2.4±1.3 mV (N=3) to -11.2±0.7 mV (N=5, p=0.007). Co-expression with two AMIGOs did not confer additional shifts over AMIGO2 alone (+AMIGO2/+AMIGO1=-13.0±2.6 mV, N=6, p=0.002; +AMIGO2/+AMIGO3=-11.6±2.2 mV, N=6, p=0.004). **B)** Voltage dependence of Kv2.1 inactivation under the four conditions. AMIGO2 alone and AMIGO2+AMIGO3 reduced inactivation, while AMIGO2+AMIGO1 did not. The inactivated fractions at +40 mV were: Kv2.1=0.40±0.02 (N=6), +AMIGO2=0.67±0.04 (N=5), +AMIGO2/+AMIGO3=0.68±0.02 (N=6), +AMIGO2/+AMIGO1=0.52±0.05 (N=5); One way ANOVA, F=13.0, p<0.0005 with pairwise Tukey tests against Kv2.1 alone: p<0.0005, p<0.0005 and p=0.1, respectively. **C)** Voltage dependence of inactivation kinetics. At +40 mV, Kv2.1 inactivation had a time constant of τ=2.8±0.2 s (N=6), which was slowed by AMIGO2 to 7.3±0.9 s (N=5, p<0.0005). +AMIGO2/+AMIGO3 did not reverse this effect (τ=7.2±0.9 s, N=6, p<0.0005) while +AMIGO2/+AMIGO1 did (τ=4.3±0.6 s, N=5, p=0.35 compared to Kv2.1 alone)(One way ANOVA F=12.0, p<0.0005). **D)** Comparison of tail current decay kinetics at -40 mV under the four conditions. Compared with Kv2.1 alone (7.4±0.74 ms, N=3 cells), AMIGO2 slowed deactivation (37.4±3.9ms, p<0.005, N=5 cells) as did +AMIGO2/+AMIGO3 (32.1±4.2 ms, p<0.05 compared to Kv2.1, N=6 cells). However, co-expression with +AMIGO2/+AMIGO1 abolished this difference (22.1±1.2 ms, p<0.05 compared to +AMIGO2, p=0.07 compared to Kv2.1, N=6 cells).

ing at the end of the inactivation protocol (Figure 4.7B, green symbols). Indeed, after a 2.5 s step to +40 mV, co-expression with AMIGO2 increased the fraction of remaining current from 0.40±0.02 for Kv2.1 alone to 0.67±0.04 ($p<0.0005$). Interestingly, co-expression with both AMIGO2 and AMIGO3 simultaneously resulted in an inactivated fraction that was not different from that of AMIGO2 alone (0.68±0.02, $p=0.99$ compared to AMIGO2 only). In contrast, co-expression of AMIGO2 and AMIGO1 simultaneously resulted in an inactivated fraction of 0.52±0.05, a value that just escaped significance from that obtained in the presence of AMIGO2 only ($p=0.06$) and was not different from the inactivated fraction of Kv2.1 alone ($p=0.09$).

We once again we fit the decay of Kv2.1 current during the inactivation protocol and compared the time constants at each voltage. Figure 4.7C shows a summary of the time constants of inactivation as a function of voltage for each condition. At +40 mV Kv2.1 current alone decayed with a time constant of 2.8±0.2 s and this was significantly slowed by co-expression with AMIGO2 to 7.3±0.8 s ($p<0.0005$). Co-expression of AMIGO2 and AMIGO3 together did not result in a different inactivation time constant from co-expression with AMIGO2 only (7.2±0.9 s, $p=0.99$ compared to +AMIGO2 only), while co-expression of AMIGO2 and AMIGO1 together reversed AMIGO2's effect (4.3±0.6 s, $p<0.05$ compared to +AMIGO2 only).

Comparable phenotypes were observed in Kv2.1 deactivation kinetics under these conditions. Figure 4.7D shows a summary of the time constants obtained from fits to deactivating tail currents at -40 mV under each of the expression conditions. As before, AMIGO2 significantly slowed the time constant of Kv2.1 deactivation from 7.4±0.74 ms to 37.4±3.9 ms ($p<0.005$). Consistent with our observations of inactivation kinetic phenotype, co-expression of AMIGO2 and AMIGO3 together did not reverse AMIGO2's effect on Kv2.1 deactivation. Indeed, when co-expressed with AMIGO2 and AMIGO3 simultaneously, Kv2.1 deactivation proceeded with a time constant of 32.1±4.2 ms, which was not different from that in the presence of AMIGO2 only ($p=0.8$). In contrast, co-expression

of AMIGO2 and AMIGO1 simultaneously reversed the effect of AMIGO2 on deactivation kinetics. The time constant of Kv2.1 deactivation in the presence of both AMIGO2 and AMIGO1 was 22.1±1.2 ms ($p<0.05$ compared to +AMIGO2 only), a value that was not significantly different from the time constant of Kv2.1 alone ($p=0.07$).

Based on the functional results, we hypothesized that AMIGO1 and AMIGO2 had higher affinity or longer-lived interactions with Kv2.1 than AMIGO3. To further explore this hypothesis, we measured the ratio of fluorescent AMIGO isoforms localized to Kv2.1 clusters in parallel with the electrophysiology experiment. We expected to find similar amounts of AMIGO1 and AMIGO2 localized to Kv2.1 clusters, and relatively less AMIGO3 than AMIGO2 localized to clusters at steady-state. Figure 4.8A shows the basal

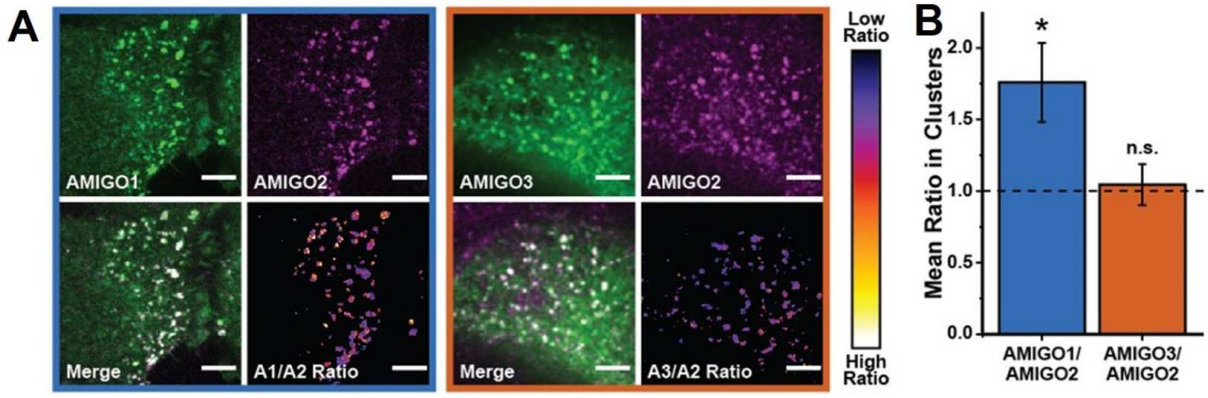

Figure 4.8: AMIGO1 and AMIGO3 compete with AMIGO2 for assembly with Kv2.1. **A)** *Left* - Cell co-expressing Kv2.1-LB (not shown), AMIGO1-GFP (green) and AMIGO2-Ruby (magenta) or *Right* - Kv2.1-LB (not shown), AMIGO3-GFP (green) and AMIGO2-Ruby (magenta). The ratio of GFP/Ruby is shown visually in the pseudocolored images in the bottom right corners. Warmer colors represent more AMIGO1 or AMIGO3 compared to AMIGO2, as indicated by the scale to the right of the images. Images are a single z-plane at the basal surface of the cell. Scale bars = 5 µm. **B)** Ratio of expression in clusters of AMIGO1 to AMIGO2 (blue bar) or AMIGO3 to AMIGO2 (orange bar). AMIGO1 had a significantly greater representation in Kv2.1 clusters than AMIGO2 ($\mu = 1.76\pm0.28$, N = 9 cells, $p<0.05$, $t = 2.75$, one-sample t-test vs test mean of 1). AMIGO3 and AMIGO2 were equally represented in Kv2.1 clusters ($\mu = 1.04\pm0.14$, N = 11 cells, non-significant, $t = 0.31$, one-sample t-test vs test mean of 1).

surface of HEK293 cells expressing Kv2.1 with AMIGO2-Ruby2 and AMIGO1-GFP simultaneously (left) or Kv2.1 with AMIGO2-Ruby2 and AMIGO3-GFP simultaneously (right). In these experiments Kv2.1 clusters contained fluorescence from both AMIGO isoforms,

however the ratio of GFP:Ruby2 fluorescence was non-uniform across cells and even across individual clusters (Figure 4.8A, ratio heatmaps). In general, the GFP:Ruby2 ratio was higher when AMIGO2 and AMIGO1 were co-expressed compared to when AMIGO2 and AMIGO3 were co-expressed, as evidenced by more white and yellow pixels in the Figure 4.8A ratio heatmaps. On average, the ratio of AMIGO1:AMIGO2 fluorescence in clusters was 1.76 ± 0.28 (Figure 4.8B, blue). This value was significantly different from 1 ($p<0.05$), suggesting that AMIGO1 was preferentially localized to clusters over AMIGO2. In contrast, the average ratio of AMIGO3:AMIGO2 fluorescence in clusters was not different from 1 (1.04 ± 0.14, $p=0.31$), indicating that AMIGO2 and AMIGO3 were found in similar amounts at Kv2.1 ER-PM junctions. The latter result was surprising, considering that the kinetic phenotype of Kv2.1 in the presence of both AMIGO2 and AMIGO3 was identical to that in the presence of AMIGO2 only. Together these results suggest that in the presence of both AMIGO2 and AMIGO3 very few of the Kv2.1 channels were exclusively associated with AMIGO3. Instead, these findings support the conclusion that multiple AMIGOs can bind to each Kv2.1 channel, and that the AMIGO2 kinetic phenotype is dominant over that conferred by AMIGO3. In contrast, AMIGO1 overcame AMIGO2 both in its ability to interact with Kv2.1 and determine the channel kinetic phenotype.

Table 4.2: Parameters from electrophysiological experiments of Kv2.1 and Kv2.2 expressed in HEK293 cells with and without AMIGO isoforms. Bold text indicates significant difference compared to the Kv2 alpha subunit expressed alone. z_{act} refers to the voltage dependence of activation kinetics. * = after a 2.5 s step to +40 mV. $^{\%}$ = at +30 mV. $^{\#}$ = at +40 mV. $^{\&}$ = at -40 mV.

Transfection	$V_{1/2\ act}$ (mV)	$V_{1/2\ inact}$ (mV)	Avail. Fraction*	τ_{act} (ms)$^{\%}$	τ_{inact} (s)$^{\#}$	τ_{deact} (ms)$^{\&}$	z_{act}
Kv2.1	-2.4±1.1 (9)	-27.1±0.7 (10)	0.43±0.02	11.9±0.7	3.2±0.1	18.6±1.0	1.76±0.14
+AMIGO1	**-8.5±1.2 (7)**	**-32.0±0.9 (9)**	0.46±0.02	**8.0±0.9**	3.2±0.2	23.2±1.3	2.16±0.13
+AMIGO2	**-10.3±1.2 (8)**	**-30.7±1.0 (8)**	**0.62±0.01**	**7.2±0.5**	**5.7±0.28**	**60.7±7.0**	2.21±0.12
+AMIGO3	**-9.1±1.2 (9)**	-28.6±0.5 (9)	0.49±0.02	**7.7±0.3**	3.9±0.2	29.2±1.2	2.17±0.16
Kv2.2	-2.2±0.9 (12)	-22.3±0.9 (10)	0.47±0.03	10.5±1.5	3.6±0.3	19.5±1.5	1.55±0.18
+AMIGO1	**-7.8±1.4 (9)**	-25.1±1.5 (8)	0.47±0.03	7.1±0.9	3.6±0.3	25.1±2.1	2.01±0.13
+AMIGO2	**-9.2±1.4 (8)**	**-27.1±0.8 (8)**	**0.59±0.03**	**5.7±0.4**	**5.4±0.4**	**70.7±11.2**	**3.23±0.71**
+AMIGO3	**-9.0±1.4 (9)**	**-27.0±0.8 (9)**	0.49±0.04	6.2±1.1	3.9±0.4	32.6±4.8	1.75±0.31
Competition Expt:							
Kv2.1	2.4±1.3 (3)	-18.8±1.4 (6)	0.40±0.02		2.8±0.2	7.4±0.74	
+AMIGO2	**-11.2±0.7 (5)**	-25.5±0.7 (6)	**0.67±0.04**		**7.3±0.9**	**37.4±3.9**	
+AMIGO2/AMIGO1	**-13.0±2.6 (6)**	**-28.1±2.1 (6)**	0.52±0.05		4.3±0.6	22.1±1.2	
+AMIGO2/AMIGO3	**-11.6±2.2 (6)**	**-26.3±2.8 (5)**	**0.68±0.02**		**7.2±0.9**	**32.1±4.2**	

4.5 Discussion

4.5.1 Summary

Kv β-subunits are well-known for their modulatory effects on channel function and localization. Our results show that all three AMIGOs do indeed modulate the activation of both Kv2.1 and 2.2 channels, and AMIGO2 specifically had an additional dramatic effect on channel inactivation and deactivation. While the effects of assembly on auxiliary subunit trafficking is often overlooked, we demonstrate that both Kv2s confer increased trafficking and a clustered localization to all three AMIGOs. Given the AMIGO family's widespread physiological functions, such as neurite growth and cell survival, assembly with Kv2 channels likely modulates some of these functions as well. Therefore, the interaction between Kv2 channels and each AMIGO represents a co-regulatory mechanism for both electrical and non-electrical cell properties.

4.5.2 On the mechanism of AMIGOs effects on Kv2 channel function

The effects of the AMIGOs on voltage-dependent activation observed in this work agree with previously published data with AMIGO1 [108]. Namely, each AMIGO conferred a 10 mV shift in the hyperpolarizing direction to both Kv2.1 and Kv2.2 channel activation. This observed increase in voltage sensitivity could be due to multiple mechanisms which were not rigorously tested in this work. We did note that all three AMIGOs tended to increase the voltage-dependence of Kv2.1 and Kv2.2 late activation kinetics, however only AMIGO2 did so significantly. Although not tested in this work, it is possible that the shifts in activation are due to increased voltage-sensitivity of the gating machinery. However, we think this mechanism unlikely. Kv2.1 channels have a characteristic separation of the Q-V and G-V curves [88, 126], and thus a leftward shift in G-V (as seen here) could be caused by increased coupling between voltage sensing and pore opening without a change in the Q-V curve. A similar mechanism has been proposed for leucine-rich-repeat-containing protein 26 (LRRC26), which is an AMIGO-like

auxiliary subunit of the large conductance potassium channel (BK) that causes a dramatic increase in the coupling between voltage sensing and pore opening [173]. In addition to speeding activation, AMIGO2 specifically slowed inactivation and deactivation of Kv2 channels by about 2-fold and 3-fold, respectively. This effect is also qualitatively similar to the effect of LRRC26 on BK [173] further supporting a similar mechanism of action for AMIGO2 on Kv2 channels. However, there is clearly a dissociation between the AMIGOs' effects on channel opening and closing, because all three isoforms shifted the G-V relationship to similar extents, while only AMIGO2 altered inactivation and deactivation kinetics. Mapping the interaction sites of the AMIGOs with Kv2 along with additional electrophysiological studies may shed light on the differences conferred by each AMIGO isoform.

The dramatic effects of AMIGO2 on channel inactivation and closing are particularly interesting in terms of Kv2 electrical function in the brain. Kv2 channels are not recruited for single AP repolarization, but are extremely important for maintaining polarized membrane potentials during high frequency firing by preventing depolarization block [86, 174]. Although the increase in activation rates seen in this work are not large enough to allow recruitment of Kv2 current during single action potentials, faster activation of the delayed rectifier current in general may improve the fidelity of high frequency AP firing. Once recruited, the additional stabilizing effect of AMIGO2 on the Kv2 open state could either enhance this fidelity or limit the AP frequency by slowing AP initiation. The physiological role of each AMIGO isoform's modulatory effects on Kv2 electrical function *in vivo* will be interesting to tease apart.

4.5.3 Consequences of Kv2-mediated increase in AMIGO surface expression

In addition to AMIGO-dependent changes in Kv2 electrical function, we also identified Kv2-dependent changes in AMIGO trafficking and localization. Expressed alone in HEK293 cells, the AMIGO isoforms showed variable levels of surface expression and surface protein was distributed evenly across the cell surface. When co-expressed with Kv2

channels, each of the three AMIGOs was trafficked more efficiently to the plasma membrane and underwent re-localization to ER-PM junctions, as was previously observed with AMIGO1 and Kv2 channels (Bishop et al., 2018). Redistribution of AMIGOs to Kv2 clusters on the cell surface likely demonstrates a direct interaction between the two proteins as has been previously shown for AMIGO1 and Kv2.1 [108]. This interaction is proposed to occur via the transmembrane (TM) domain of AMIGO1 and an unidentified TM domain of Kv2.1. Since the TM domains of the 3 AMIGOs are fairly homologous (48% identical, 81% similar, Uniprot), interaction between each AMIGO and Kv2 likely occurs via a similar mechanism, although the specific residues involved in interaction have yet to be determined.

Each of the AMIGOs showed variable levels of surface expression and of the AMIGOs, AMIGO3 showed the lowest surface expression, with much of the internal AMIGO3 appearing to reside in the ER. Although an ER-retention motif has not yet been identified in any of the AMIGOs, AMIGO3 has an additional 6 amino acids in the proximal C-terminus (RCRRWP) that contain a di-arginine motif, which is a sequence involved in general ER retention [175]. Internal AMIGO1 and AMIGO2 appeared to be localized in trafficking vesicles, which may represent a forward trafficking or recycling pool. Future studies may wish to determine in which pool these vesicles belong, and whether assembly with Kv2 channels or transcellular homophilic AMIGO adhesion prolongs the lifetime at the plasma membrane.

The effect of Kv2 channels on AMIGO surface expression represents a gain-of-function phenotype that likely has downstream effects due to AMIGO functions at the cell surface. For example, AMIGO2 localization to the PM may upregulate lipid-dependent phosphorylation of Akt, leading to increased growth and survivability [169]. Likewise, since all 3 AMIGOs are thought to act as cell adhesion molecules [160], increased surface expression could increase the size, number or location of cell-cell adhesions. Indeed, EM micrographs of Kv2.1 clusters in the rat hippocampus have been identified as sites of astrocyte

adhesion [60], and more recently, it was reported that microglia often contact neurons at Kv2.1 clusters [107]. Although neither of these neuron-glia adhesions have been attributed to AMIGO family interactions, it is tempting to speculate that AMIGOs residing in Kv2 clusters play a role in adhesion.

4.5.4 The stoichiometry of the AMIGO - Kv2 complex

The stoichiometry of the AMIGO-Kv2 interaction has not yet been addressed to our knowledge. However, the combination of quantitative imaging and electrophysiology in the competition experiments undertaken in this work can offer some new insights. When expressed together, we found that AMIGO1 reversed AMIGO2's effects on inactivation and deactivation and outcompeted AMIGO2 in localization to clusters. In contrast, AMIGO3 did not compete with the AMIGO2 functional effects despite its equal representation in Kv2 clusters. The inability of AMIGO3 to compete with the AMIGO2 kinetic phenotype suggests that no Kv2 channels in the AMIGO2/AMIGO3 condition were associated exclusively with AMIGO3. Instead, almost all channels were likely associated with both AMIGO2 and AMIGO3 and took on the AMIGO2 inactivation/deactivation phenotype. Therefore, Kv2 channels can likely bind more than one AMIGO subunit simultaneously but the presence of one AMIGO2 subunit appears to be sufficient to slow inactivation and deactivation. Assembly of Kv2 channels with variable numbers of AMIGO subunits could also explain some of the scatter in our data, such as was seen in measurements of deactivation kinetics. KCNEs are another family of type-1 transmembrane proteins that act as Kv channel auxiliary subunits. Although the stoichiometry of interaction between KCNE and Kv channels is still under debate, it is well accepted that each channel can bind multiple KCNE subunits [176–178]. In further support of our conclusion, a single KCNE subunit is sufficient to maximally alter Kv1.3 inactivation kinetics [177]. In summary, our data can be explained by assuming that all AMIGO isoforms compete for similar binding sites on Kv2 channels, but that they have different potency for modulating channel function. Although this may be the most parsimonious explanation for our results, we

cannot rule out the possibility that AMIGO3 has a binding site separate from the one that AMIGO1 and AMIGO2 seemed to compete for. If this is the case, allosteric effects could underlie AMIGO2's ability to overcome the AMIGO3 inactivation/deactivation phenotype.

4.5.5 Conclusion and Future Directions

Until recently, the Kv2 literature and AMIGO literature have been largely distinct bodies of work. The 2011 finding that AMIGO1 is a Kv2.1 auxiliary subunit marks the merging of the two fields. In this work we further intertwine the AMIGO and Kv2 fields by showing functional interactions between all members of both families. This result will inevitably lead to new and renewed interest in various aspects of each family's physiological function. For example, could AMIGOs reduce or exacerbate effects of the known pathogenic de novo Kv2.1 mutations [95,96,179]? Are Kv2 channels somehow involved in the activity-dependence of AMIGO expression [165]? What are the consequences of concentrating each of the three AMIGOs at the extracellular surface of Kv2-induced ER-PM junctions? These and other questions await future investigation.

Chapter 5

Conclusions

5.1 Studying silent channels

Electrophysiology is an extremely powerful method to probe the behavior of single channels, single cells, cellular networks and even whole nervous systems. Since the late 1700s, scientists have studied the interactions between electricity and physiology and have made ground breaking discoveries along the way. Not the least of which is a detailed description of the function of individual voltage-gated ion channel molecules that underlie a myriad of cell functions - from action potential generation to apoptosis, cell volume regulation to synaptic communication, among others.

Electrophysiologists are well-versed in the study of well-behaved ion channels. These channels open and close as predicted and contribute to the aforementioned processes. However, the research in this dissertation suggests that "badly-behaved" channels are deserving of our attention as well. These channels defy the predictions of gating models and are recalcitrant to opening despite strong stimulation. Inevitably, silent channels are difficult to study with electrophysiology because they do not contribute to the ionic current flowing across the cell membrane. In this work we avoided this problem by relying on the electrogenic nature of ion channel activation. That is, by detecting the current associated with conformational changes in the protein structure we could infer the presence of channels that did not open. Might there be a better way to study silent channels? A method that does not rely on the absence of signal to report "bad" behavior?

My opinion is that optical methods will solve this problem in the future. Voltage-clamp fluorometry is a well-established method to visually observe structural rearrangements in ion channels during gating [180]. This technique has been used to show rearrangements in the voltage sensor during activation as well as rearrangements in the pore region during slow inactivation [181, 182]. Ion selective fluorescent dyes are also com-

monly used to image changes in ion concentrations due to ion channel activity in real time [183–185]. One could imagine a method whereby voltage sensor and/or pore conformation is reported by voltage-clamp fluorometry while channel conductance is monitored by a potassium sensitive dye. Of course, resolution of these signals at the single channel level are impossible with the current fluorescent potassium sensor reagents. Given the rapid development in this technical area over the past several years, I have no doubt that this experiment will one day be feasible.

5.2 Kv silencing is related to channel density

Despite less-than-perfect methods to measure non-conducting channels, we showed that the silencing of Kv2.1, and now Kv2.2, Kv1.4 and Kv1.5, is favored by an increased density of those channels in the membrane, i.e. their expression level. We showed this by comparing the numbers of gating and conducting channels in individual HEK293 cells, finding that the conducting fraction decreased with the number of gating channels. This was true for all four channels tested. However, there was a distinction in the sensitivity of Kv1.4 channels to the silencing effect. While Kv2.1, Kv2.2 and Kv1.5 had significant numbers of non-conducting channels below a density of 100 channels/μm^2, Kv1.4 did not. Instead, non-conducting Kv1.4 channels were only detected above a density of 100 channels/μm^2. If we assume the non-conducting state arises due to saturation of a binding partner required for "good" channel behavior, then we might hypothesize that Kv1.4 has a less stringent requirement for that partner. Alternatively, expression of Kv1.4 may specifically alter the available amount of that partner in some unknown way. It is difficult to speculate on the mechanism distinguishing Kv1.4 from the other channels without a better understanding of the mechanism of channel silencing in general.

Interestingly, we also found that Kv1.4 had a higher unitary charge than the other three channels examined in this work. It should be noted that unitary charge in this work meant the charge per channel that moves during the first 3 ms after a depolariz-

ing stimulus to +40 mV. Therefore, our results do not necessarily contradict previously published studies finding that Kv1 and Kv2 channels have similar amounts of total unitary charge. We believe the differences uncovered here represent differences in gating between Kv1.4 and the other three channels. A slow component to Kv2.1 channel activation was suggested by a study showing that the first 10 ms of ON gating do not contain the total gating charge [126]. Sequential voltage sensor activation has been described in Kv1.5 [186], *Shaker* channels [187], and even the voltage sensitive phosphatase from *Ciona intestinalis* [188]. We suggest that the underestimation of unitary charge obtained in this work from Kv2.1, Kv2.2 and Kv1.5 represents the detection of early voltage sensor transitions and not late ones. If true, Kv1.4 was the outlier in terms of voltage sensor activation in our studies, because we detected the full predicted number of elementary charges in the first few milliseconds after depolarization. Whether this distinction also underlies the less prevalent non-conducting state in Kv1.4 remains to be seen, but is an intriguing idea.

5.3 AMIGO and Kv2 functions are inextricably linked

Kv2 channels are complex proteins. As reviewed in the introduction to this dissertation, Kv2 channels do act as canonical voltage-gated potassium channels but the majority of their known functions are not related to their ion conductance. The discovery that Kv2 channels assemble with a cell adhesion molecule-like protein, AMIGO1, in 2011 added to this growing list of non-canonical functions associated with Kv2 channels. In chapter 4 of this dissertation, we expanded on this finding and showed that Kv2s assemble with two additional AMIGO isoforms and localize these proteins to ER-PM junctions. In addition to their effects on AMIGO localization and trafficking, the AMIGOs conferred functional differences to Kv2 channel conductance. The most striking effects were seen upon assembly with AMIGO2. Specifically, AMIGO2 slowed Kv2 inactivation and deactivation by 2- and 3-fold, respectively, resulting in channels spending more time in the open, conduct-

ing state. Whether the AMIGO2 functional phenotype confers altered electrical properties onto neurons or other excitable cells remains to be seen.

Both AMIGOs and Kv2 proteins are expressed in tissues throughout the body [160]. However, the cell-type and subcellular compartment-specific expression of each AMIGO isoform remains largely unexplored. This is mostly due to the relatively recent discovery of these proteins and the consequential lack of tools being used to study them. However, the connection between the AMIGO and Kv2 families' functions will likely accelerate these investigations. It will be interesting to know whether Kv2s are always associated with an AMIGO *in vivo* or if certain conditions favor assembly and/or disassembly. Studies of the relative abundance of AMIGO isoforms across tissues, cells and throughout development will also be intriguing. Perhaps most exciting is the idea that AMIGOs could mediate transcellular contacts between the cell types that express them. The finding that Kv2s improve surface trafficking of AMIGOs to the PM of HEK293 cells suggests that where Kv2s are highly expressed, AMIGOs will also be localized. Intercellular binding partners of the Kv2-AMIGO complex await discovery, as do the downstream effects of their interaction.

5.4 The big picture

The nervous system is a fascinating thing. My motivations for studying neuroscience were largely based on my awe for the way arrangements of atoms and molecules bring about the human experience. It has been a privilege to study a small corner of this field over the past six years. I am not sure how much the work in this dissertation will contribute to our understanding of complex neurological phenomena. However, throughout the course of these studies I have become more aware and even more in awe at the complexities within us, indeed within each of our individual cells. The prospect of scientists one day explaining all the intricacies of molecular neuroscience is actually more daunting now than before I started. But that is the journey of science - learning what you do not

know, in the hope that you can contribute a bit of knowledge of your own and push the boundaries of human understanding.

Bibliography

[1] Marco Bresadola. Medicine and science in the life of Luigi Galvani (1737-1798). *Brain Res. Bull.*, 46(5):367–380, 1998.

[2] Bertil Hille. *Ionic channels of excitable membranes*. Sinauer Associates, Inc., Sunderland, Massachusetts, 2nd edition, 1991.

[3] A.L. Hodgkin and A.F. Huxley. Action potentials recorded from inside a nerve fiber. *Nature*, 144(3651):710–711, 1939.

[4] HJ Curtis and KS Cole. Membrane resting and action potentials from the squid giant axon. *J. Cell. Comp. Physiol.*, 19(2):135–144, 1942.

[5] Osvaldo Alvarez and Ramón Latorre. The enduring legacy of the "constant-field equation" in membrane ion transport. *J. Gen. Physiol.*, 149(10):1–10, 2017.

[6] David E. Goldman. Potential, impedance, and rectification in membranes. *J. Gen. Physiol.*, 27(1):37–60, 1943.

[7] A. L. Hodgkin and B Katz. The effect of sodium ions on the electrical activity of the giant axon of the squid. *J. Physiol.*, 108:37–77, 1949.

[8] G Marmont. Studies on the axon membrane. *J. Cell. Comp. Physiol.*, 34(3):351–382, 1949.

[9] A. L. Hodgkin, A. F. Huxley, and B. Katz. Measurement of current-voltage relations in the membrane of the giant axon of Loligo. *J. Physiol.*, 116:424–448, 1952.

[10] A L Hodgkin and A F Huxley. Currents carried by sodium and potassium ions through the membrane of the giant axon of loligo. *J. Physiol.*, 116:449–472, 1952.

[11] A.L. Hodgkin and A.F. Huxley. A quantitative description of membrane current and its application to conduction and excitation in nerve. *J. Physiol.*, 117(4):500–544, 1952.

[12] A. L. Hodgkin and R. D. Keynes. The potassium permeability of a giant nerve fibre. *J. Physiol.*, 128(1):61–88, 1955.

[13] C. M. Armstrong. Time course of TEA(+)-induced anomalous rectification in squid giant axons. *J. Gen. Physiol.*, 50(2):491–503, 1966.

[14] T. I. Benzer and M. A. Raftery. Partial characterization of a tetrodotoxin-binding component from nerve membrane. *Proc. Natl. Acad. Sci. U. S. A.*, 69(12):3634–3637, 1972.

[15] W. Almers and S. R. Levinson. Tetrodotoxin binding to normal and depolarized frog muscle and the conductance of a single sodium channel. *J. Physiol.*, 247(2):483–509, 1975.

[16] Clay M. Armstrong. Ionic pores, gates, and gating currents. *Q. Rev. Biophys.*, 7(2):179–210, 1975.

[17] W. S. Agnew, S. R. Levinson, J. S. Brabson, and M. A. Raftery. Purification of the tetrodotoxin-binding component associated with the voltage-sensitive sodium channel from Electrophorus electricus electroplax membranes. *Proc. Natl. Acad. Sci.*, 75(6):2606–2610, 1978.

[18] M. M. Tamkun, J. A. Talvenheimo, and W. A. Catterall. The sodium channel from rat brain. *J. Biol. Chem.*, 259(3):1676–1688, 1984.

[19] R. P. Hartshorne and W. A. Catterall. The sodium channel from rat brain. Purification and subunit composition. *J. Biol. Chem.*, 259(3):1667–1675, 1984.

[20] Robert P. Hartshorne, Bernhard U. Keller, Jane A. Talvenheimo, William A. Catterall, and Mauricio Montal. Functional Reconstitution of the Purified Brain Sodium Channel in Planar Lipid Bilayers. *Proc. Natl. Acad. Sci.*, 82:240–244, 1985.

[21] Masaharu Noda, Shin Shimizu, Tsutomu Tanabe, Toshiyuki Takai, Toshiaki Kayano, Takayuki Ikeda, Hideo Takahashi, Hitoshi Nakayama, Yuichi Kanaoka, Naoto Minamino, Kenji Kangawa, Hisayuki Matsuo, Michael A. Raftery, Tadaaki Hirose, Seiichi Inayama, Hidenori Hayashida, Takashi Miyata, and Shosaku Numa. Primary structure of Electrophorus electricus sodium channel deduced from cDNA sequence. *Nature*, 312(5990):121–127, 1984.

[22] Bruce L Tempel, Diane M Papazian, Thomas L Schwarz, Yuh Nung Jan, and Lily Yeh Jan. Sequence of a Probable Potassium Channel Component Encoded at Shaker Locus of Drosophila. *Science (80-.).*, 237(4816):770–774, 1987.

[23] Diane M. Papazian, Thomas L. Schwarz, Bruce L. Tempel, Yuh Nung Jan, and Lily Y. Jan. Cloning of genomic and complementary DNA from Shaker, a putative potassium channel gene from Drosophila. *Science (80-.).*, 237(4816):749–753, 1987.

[24] Alexander Kamb, Linda E. Iverson, and Mark A. Tanouye. Molecular characterization of Shaker, a Drosophila gene that encodes a potassium channel. *Cell*, 50(3):405–413, 1987.

[25] D. A. Doyle. The Structure of the Potassium Channel: Molecular Basis of K+ Conduction and Selectivity. *Science (80-.).*, 280(5360):69–77, 1998.

[26] Youxing Jiang, Alice Lee, Jiayun Chen, Vanessa Ruta, Martine Cadene, Brian T. Chait, and Roderick MacKinnon. X-ray structure of a voltage-dependent K+ channel. *Nature*, 423(6935):33–41, 2003.

[27] Youxing Jiang, Vanessa Ruta, Jiayun Chen, Alice Lee, and Roderick Mackinnon. The principle of gating charge movement in a voltage-dependent K channel. *Nature*, 423(6935):42–48, 2003.

[28] Stephen B Long, Ernest B Campbell, and Roderick Mackinnon. Crystal Structure of a Mammalian Voltage-Dependent Shaker Family K+ Channel. *Science (80-.).*, 309(5736):897–903, 2005.

[29] Stephen B Long, Ernest B Campbell, and Roderick Mackinnon. Voltage Sensor of Kv1.2 : Structural Basis of Electromechanical Coupling. *Science (80-.).*, 309(5736):903–908, 2005.

[30] Stephen B. Long, Xiao Tao, Ernest B. Campbell, and Roderick MacKinnon. Atomic structure of a voltage-dependent K+ channel in a lipid membrane-like environment. *Nature*, 450(7168):376–382, 2007.

[31] Yi Liu, Miguel Holmgren, Mark E. Jurman, and Gary Yellen. Gated access to the pore of a voltage-dependent K+ channel. *Neuron*, 19(1):175–184, 1997.

[32] Donato Del Camino and Gary Yellen. Tight steric closure at the intracellular activation gate of a voltage-gated K+ channel. *Neuron*, 32(4):649–656, 2001.

[33] Zhe Lu, Angela M. Klem, and Yajamana Ramu. Coupling between voltage sensors and activation gate in voltage-gated K+ channels. *J. Gen. Physiol.*, 120(5):663–676, 2002.

[34] Rikard Blunck and Zarah Batulan. Mechanism of electromechanical coupling in voltage-gated potassium channels. *Front. Pharmacol.*, 3:1–16, 2012.

[35] Francisco Barros, Luis A. Pardo, Pedro Domínguez, Luisa Maria Sierra, and Pilar de la Peña. New structures and gating of voltage-dependent potassium (Kv) channels and their relatives: A multi-domain and dynamic question. *Int. J. Mol. Sci.*, 20(2), 2019.

[36] Y. M. Cheng, J. Azer, C. M. Niven, P. Mafi, C. R. Allard, J. Qi, S. Thouta, and T. W. Claydon. Molecular determinants of U-type inactivation in Kv2.1 channels. *Biophys. J.*, 101(3):651–661, 2011.

[37] Mayra Delgado-Ramírez, José J. De Jesús-Pérez, Iván A. Aréchiga-Figueroa, Jorge Arreola, Scott K. Adney, Carlos A. Villalba-Galea, Diomedes E. Logothetis, and Aldo A. Rodríguez-Menchaca. Regulation of Kv2.1 channel inactivation by phosphatidylinositol 4,5-bisphosphate. *Sci. Rep.*, 8(1):1–13, 2018.

[38] Toshinori Hoshi, William N. Zagotta, and Richard W. Aldrich. Biophysical and molecular mechanisms of Shaker potassium channel inactivation. *Science (80-.).*, 250(4980):533–538, 1990.

[39] Jing Li, Jared Ostmeyer, Luis G. Cuello, Eduardo Perozo, and Benoît Roux. Rapid constriction of the selectivity filter underlies C-type inactivation in the KcsA potassium channel. *J. Gen. Physiol.*, 215(10):1408–1420, 2018.

[40] Laszlo Kiss and Stephen J. Korn. Modulation of C-type inactivation by K+ at the potassium channel selectivity filter. *Biophys. J.*, 74(4):1840–1849, 1998.

[41] Alice Butler, Aguan Wei, Keith Baker, and Lawrence Salkoff. A family of putative potassium channel genes in Drosophila. *Science (80-.).*, 243(4893):943–947, 1989.

[42] Aguan Wei, Manuel Covarrubias, Alice Butler, Keith Baker, Michael Pak, and Lawrence Salkoff. K+ current diversity is produced by an extended gene family conserved in Drosophila and mouse. *Science (80-.).*, 248(4955):599–603, 1990.

[43] T. Mccormack, E. C. Vega-Saenz De Miera, and B. Rudy. Molecular cloning of a member of a third class of Shaker-family K+ channel genes in mammals. *Proc. Natl. Acad. Sci. U. S. A.*, 87(13):5227–5231, 1990.

[44] Bruce L. Tempel, Yuh Nung Jan, and Lily Y. Jan. Cloning of a probable potassium channel gene from mouse brain. *Nature*, 332(6167):837–839, 1988.

[45] Georges C. Frech, Antonius M.J. VanDongen, Gabriele Schuster, Arthur M. Brown, and Rolf H. Joho. A novel potassium channel with delayed rectifier properties isolated from rat brain by expression cloning. *Nature*, 340(6235):642–645, 1989.

[46] Walter Stuhmer, Johann Peter Ruppersberg, Klaus Hasso Schroter, Bert Sakmann, Martin Stocker, Karl Peter Giese, Astrid Perschke, Arnd Baumann, and Olaf Pongs. Molecular basis of functional diversity of voltage-gated potassium channels in mammalian brain. *EMBO J.*, 8(11):3235–3244, 1989.

[47] S L Roberds and M M Tamkun. Cloning and tissue-specific expression of five voltage-gated potassium channel cDNAs expressed in rat heart. *Proc. Natl. Acad. Sci. U. S. A.*, 88(March 1991):1798–802, 1991.

[48] G. A. Gutman, K. G. Chandy, S. Grissmer, M. Lazdunski, D. McKinnon, L. A. Pardo, G. A. Robertson, B. Rudy, M. C. Sanguinetti, W. Stuhmer, and X. Wang. International Union of Pharmacology. LIII. Nomenclature and Molecular Relationships of Voltage-Gated Potassium Channels. *Pharmacol. Rev.*, 57(4):473–508, dec 2005.

[49] Carlos González, David Baez-Nieto, Ignacio Valencia, Ingrid Oyarzún, Patricio Rojas, David Naranjo, and Ramón Latorre. K+ channels: Function-structural overview. *Compr. Physiol.*, 2(3):2087–2149, 2012.

[50] Rajnish Ranjan, Emmanuelle Logette, Michela Marani, Mirjia Herzog, Valérie Tâche, Enrico Scantamburlo, Valérie Buchillier, and Henry Markram. A Kinetic Map of the Homomeric Voltage-Gated Potassium Channel (Kv) Family. *Front. Cell. Neurosci.*, 13(August):1–25, 2019.

[51] Min Li, Yuh Nung Jan, and Lily Yeh Jan. Specification of subunit assembly by the hydrophilic amino-terminal domain of the Shaker potassium channel. *Science (80-.).*, 257(5074):1225–1230, 1992.

[52] Clay M. Armstrong and Francisco Bezanilla. Currents related to movement of the gating particles of the sodium channels. *Nature*, 242(5398):459–461, 1973.

[53] Sara I. Börjesson and Fredrik Elinder. Structure, function, and modification of the voltage sensor in voltage-gated ion channels. *Cell Biochem. Biophys.*, 52(3):149–174, 2008.

[54] Leon D Islas and Fred J Sigworth. Voltage sensitivity and gating charge in Shaker and Shab family potassium channels. *J. Gen. Physiol.*, 114(5):723–741, 1999.

[55] A. Scholle, S. Dugarmaa, T. Zimmer, M. Leonhardt, R. Koopmann, B. Engeland, O. Pongs, and K. Benndorf. Rate-limiting Reactions Determining Different Activation Kinetics of Kv1.2and Kv2.1 Channels. *J. Membr. Biol.*, 198(2):103–112, 2004.

[56] Catherine J. Smith-Maxwell, Jennifer L. Ledwell, and Richard W. Aldrich. Uncharged S4 residues and cooperativity in voltage-dependent potassium channel activation. *J. Gen. Physiol.*, 111(3):421–439, 1998.

[57] Jennifer L. Ledwell and Richard W. Aldrich. Mutations in the S4 region isolate the final voltage-dependent cooperative step in potassium channel activation. *J. Gen. Physiol.*, 113(3):389–414, 1999.

[58] Dominique G. Gagnon and Francisco Bezanilla. The contribution of individual subunits to the coupling of the voltage sensor to pore opening in Shaker K channels: Effect of ILT mutations in heterotetramers. *J. Gen. Physiol.*, 136(5):555–568, 2010.

[59] James S. Trimmer. Immunological identification and characterization of a delayed rectifier K+ channel polypeptide in rat brain. *Proc. Natl. Acad. Sci. U. S. A.*, 88(23):10764–10768, 1991.

[60] J. Du, J. H. Tao-Cheng, P. Zerfas, and C. J. McBain. The K+ channel, Kv2.1, is apposed to astrocytic processes and is associated with inhibitory postsynaptic mem-

branes in hippocampal and cortical principal neurons and inhibitory interneurons. *Neuroscience*, 84(1):37–48, 1998.

[61] Patrick D Sarmiere, Cecile M Weigle, and Michael M Tamkun. The Kv2.1 K+ channel targets to the axon initial segment of hippocampal and cortical neurons in culture and in situ. *BMC Neurosci.*, 9(1):112, 2008.

[62] H. I. Bishop, D. Guan, E. Bocksteins, L. K. Parajuli, K. D. Murray, M. M. Cobb, H. Misonou, K. Zito, R. C. Foehring, and J. S. Trimmer. Distinct Cell- and Layer-Specific Expression Patterns and Independent Regulation of Kv2 Channel Subtypes in Cortical Pyramidal Neurons. *J. Neurosci.*, 35(44):14922–14942, 2015.

[63] Elizabeth A.L. Muennich and Robert E.W. Fyffe. Focal aggregation of voltage-gated, Kv2.1 subunit-containing, potassium channels at synaptic sites in rat spinal motoneurones. *J. Physiol.*, 554(3):673–685, 2004.

[64] Lizhen Yan, David J. Figueroa, Christopher P. Austin, Yuan Liu, Randal M. Bugianesi, Robert S. Slaughter, Gregory J. Kaczorowski, and Martin G. Kohler. Expression of Voltage-Gated Potassium Channels in Human and Rhesus Pancreatic Islets. *Diabetes*, 53(3):597–607, 2004.

[65] Jianyang Fu, Xiaoqing Dai, Gregory Plummer, Kunimasa Suzuki, Austin Bautista, John M. Githaka, Laura Senior, Mette Jensen, Dafna Greitzer-Antes, Jocelyn E.Manning Fox, Herbert Y. Gaisano, Christopher B. Newgard, Nicolas Touret, and Patrick E. MacDonald. Kv2.1 clustering contributes to insulin exocytosis and rescues human β-cell dysfunction. *Diabetes*, 66(7):1890–1900, 2017.

[66] K. M. S. O'Connell, J. D. Whitesell, and M. M. Tamkun. Localization and mobility of the delayed-rectifer K+ channel Kv2.1 in adult cardiomyocytes. *AJP Hear. Circ. Physiol.*, 294(1):H229–H237, 2007.

[67] D.R. Van Wagoner, A.L. Pond, P.M. McCarthy, J. S. Trimmer, and J.M. Nerbonne. Outward K+ current densities and Kv1.5 expression are reduced in chronic human atrial fibrillation. *Circ. Res.*, 80(6):772–781, 1997.

[68] Gregory C. Amberg and Luis F. Santana. Kv2 channels oppose myogenic constriction of rat cerebral arteries. *Am. J. Physiol. - Cell Physiol.*, 291(2):348–356, 2006.

[69] Paul M. Hwang, Charles E. Glatt, David S. Bredt, Gary Yellen, and Solomon H. Snyder. A novel K+ channel with unique localizations in mammalian brain: Molecular cloning and characterization. *Neuron*, 8(3):473–481, 1992.

[70] Yoshitaka Kihira, Tracey O Hermanstyne, and Hiroaki Misonou. Formation of Heteromeric Kv2 Channels in Mammalian Brain Neurons. *J. Biol. Chem.*, 285(20):15048–15055, 2010.

[71] Hannah I. Bishop, Melanie M. Cobb, Michael Kirmiz, Laxmi K. Parajuli, Danielle Mandikian, Ashleigh M. Philp, Mikhail Melnik, Juha Kuja-Panula, Heikki Rauvala, Ryuichi Shigemoto, Karl D. Murray, and James S. Trimmer. Kv2 Ion Channels Determine the Expression and Localization of the Associated AMIGO-1 Cell Adhesion Molecule in Adult Brain Neurons. *Front. Mol. Neurosci.*, 11(January):1–20, jan 2018.

[72] K. M. S. O'Connell and M. M. Tamkun. Targeting of voltage-gated potassium channel isoforms to distinct cell surface microdomains. *J. Cell Sci.*, 118(10):2155–2166, may 2005.

[73] Durga P. Mohapatra and James S. Trimmer. The Kv2.1 C terminus can autonomously transfer Kv2.1-like phosphorylation-dependent localization, voltage-dependent gating, and muscarinic modulation to diverse Kv channels. *J. Neurosci.*, 26(2):685–695, 2006.

[74] Ben Johnson, Ashley N. Leek, Laura Solé, Emily E. Maverick, Tim P. Levine, and Michael M. Tamkun. Kv2 potassium channels form endoplasmic reticulum/plasma

membrane junctions via interaction with VAPA and VAPB. *Proc. Natl. Acad. Sci.*, 115(31):E7331–E7340, jul 2018.

[75] Robert H. Scannevin, Hideyuki Murakoshi, Kenneth J. Rhodes, and James S. Trimmer. Identification of a cytoplasmic domain important in the polarized expression and clustering of the Kv2.1 K+ channel. *J. Cell Biol.*, 135(6):1619–1632, 1996.

[76] Hideyuki Murakoshi and James S. Trimmer. Identification of the Kv2.1 K+ channel as a major component of the delayed rectifier K+ current in rat hippocampal neurons. *J. Neurosci.*, 19(5):1728–1735, 1999.

[77] K. M. S. O'Connell, A. S. Rolig, J. D. Whitesell, and M. M. Tamkun. Kv2.1 Potassium Channels Are Retained within Dynamic Cell Surface Microdomains That Are Defined by a Perimeter Fence. *J. Neurosci.*, 26(38):9609–9618, sep 2006.

[78] M. M. Tamkun, K. M. S. O'Connell, and A. S. Rolig. A cytoskeletal-based perimeter fence selectively corrals a sub-population of cell surface Kv2.1 channels. *J. Cell Sci.*, 120(14):2413–2423, jul 2007.

[79] P. D. Fox, C. J. Haberkorn, E. J. Akin, P. J. Seel, D. Krapf, and M. M. Tamkun. Induction of stable ER-plasma-membrane junctions by Kv2.1 potassium channels. *J. Cell Sci.*, 128(11):2096–2105, 2015.

[80] Philip D. Fox, Christopher J. Haberkorn, Aubrey V. Weigel, Jenny L. Higgins, Elizabeth J. Akin, Matthew J. Kennedy, Diego Krapf, and Michael M. Tamkun. Plasma membrane domains enriched in cortical endoplasmic reticulum function as membrane protein trafficking hubs. *Mol. Biol. Cell*, 24(17):2703–2713, 2013.

[81] Michael Kirmiz, Stephanie Palacio, Parashar Thapa, Anna N. King, Jon T. Sack, and James S. Trimmer. Remodeling neuronal ER-PM junctions is a conserved nonconducting function of Kv2 plasma membrane ion channels. *Mol. Biol. Cell*, 29(20):2410–2432, 2018.

[82] Seung T Lim, Dana E Antonucci, Robert H Scannevin, and James S Trimmer. A Novel Targeting Signal for Proximal Clustering of the Kv2.1 K+ Channel in Hippocampal Neurons. *Neuron*, 25(2):385–397, 2000.

[83] Hiroaki Misonou, Durga P Mohapatra, Eunice W Park, Victor Leung, Dongkai Zhen, Kaori Misonou, Anne E Anderson, and James S Trimmer. Regulation of ion channel localization and phosphorylation by neuronal activity. *Nat. Neurosci.*, 7(7):711–718, jul 2004.

[84] Ben Johnson, Ashley N. Leek, and Michael M. Tamkun. Kv2 channels create endoplasmic reticulum / plasma membrane junctions: a brief history of Kv2 channel subcellular localization. *Channels*, 13(1):88–101, 2019.

[85] Jing Du, Laurel L Haak, Emily Phillips-tansey, James T Russell, and Chris J Mcbain. Frequency-dependent regulation of rat hippocampal somato-dendritic excitability by the K+ channel subunit Kv2.1. *J. Physiol.*, 522(1):19–31, 2000.

[86] Dongxu Guan, William E. Armstrong, and Robert C. Foehring. Kv2 channels regulate firing rate in pyramidal neurons from rat sensorimotor cortex. *J. Physiol.*, 591(19):4807–4825, 2013.

[87] Durga P. Mohapatra, Hiroaki Misonou, Sheng Jun Pan, Joshua E. Held, D. James Surmeier, and James S. Trimmer. Regulation of intrinsic excitability in hippocampal neurons by activity-dependent modulation of the KV2.1 potassium channel. *Channels*, 3(1):46–56, 2009.

[88] K. M. S. O'Connell, R. Loftus, and M. M. Tamkun. Localization-dependent activity of the Kv2.1 delayed-rectifier K+ channel. *Proc. Natl. Acad. Sci.*, 107(27):12351–12356, jul 2010.

[89] Scott B. Baver and Kristen M.S. O'Connell. The C-terminus of neuronal Kv2.1 channels is required for channel localization and targeting but not for NMDA-receptor mediated regulation of channel function. *Neuroscience*, 217:56–66, 2012.

[90] Sumon Pal, Karen A. Hartnett, Jeanne M. Nerbonne, Edwin S. Levitan, and Elias Aizenman. Mediation of Neuronal Apoptosis by Kv2.1-Encoded Potassium Channels. *J. Neurosci.*, 23(12):4798–4802, 2003.

[91] Meghan C Mccord and Elias Aizenman. Convergent Ca2+ and Zn2+ signaling regulates apoptotic Kv2.1 K+ currents. *Proc. Natl. Acad. Sci.*, 110(34):13988–13993, 2013.

[92] Chung Yang Yeh, Ashlyn M. Bulas, Aubin Moutal, Jami L. Saloman, Karen A. Hartnett, Charles T. Anderson, Thanos Tzounopoulos, Dandan Sun, Rajesh Khanna, and Elias Aizenman. Targeting a potassium channel/syntaxin interaction ameliorates cell death in ischemic stroke. *J. Neurosci.*, 37(23):5648–5658, 2017.

[93] Anthony J Schulien, Chung-yang Yeh, Bailey N Orange, Olivia J Pav, Madelynn P Hopkins, Aubin Moutal, Rajesh Khanna, Dandan Sun, Jason A Justice, and Elias Aizenman. Targeted disruption of Kv2.1-VAPA association provides neuroprotection against ischemic stroke in mice by declustering Kv2.1 channels. *Sci. Adv.*, 6(July), 2020.

[94] D. J. Speca, G. Ogata, D. Mandikian, H. I. Bishop, S. W. Wiler, K. Eum, H. Jürgen Wenzel, E. T. Doisy, L. Matt, K. L. Campi, M. S. Golub, J. M. Nerbonne, J. W. Hell, B. C. Trainor, J. T. Sack, P. A. Schwartzkroin, and J. S. Trimmer. Deletion of the Kv2.1 delayed rectifier potassium channel leads to neuronal and behavioral hyperexcitability. *Genes, Brain Behav.*, 13(4):394–408, 2014.

[95] Carolien G.F. De Kovel, Steffen Syrbe, Eva H. Brilstra, Nienke Verbeek, Bronwyn Kerr, Holly Dubbs, Allan Bayat, Sonal Desai, Sakkubai Naidu, Siddharth Srivastava, Hande Cagaylan, Uluc Yis, Carol Saunders, Martin Rook, Susanna

Plugge, Hiltrud Muhle, Zaid Afawi, Karl Martin Klein, Vijayakumar Jayaraman, Ramakrishnan Rajagopalan, Ethan Goldberg, Eric Marsh, Sudha Kessler, Christina Bergqvist, Laura K. Conlin, Bryan L. Krok, Isabelle Thiffault, Manuela Pendziwiat, Ingo Helbig, Tilman Polster, Ingo Borggraefe, Johannes R. Lemke, Marie José Van Den Boogaardt, Rikke S. Møller, and Bobby P.C. Koeleman. Neurodevelopmental disorders caused by de novo variants in KCNB1 genotypes and phenotypes. *JAMA Neurol.*, 74(10):1228–1236, 2017.

[96] Seok Kyu Kang, Carlos G. Vanoye, Sunita N. Misra, Dennis M. Echevarria, Jeffrey D. Calhoun, John B. O'Connor, Katarina L. Fabre, Dianalee McKnight, Laurie Demmer, Paula Goldenberg, Lauren E. Grote, Isabelle Thiffault, Carol Saunders, Kevin A. Strauss, Ali Torkamani, Jasper van der Smagt, Koen van Gassen, Robert P. Carson, Jullianne Diaz, Eyby Leon, Joseph E. Jacher, Mark C. Hannibal, Jessica Litwin, Neil R. Friedman, Allison Schreiber, Bryan Lynch, Annapurna Poduri, Eric D. Marsh, Ethan M. Goldberg, John J. Millichap, Alfred L. George, and Jennifer A. Kearney. Spectrum of KV2.1 Dysfunction in KCNB1-Associated Neurodevelopmental Disorders. *Ann. Neurol.*, 86(6):899–912, 2019.

[97] K Benndorf, R Koopmann, C Lorra, and O Pongs. Gating and conductance properties of a human delayed rectifier K + channel expressed in frog oocytes. *J. Physiol.*, 477(1):1–14, 1994.

[98] Samantha C. O'Dwyer, Stephanie Palacio, Collin Matsumoto, Laura Guarina, Nicholas R Klug, Sendoa Tajada, Barbara Rosati, David McKinnon, James S Trimmer, and L Fernando Santana. Kv2.1 channels play opposing roles in regulating membrane potential, Ca 2+ channel function, and myogenic tone in arterial smooth muscle. *Proc. Natl. Acad. Sci.*, page 201917879, 2020.

[99] Gregory C. Amberg, Charles F. Rossow, Manuel F. Navedo, and Luis F. Santana. NFATc3 regulates Kv2.1 expression in arterial smooth muscle. *J. Biol. Chem.*, 279(45):47326–47334, 2004.

[100] Alexa L. Mattheyses, Sanford M. Simon, and Joshua Z. Rappoport. Imaging with total internal reflection fluorescence microscopy for the cell biologist. *J. Cell Sci.*, 123(21):3621–3628, 2010.

[101] P. D. Fox, R. J. Loftus, and M. M. Tamkun. Regulation of Kv2.1 K+ Conductance by Cell Surface Channel Density. *J. Neurosci.*, 33(3):1259–1270, jan 2013.

[102] E. Deutsch, A. V. Weigel, E. J. Akin, P. Fox, G. Hansen, C. J. Haberkorn, R. Loftus, D. Krapf, and M. M. Tamkun. Kv2.1 cell surface clusters are insertion platforms for ion channel delivery to the plasma membrane. *Mol. Biol. Cell*, 23(15):2917–2929, 2012.

[103] Dafna Singer-Lahat, Anton Sheinin, Dodo Chikvashvili, Sharon Tsuk, Dafna Greitzer, Reut Friedrich, Lori Feinshreiber, Uri Ashery, Morris Benveniste, Edwin S. Levitan, and Ilana Lotan. K+ channel facilitation of exocytosis by dynamic interaction with syntaxin. *J. Neurosci.*, 27(7):1651–1658, 2007.

[104] Lori Feinshreiber, Dafna Singer-Lahat, Reut Friedrich, Ulf Matti, Anton Sheinin, Ofer Yizhar, Rachel Nachman, Dodo Chikvashvili, Jens Rettig, Uri Ashery, and Ilana Lotan. Non-conducting function of the Kv2.1 channel enables it to recruit vesicles for release in neuroendocrine and nerve cells. *J. Cell Sci.*, 123:1940–1947, 2010.

[105] X. Q. Dai, J. E. Manning Fox, D. Chikvashvili, M. Casimir, G. Plummer, C. Hajmrle, A. F. Spigelman, T. Kin, D. Singer-Lahat, Y. Kang, A. M.J. Shapiro, H. Y. Gaisano, I. Lotan, and P. E. MacDonald. The voltage-dependent potassium channel subunit

Kv2.1 regulates insulin secretion from rodent and human islets independently of its electrical function. *Diabetologia*, 55(6):1709–1720, 2012.

[106] P. T. Redman, K. He, K. A. Hartnett, B. S. Jefferson, L. Hu, P. A. Rosenberg, E. S. Levitan, and E. Aizenman. Apoptotic surge of potassium currents is mediated by p38 phosphorylation of Kv2.1. *Proc. Natl. Acad. Sci.*, 104(9):3568–3573, 2007.

[107] Csaba Cserep, Balazs Posfai, Nikolett Lenart, Rebeka Fekete, Zsofia I. Laszlo, Zsolt Lele, Barbara Orsolits, Gabor Molnar, Steffanie Heindl, Anett D. Schwarcz, Katinka Ujvari, Zsuzsanna Kornyei, Krisztina Toth, Eszter Szabadits, Beata Sperlagh, Maria Baranyi, Laszlo Csiba, Tibor Hortobagyi, Zsofia Magloczky, Bernadett Martinecz, Gabor Szabo, Ferenc Erdelyi, Robert Szipocs, Michael M. Tamkun, Benno Gesierich, Marco Duering, Istvan Katona, Arthur Liesz, Gabor Tamas, and Adam Denes. Microglia monitor and protect neuronal function iva specialized somatic purinurgic junctions. *Science (80-.).*, 6752(December):5–10, 2019.

[108] Marjaana A. Peltola, Juha Kuja-Panula, Sari E. Lauri, Tomi Taira, and Heikki Rauvala. AMIGO is an auxiliary subunit of the Kv2.1 potassium channel. *EMBO Rep.*, 12(12):1293–1299, 2011.

[109] E Neher and B Sakmann. Single-channel currents recorded from membrane. *Nature*, 260:799–802, 1976.

[110] O. P. Hamill, A. Marty, E. Neher, B. Sakmann, and F. J. Sigworth. Improved patch-clamp techniques for high-resolution current recording from cells and cell-free membrane patches. *Pflügers Arch. Eur. J. Physiol.*, 391(2):85–100, 1981.

[111] J. López-Barneo, T. Hoshi, S. H. Heinemann, and R. W. Aldrich. Effects of external cations and mutations in the pore region on C-type inactivation of Shaker potassium channels. *Receptors Channels*, 1(1):61–71, 1993.

[112] L A Pardo, S H Heinemann, H Terlau, U Ludewig, C Lorra, O Pongs, and W Stuhmer. Extracellular K+ specifically modulates a rat brain K+ channel. *Proc. Natl. Acad. Sci.*, 89:2466–2470, 1992.

[113] Josef G Trapani, Payam Andalib, Joseph F Consiglio, and Stephen J Korn. Control of Single Channel Conductance in the Outer Vestibule of the Kv2.1 Potassium Channel. *J. Gen. Physiol.*, 128(2):231–246, 2006.

[114] C.R. Anderson and C.F. Stevens. Voltage clamp analysis of acetylcholine produced end-plate current fluctuations at frog neuromuscular junction. *J. Physiol.*, 235(3):655–691, 1973.

[115] E. Neher and C. F. Stevens. Conductance fluctuations and ionic pores in membranes. *Ann. Rev. Biophys. Bioeng.*, 6:345–381, 1977.

[116] Stefan H Heinemann and Franco Conti. Nonstationary noise analysis and application to patch clamp recordings. *Methods Enzymol.*, 207:131–148, 1992.

[117] Christopher J. Lingle. Empirical considerations regarding the use of ensemble-variance analysis of macroscopic currents. *J. Neurosci. Methods*, 158(1):121–132, 2006.

[118] Chang Liu, Changan Xie, Khade Grant, Zhuocheng Su, Weihua Gao, Qinglian Liu, and Lei Zhou. Patch-clamp fluorometry-based channel counting to determine HCN channel conductance. *J. Gen. Physiol.*, 148(1):65–76, 2016.

[119] Lori Feinshreiber, Dafna Singer-Lahat, Uri Ashery, and Ilana Lotan. Voltage-gated Potassium Channel as a Facilitator of Exocytosis. *Ann. N. Y. Acad. Sci.*, 1152:87–92, 2009.

[120] D. E. Antonucci, S. T. Lim, S. Vassanelli, and J. S. Trimmer. Dynamic localization and clustering of dendritic Kv2.1 voltage-dependent potassium channels in developing hippocampal neurons. *Neuroscience*, 108(1):69–81, dec 2001.

[121] Nicholas C. Vierra, Michael Kirmiz, Deborah van der List, L. Fernando Santana, and James S. Trimmer. KV2.1 mediates spatial and functional coupling of l-type calcium channels and ryanodine receptors in mammalian neurons. *Elife*, 8:1–42, 2019.

[122] M Taglialatela and E Stefani. Gating currents of the cloned delayed-rectifier K+ channel DRK1. *Proc. Natl. Acad. Sci. U. S. A.*, 90(10):4758–4762, 1993.

[123] Aubrey V. Weigel, Blair Simon, Michael M. Tamkun, and Diego Krapf. Ergodic and nonergodic processes coexist in the plasma membrane as observed by single-molecule tracking. *Proc. Natl. Acad. Sci. U. S. A.*, 108(16):6438–6443, 2011.

[124] Aubrey V. Weigel, Michael M. Tamkun, and Diego Krapf. Quantifying the dynamic interactions between a clathrin-coated pit and cargo molecules. *Proc. Natl. Acad. Sci. U. S. A.*, 110(48):E4591–E4600, 2013.

[125] Luc J. Gentet, Greg J. Stuart, and John D. Clements. Direct measurement of specific membrane capacitance in neurons. *Biophys. J.*, 79(1):314–320, 2000.

[126] Drew C. Tilley, Juan M. Angueyra, Kenneth S. Eum, Heesoo Kim, Luke H. Chao, Anthony W. Peng, and Jon T. Sack. The tarantula toxin GxTx detains K + channel gating charges in their resting conformation . *J. Gen. Physiol.*, 151(3):292–315, 2019.

[127] L. Heginbotham and R. MacKinnon. Conduction properties of the cloned Shaker K+ channel. *Biophys. J.*, 65(5):2089–2096, 1993.

[128] John R. Clay. Determining K+ channel activation curves from K+ channel currents often requires the Goldman-Hodgkin-Katz equation. *Front. Cell. Neurosci.*, 3(DEC):1–6, 2009.

[129] Michael J Wood and Stephen J Korn. Two Mechanisms of K+-Dependent Potentiation in Kv2 . 1 Potassium Channels. *Biophys. J.*, 79(5):2535–2546, 2000.

[130] Payam Andalib, Michael J Wood, and Stephen J Korn. Control of outer vestibule dynamics and current magnitude in the Kv2.1 Potassium channel. *J. Gen. Physiol.*, 120(5):739–755, 2002.

[131] Sanjay Kumar Aggarwal and Roderick MacKinnon. Contribution of the S4 segment to gating charge in the Shaker K+ channel. *Neuron*, 16(6):1169–1177, 1996.

[132] Itzel G Ishida, Gisela E Rangel-yescas, Julia Carrasco-zanini, and León D Islas. Voltage-dependent gating and gating charge measurements in the Kv1 . 2 potassium channel. *J. Gen. Phys.*, 145(4):345–358, 2015.

[133] Jie Zhang, Chase M. Carver, Frank S. Choveau, and Mark S. Shapiro. Clustering and Functional Coupling of Diverse Ion Channels and Signaling Proteins Revealed by Super-resolution STORM Microscopy in Neurons. *Neuron*, 92(2):461–478, sep 2016.

[134] Elizabeth J. Akin, Laura Solé, Ben Johnson, Mohamed el Beheiry, Jean-Baptiste Masson, Diego Krapf, and Michael M. Tamkun. Single-Molecule Imaging of Nav1.6 on the Surface of Hippocampal Neurons Reveals Somatic Nanoclusters. *Biophys. J.*, 111(6):1235–1247, sep 2016.

[135] Mihaly Kollo, Noémi Holderith, Miklós Antal, and Zoltan Nusser. Unique clustering of A-type potassium channels on different cell types of the main olfactory bulb. *Eur. J. Neurosci.*, 27(7):1686–1699, apr 2008.

[136] A. Bhargava, X. Lin, P. Novak, K. Mehta, Y. Korchev, M. Delmar, and J. Gorelik. Super-resolution scanning patch-clamp reveals clustering of functional ion channels in the adult ventricular myocyte. *Circ. Res.*, 112(8):1112–1120, 2013.

[137] Ayumi Sumino, Daisuke Yamamoto, Masayuki Iwamoto, Takehisa Dewa, and Shigetoshi Oiki. Gating-associated clustering-dispersion dynamics of the KcsA potassium channel in a lipid membrane. *J. Phys. Chem. Lett.*, 5(3):578–584, 2014.

[138] Koen M. Visscher, João Medeiros-Silva, Deni Mance, João P.G.L.M. Rodrigues, Mark Daniëls, Alexandre M.J.J. Bonvin, Marc Baldus, and Markus Weingarth. Supramolecular Organization and Functional Implications of K+ Channel Clusters in Membranes. *Angew. Chemie - Int. Ed.*, 56(43):13222–13227, 2017.

[139] Rose E. Dixon, Claudia M. Moreno, Can Yuan, Ximena Opitz-Araya, Marc D. Binder, Manuel F. Navedo, and Luis F. Santana. Graded Ca2+/calmodulin-dependent coupling of voltage-gated CaV1.2 channels. *Elife*, 2015(4):1–21, 2015.

[140] Claudia M. Moreno, Rose E. Dixon, Sendoa Tajada, Can Yuan, Ximena Opitz-Araya, Marc D. Binder, and Luis F. Santana. Ca2+ entry into neurons is facilitated by co-operative gating of clustered Cav1.3 channels. *Elife*, 5(MAY2016):e15744, 2016.

[141] Grace E. Kim, Jack Kronengold, Giulia Barcia, Imran H. Quraishi, Hilary C. Martin, Edward Blair, Jenny C. Taylor, Olivier Dulac, Laurence Colleaux, Rima Nabbout, and Leonard K. Kaczmarek. Human Slack Potassium Channel Mutations Increase Positive Cooperativity between Individual Channels. *Cell Rep.*, 9(5):1661–1672, dec 2014.

[142] D. J. Mays, J. M. Foose, L. H. Philipson, and M. M. Tamkun. Localization of the Kv1.5 K+ channel protein in explanted cardiac tissue. *J. Clin. Invest.*, 96(1):282–292, 1995.

[143] Jodene Eldstrom, David R. Van Wagoner, Edwin D. Moore, and David Fedida. Localization of Kv1.5 channels in rat and canine myocyte sarcolemma. *FEBS Lett.*, 580(26):6039–6046, 2006.

[144] Marina A. Kasimova, Mark A. Zaydman, Jianmin Cui, and Mounir Tarek. PIP2-dependent coupling is prominent in Kv7.1 due to weakened interactions between S4-S5 and S6. *Sci. Rep.*, 5:2–10, 2015.

[145] Donald W. Hilgemann. Fitting KV potassium channels into the PIP2 puzzle: Hille group connects dots between illustrious HH groups. *J. Gen. Physiol.*, 140(3):245–248, 2012.

[146] Martin Kruse, Gerald R.V. Hammond, and Bertil Hille. Regulation of voltage-gated potassium channels by PI(4,5)P2. *J. Gen. Physiol.*, 140(2):189–205, 2012.

[147] Helgi I. Ingólfsson, Timothy S. Carpenter, Harsh Bhatia, Peer Timo Bremer, Siewert J. Marrink, and Felice C. Lightstone. Computational Lipidomics of the Neuronal Plasma Membrane. *Biophys. J.*, 113(10):2271–2280, 2017.

[148] Melanie M. Cobb, Daniel C. Austin, Jon T. Sack, and James S. Trimmer. Cell cycle-dependent changes in localization and phosphorylation of the plasma membrane Kv2.1 K+ channel impact endoplasmic reticulum membrane contact sites in COS-1 cells. *J. Biol. Chem.*, 290(49):29189–29201, 2015.

[149] Rosie Dawaliby, Cataldo Trubbia, Cédric Delporte, Caroline Noyon, Jean Marie Ruysschaert, Pierre Van Antwerpen, and Cédric Govaerts. Phosphatidylethanolamine is a key regulator of membrane fluidity in eukaryotic cells. *J. Biol. Chem.*, 291(7):3658–3667, 2016.

[150] Masashi Maekawa and Gregory D. Fairn. Molecular probes to visualize the location, organization and dynamics of lipids. *J. Cell Sci.*, 127(22):4801–4812, 2014.

[151] Yan Li, Yon Um Sung, and Thomas V. McDonald. Voltage-gated potassium channels: Regulation by accessory subunits. *Neuroscientist*, 12(3):199–210, 2006.

[152] Olaf Pongs and Jürgen R. Schwarz. Ancillary subunits associated with voltage-dependent K+ channels. *Physiol. Rev.*, 90(2):755–796, 2010.

[153] Xiaohui Sun, Mark A. Zaydman, and Jianmin Cui. Regulation of voltage-activated K+ channel gating by transmembrane β subunits. *Front. Pharmacol.*, 3 APR(April):1–10, 2012.

[154] Sarah K. England, Victor N. Uebele, Holly Shear, Jayaveera Kodali, Paul B. Bennett, and Michael M. Tamkun. Characterization of a voltage-gated K+ channel β subunit expressed in human heart. *Proc. Natl. Acad. Sci. U. S. A.*, 92(14):6309–6313, 1995.

[155] T. Leicher, J. Roeper, K. Weber, X. Wang, and O. Pongs. Structural and functional characterization of human potassium channel subunit β1 (KCNA1B). *Neuropharmacology*, 35(7):787–795, 1996.

[156] Geoffrey W. Abbott, Federico Sesti, Igor Splawski, Marianne E. Buck, Michael H. Lehmann, Katherine W. Timothy, Mark T. Keating, and Steve A.N. Goldstein. MiRP1 forms IKr potassium channels with HERG and is associated with cardiac arrhythmia. *Cell*, 97(2):175–187, 1999.

[157] Yumei Wu, Christina Whiteus, C. Shan Xu, Kenneth J. Hayworth, Richard J. Weinberg, Harald F. Hess, and Pietro De Camilli. Contacts between the endoplasmic reticulum and other membranes in neurons. *Proc. Natl. Acad. Sci. U. S. A.*, 114(24):E4859–E4867, 2017.

[158] Hiroaki Misonou, Durga P Mohapatra, Milena Menegola, and James S Trimmer. Calcium- and metabolic state-dependent modulation of the voltage-dependent Kv2.1 channel regulates neuronal excitability in response to ischemia. *J. Neurosci.*, 25(48):11184–11193, 2005.

[159] Kang-sik Park, Durga P Mohapatra, Hiroaki Misonou, and James S Trimmer. Graded Regulation of the Kv2.1 Potassium Channel by Variable Phosphorylation. *Science (80-.).*, 313(5789):976–980, 2006.

[160] Juha Kuja-Panula, Marjaana Kiiltomäki, Takashi Yamashiro, Ari Rouhiainen, and Heikki Rauvala. AMIGO, a transmembrane protein implicated in axon tract development, defines a novel protein family with leucine-rich repeats. *J. Cell Biol.*, 160(6):963–973, 2003.

[161] Tommi Kajander, Juha Kuja-Panula, Heikki Rauvala, and Adrian Goldman. Crystal structure and role of glycans and dimerization in folding of neuronal leucine-rich repeat protein AMIGO-1. *J. Mol. Biol.*, 413(5):1001–1015, 2011.

[162] Yanan Chen, Hong Huan Hor, and Bor Luen Tang. AMIGO is expressed in multiple brain cell types and may regulate dendritic growth and neuronal survival. *J. Cell. Physiol.*, 227(5):2217–2229, 2012.

[163] Zubair Ahmed, Michael R. Douglas, Gabrielle John, Martin Berry, and Ann Logan. AMIGO3 Is an NgR1/p75 Co-Receptor Signalling Axon Growth Inhibition in the Acute Phase of Adult Central Nervous System Injury. *PLoS One*, 8(4):e61878, apr 2013.

[164] Florentina Soto, Nai Wen Tien, Anurag Goel, Lei Zhao, Philip A. Ruzycki, and Daniel Kerschensteiner. AMIGO2 Scales Dendrite Arbors in the Retina. *Cell Rep.*, 29(6):1568–1578.e4, 2019.

[165] Tomio Ono, Naoko Sekino-Suzuki, Yoshiaki Kikkawa, Hiromichi Yonekawa, and Seiichi Kawashima. Alivin 1, a novel neuronal activity-dependent gene, inhibits apoptosis and promotes survival of cerebellar granule neurons. *J. Neurosci.*, 23(13):5887–5896, 2003.

[166] Sharmin Hossain, Minhaz Uddin Ahmed, Shamiul Alam, Akuo Watanabe, Ai Harashima, Hideto Yonekura, and Hiroshi Yamamoto. Expressions and Roles of AMIGO Gene Family in Vascular Endothelial Cells. *Int. J. Biosci. Biochem. Bioinforma.*, 2(1):1–5, 2012.

[167] Karen E. Rabenau, Jennifer M. O'Toole, Rajiv Bassi, Helen Kotanides, Larry Witte, Dale L. Ludwig, and Daniel S. Pereira. DEGA/AMIGO-2, a leucine-rich repeat family member, differentially expressed in human gastric adenocarcinoma: Effects on

ploidy, chromosomal stability, cell adhesion/migration and tumorigenicity. *Oncogene*, 23(29):5056–5067, 2004.

[168] Barbara Fontanals-Cirera, Dan Hasson, Chiara Vardabasso, Raffaella Di Micco, Praveen Agrawal, Asif Chowdhury, Madeleine Gantz, Ana de Pablos-Aragoneses, Ari Morgenstern, Pamela Wu, Dan Filipescu, David Valle-Garcia, Farbod Darvishian, Jae Seok Roe, Michael A Davies, Christopher R Vakoc, Eva Hernando, and Emily Bernstein. Harnessing BET Inhibitor Sensitivity Reveals AMIGO2 as a Melanoma Survival Gene. *Mol. Cell*, 68(4):731–744.e9, 2017.

[169] Hyojin Park, Sungwoon Lee, Pravesh Shrestha, Jihye Kim, Jeong Ae Park, Yeongrim Ko, Young Ho Ban, Dae-Young Young Park, Sang-Jun Jun Ha, Gou Young Koh, Victor Sukbong Hong, Naoki Mochizuki, Young-Myeong Myeong Kim, Weontae Lee, and Young-Guen Guen Kwon. AMI GO2, a novel membrane anchor of PDK1, controls cell survival and angiogenesis via Akt activation. *J. Cell Biol.*, 211(3):619–637, nov 2015.

[170] Irwin Chen, Mark Howarth, Weiying Lin, and Alice Y. Ting. Site-specific labeling of cell surface proteins with biophysical probes using biotin ligase. *Nat. Methods*, 2(2):99–104, 2005.

[171] Kathryn G. Klemic, Char Chang Shieh, Glenn E. Kirsch, and Stephen W. Jones. Inactivation of Kv2.1 potassium channels. *Biophys. J.*, 74(4):1779–1789, 1998.

[172] Elisa Carrillo, Imilla I Arias-olguín, León D Islas, and Froylan Gómez-lagunas. Shab K+ channel slow inactivation: A test for U-type inactivation and a hypothesis regarding K+-facilitated inactivation mechanisms. *Channels*, 7(2):97–108, 2013.

[173] Jiusheng Yan and Richard W. Aldrich. LRRC26 auxiliary protein allows BK channel activation at resting voltage without calcium. *Nature*, 466(7305):513–516, 2010.

[174] Pin W. Liu and Bruce P. Bean. Kv2 channel regulation of action potential repolarization and firing patterns in superior cervical ganglion neurons and hippocampal CA1 pyramidal neurons. *J. Neurosci.*, 34(14):4786–4800, 2014.

[175] Parveen Sharma, Vladimir Ignatchenko, Kevin Grace, Claudia Ursprung, Thomas Kislinger, and Anthony O. Gramolini. Endoplasmic reticulum protein targeting of phospholamban: A common role for an N-terminal di-arginine motif in ER retention? *PLoS One*, 5(7), 2010.

[176] L. D. Plant, D. Xiong, H. Dai, and S. A. N. Goldstein. Individual IKs channels at the surface of mammalian cells contain two KCNE1 accessory subunits. *Proc. Natl. Acad. Sci.*, 111(14):E1438–E1446, apr 2014.

[177] Laura Solé, Daniel Sastre, Magalí Colomer-Molera, Albert Vallejo-Gracia, Sara R. Roig, Mireia Pérez-Verdaguer, Pilar Lillo, Michael M. Tamkun, and Antonio Felipe. Functional Consequences of the Variable Stoichiometry of the Kv1.3-KCNE4 Complex. *Cells*, 9(5):1–17, 2020.

[178] Koichi Nakajo, Maximilian H. Ulbrich, Yoshihiro Kubo, and Ehud Y. Isacoff. Stoichiometry of the KCNQ1 - KCNE1 ion channel complex. *Proc. Natl. Acad. Sci. U. S. A.*, 107(44):18862–18867, 2010.

[179] Isabelle Thiffault, David J. Speca, Daniel C. Austin, Melanie M. Cobb, Kenneth S. Eum, Nicole P. Safina, Lauren Grote, Emily G. Farrow, Neil Miller, Sarah Soden, Stephen F. Kingsmore, James S. Trimmer, Carol J. Saunders, and Jon T. Sack. A novel epileptic encephalopathy mutation in KCNB1 disrupts Kv2.1 ion selectivity, expression, and localization. *J. Gen. Physiol.*, 146(5):399–410, 2015.

[180] John Cowgill and Baron Chanda. The contribution of voltage clamp fluorometry to the understanding of channel and transporter mechanisms. *J. Gen. Physiol.*, 151(10):1163–1172, 2019.

[181] Christian J. Peters, David Fedida, and Eric A. Accili. Allosteric coupling of the inner activation gate to the outer pore of a potassium channel. *Sci. Rep.*, 3:1–8, 2013.

[182] Georges A. Haddad and Rikard Blunck. Mode shift of the voltage sensors in Shaker K+ channels is caused by energetic coupling to the pore domain. *J. Gen. Physiol.*, 137(5):455–472, 2011.

[183] Junji Suzuki, Kazunori Kanemaru, Kuniaki Ishii, Masamichi Ohkura, Yohei Okubo, and Masamitsu Iino. Imaging intraorganellar Ca2+ at subcellular resolution using CEPIA. *Nat. Commun.*, 5(May):1–13, 2014.

[184] Tsai-wen Chen, Trevor J Wardill, Yi Sun, Stefan R Pulver, Sabine L Renninger, Amy Baohan, Eric R Schreiter, Rex A Kerr, Michael B Orger, Vivek Jayaraman, Loren L Looger, Karel Svoboda, and Douglas S Kim. Ultra-sensitive fluorescent proteins for imaging neuronal activity. *Nature*, 499(7458):295–300, 2013.

[185] Yi Shen, Sheng Yi Wu, Vladimir Rancic, Abhi Aggarwal, Yong Qian, Shin Ichiro Miyashita, Klaus Ballanyi, Robert E. Campbell, and Min Dong. Genetically encoded fluorescent indicators for imaging intracellular potassium ion concentration. *Commun. Biol.*, 2(1):1–10, 2019.

[186] J C Hesketh and D Fedida. Sequential gating in the human heart K(+) channel Kv1.5 incorporates Q(1) and Q(2) charge components. *Am. J. Physiol.*, 277(5 Pt 2):H1956–66, 1999.

[187] F. Bezanilla, E. Perozo, and E. Stefani. Gating of Shaker K+ channels: II. The components of gating currents and a model of channel activation. *Biophys. J.*, 66(4):1011–1021, 1994.

[188] Sasha S. Grimm and Ehud Y. Isacoff. Allosteric substrate switching in a voltage-sensing lipid phosphatase. *Nat. Chem. Biol.*, 12(4):261–267, 2016.

[189] Elke Bocksteins. Kv5, Kv6, Kv8, and Kv9 subunits: No simple silent bystanders. *J. Gen. Physiol.*, 147(2):105–125, 2016.

[190] Daniel Kerschensteiner and Martin Stocker. Heteromeric assembly of Kv2.1 with Kv9.3: Effect on the state dependence of inactivation. *Biophys. J.*, 77(1):248–257, 1999.

[191] Daniel Kerschensteiner, Francisco Monje, and Martin Stocker. Structural determinants of the regulation of the voltage-gated potassium channel Kv2.1 by the Modulatory α-subunit Kv9.3. *J. Biol. Chem.*, 278(20):18154–18161, 2003.

[192] A J Patel, M Lazdunski, and E Honoré. Kv2.1/Kv9.3, a novel ATP-dependent delayed-rectifier K+ channel in oxygen-sensitive pulmonary artery myocytes. *EMBO J.*, 16(22):6615–25, 1997.

[193] Joanne T. Hulme, Elizabeth A. Coppock, Antonio Felipe, Jeffery R. Martens, and Michael M. Tamkun. Oxygen sensitivity of cloned voltage-gated K+ channels expressed in the pulmonary vasculature. *Circ. Res.*, 85(6):489–497, 1999.

[194] Elke Bocksteins, Dirk J Snyders, and Miguel Holmgren. Independent movement of the voltage sensors in KV2.1/KV6.4 heterotetramers. *Sci. Rep.*, 7(41646), 2017.

Appendix A

Non-stationary noise fluctuation analysis: Theory and Validation

A.1 The accuracy of our noise fluctuation measurements

In Figure 2.9 I showed the single channel conductance of Kv2.1 measured from noise fluctuations as a function of channel expression. There was no relationship between those parameters. Noise fluctuation analysis also yields an estimate of the number of channels contributing to the macroscopic current. In Figure A.1 below I show the number of channels estimated from HEK293 cells expressing Kv2.1 as a function of the peak membrane conductance during the recording. It is immediately clear that the number of channels is a linear function of the membrane conductance, and this relationship does not deviate across the range tested. This is strong evidence that noise fluctuation analysis was accurate across the expression range.

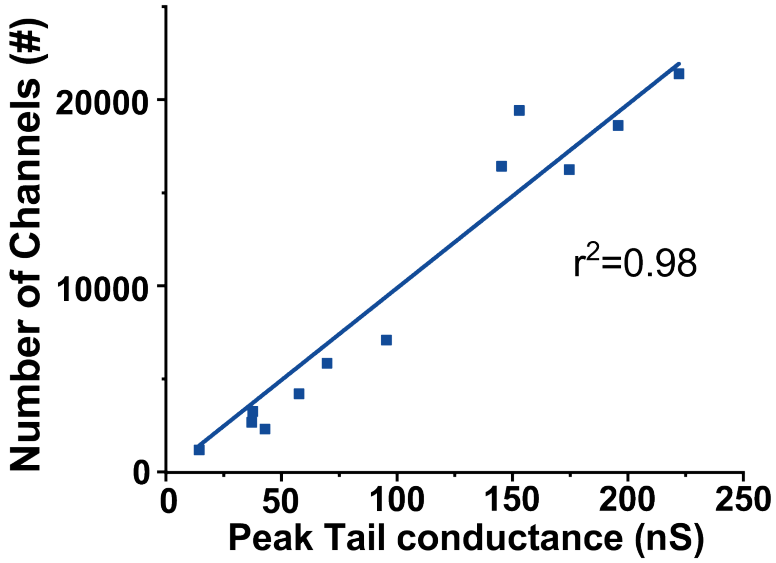

Figure A.1: N from noise analysis is a function of channel expression. A plot of the number of channels in each cell estimated using noise fluctuation analysis of Kv2.1 in Flipped K^+. The relationship was fit well with a line, suggesting that our analysis method was accurate across the range tested. Each data point is one cell. The data is from the same cells whose single channel conductance values are shown in Figure 2.9.

A.2 Derivations

Here I will walk through the theory that predicts the parabolic nature of gating fluctuations as a function of mean current. I have mostly followed the work of `Alvarez et al 2002` but included a few more mathematical steps here for my own benefit.

A.2.1 One Channel, one open state

Variables:

$< I >$ Mean Current

i Unitary Current

p Open probability

q Closed probability

Note that $p + q = 1$.

The mean current is the single channel current time the open probability:

$$< I >= ip$$

The variance in the current is the sum of the squared deviations from the mean. In other words, the sum of each state times the probability of finding the channel in that state. In the case of a single channel, there are only two states that deviate from the mean, open and closed (we are ignoring the variance in the mean current that flows through a single open channel). The probability of finding the channel in the open or closed state is given by p and q, respectively:

$$\sigma^2 = q(0 - ip)^2 + p(i - ip)^2$$

$$\sigma^2 = q(i^2p^2) + p(i^2 - 2i^2p + i^2p^2)$$

$$\sigma^2 = i^2p^2q + i^2p - 2i^2p^2 + i^2p^3$$

$$\sigma^2 = i^2p(pq + 1 - 2p + p^2)$$

At this point we will make the following substitution: $p^2 = (1-q)^2 = (-1+2p+q^2)$.

$$\sigma^2 = i^2 p(pq + 1 - 2p - 1 + 2p + q^2)$$

$$\sigma^2 = i^2 p(pq + q^2)$$

$$\sigma^2 = i^2 pq(p + q)$$

$$\sigma^2 = i^2 pq$$

A.2.2 N Channels, one open state

The mean and variance are similar to above but scaled by the number of channels in the membrane, N:

$$< I >= Nip$$

$$\sigma^2 = Ni^2 pq$$

Let us write the variance in terms of $< I >$:

$$\sigma^2 = Nip(iq)$$

$$\sigma^2 =< I > (iq)$$

Let us substitute $iq = i(1-p) = (i - ip)$:

$$\sigma^2 =< I > (i - ip)$$

$$\sigma^2 = i < I > -ip < I >$$

And one more substitution where $ip = \frac{<I>}{N}$ from the definition of mean current above:

$$\sigma^2 = i < I > -\frac{< I >}{N} < I >$$

$$\sigma^2 = i < I > - \frac{< I >^2}{N}$$

We have arrived at a second order polynomial (parabola) that relates the statistical noise associated with channel gating to the mean current. Ideally the data we collect will be fit well with a parabola. If it is not, artifacts due to filtering, channel rundown or excess noise are likely present.

If we take the derivative with respect to $< I >$:

$$\frac{d\sigma^2}{d < I >} = i - \frac{2 < I >}{N}$$

we see that as $< I >$ approaches 0, the derivative approaches i. Therefore, the slope of the parabola near $< I >= 0$ is equal to the single channel current. This is the basis for our treatment of noise fluctuation data to estimate unitary current.

Appendix B

Silent subunit Kv9.3 does not alter the non-conducting fraction of Kv2.1

Kv9.3 is a member of one of the Kv channel silent subunit families [189]. Kv9.3 is widely expressed throughout the nervous system and body where it associates with Kv2 channels and modulates their gating behavior [189–191]. Interestingly, Kv9.3 is highly expressed in smooth muscle where it may impart ATP- and oxygen sensitivity to the delayed rectifier current [192, 193]. Given the large number of non -conducting Kv2.1

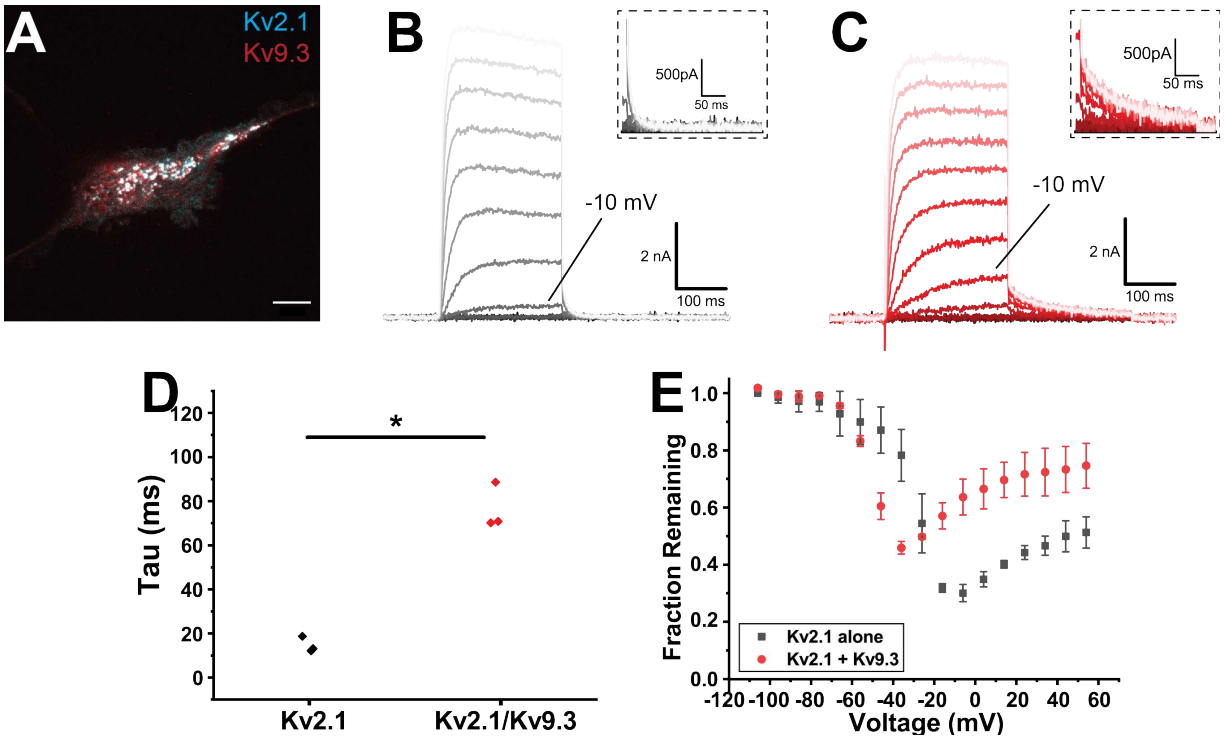

Figure B.1: Kv9.3 assembles with and modulates Kv2.1 function in HEK293 cells. **A)** TIRF image of the basal surface of a HEK293 cell co-expressing GFP-Kv2.1 (cyan) and RFP-Kv9.3 (red) showing co-localization of the two subunits. Scale bar = 10 microns **B)** Whole-cell currents from a HEK293 cell expressing GFP-Kv2.1 alone. The command potentials were between -60 and +60 mV. *Inset* - Zoom of tail currents recorded at -40 mV after the depolarizing pulses. Note that tail currents decayed to baseline within 50 ms. **C)** Currents from HEK293 cell expressing both GFP-Kv2.1 and RFP-Kv9.3. *Inset* - Zoom of tail currents recorded at -40 mV. Note that tail currents do not reach baseline within several hundred milliseconds. **D)** Time constants of current deactivation at -40 mV from 3 cells expressing GFP-Kv2.1 alone (grey) or GFP-Kv2.1 and RFP-Kv9.3 together (red). **E)** Voltage-dependence of current inactivation from HEK293 cells expressing GFP-Kv2.1 only (grey) or GFP-Kv2.1+RFP-Kv9.3 (red). The midpoint of inactivation was hyperpolarized in the presence of Kv9.3.

channels recently identified in arterial smooth muscle cells, we wondered weather Kv9.3 could promote the non-conducting state of Kv2.1 channels. To that end, we co-expressed Kv2.1 and Kv9.3 subunits in HEK293 cells and counted non-conducting channels.

First, we convinced ourselves that Kv2.1 and Kv9.3 would co-assemble when expressed together in HEK293 cells. Figure B.1A shows a TIRF image of a HEK293 cell expressing the two subunits. GFP-Kv2.1 and RFP-Kv9.3 were largely co-localized both within and outside of Kv2.1 clusters. We also recorded whole-cell currents from cells expressing both subunits in physiological K^+ solutions. Figure B.1B and C show representative currents from cells expressing Kv2.1 alone or Kv2.1+Kv9.3, respectively. The currents were similar, although there were subtle differences in the voltage dependence of activation (not shown) and the kinetics of inactivation (not shown). Co-expression with Kv9.3 did impart a dramatic slowing to Kv2.1 deactivating tail currents, strongly suggesting that the two subunits assembled into functional heterotetramers. Further supporting this conclusion was that Kv9.3 shifted the voltage dependence of Kv2.1 inactivation by -20 mV, as shown in Figure B.1E. This finding is in good agreement with the published effects of Kv9.3 on Kv2.1 inactivation [190].

We next co-expressed Kv2.1 and Kv9.3 subunits in HEK293 cells bathed in Flipped K^+. We voltage-clamped them as described in Chapter 2 of this dissertation and recorded the macroscopic gating charge and membrane conductance associated with the heteromers. Figure B.2A shows the numbers of conducting and gating heteromers we obtained from HEK293 cells. The number of gating channels was consistently higher than the number of conducting channels. Indeed, when we calculated the average conducting fraction, we found that about 45% of channels were conducting, as shown in Figure B.2B. Similar to our findings from the other channels in this dissertation, the Kv2.1/Kv9.3 conducting fraction was a function of the density of channels in the membrane, as seen in Figure B.2C. These results were extremely similar to the measurements we made from Kv2.1 alone in Chapter 2. There certainly was no evidence that 10 fold fewer channels were conduct-

ing upon co-expression of Kv9.3. Therefore, we do not believe that this silent subunit regulates entry into the non-conducting state we measured here.

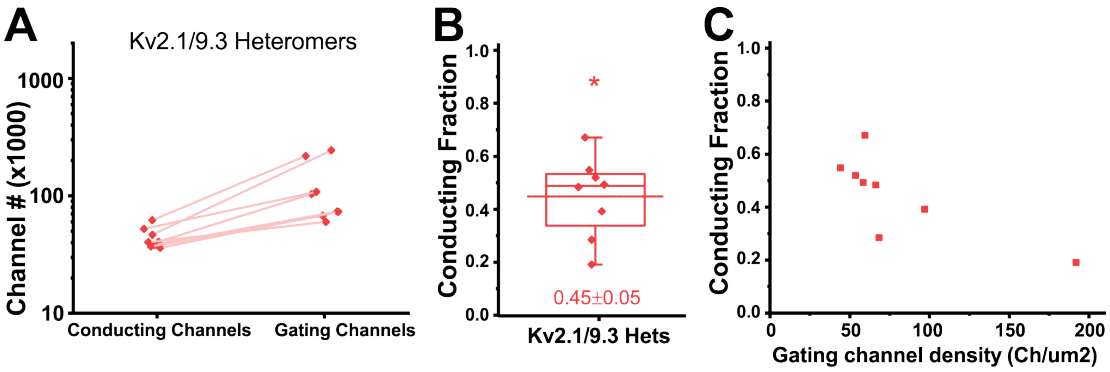

Figure B.2: Non-conducting fraction of Kv2.1/Kv9.3 heteromers. **A)** Comparison of the number of conducting and gating Kv2.1/Kv9.3 heteromers expressed in HEK293 cells as determined from the macroscopic gating charge and membrane conductance in Flipped K^+. We used the unitary values of gating charge, single channel conductance and open probability from Kv2.1 alone (Chapter 2) to calculate channel numbers here. **B)** The same data in A shown as the fraction of gating channels that were conducting. The average fraction was 0.45±0.05, which was significantly different from 1 ($p<0.0005$, One sample T-test).**C)** The conducting fraction from B shown as a function of the density of gating channels in each cell. The relationship shows that silencing of Kv2.1/Kv9.3 heteromers is sensitive to expression level.

One caveat to these data is that we did not make measurements of unitary charge or single channel conductance from Kv2.1/Kv9.3 heteromers. We used the unitary measurements from Kv2.1 alone to estimate the numbers of gating and conducting heteromers. Patel and coworkers found that Kv2.1/Kv9.3 heteromers had a larger single channel conductance than Kv2.1 alone in physiological K^+ [192]. Therefore, it is possible that we overestimated the number of conducting channels in this work. To our knowledge, the unitary charge of Kv2.1/Kv9.3 has not been measured. Bocksteins et al. found that the voltage sensors of Kv2.1 and Kv6.4 subunits moved independently and with different voltage dependence when assembled into Kv2.1/Kv6.4 heteromers [194]. Whether the same is true of heteromers formed with Kv9.3 is unknown. Furthermore, whether this would alter the charge moved in the first 3 ms after maximal activation is also unknown. For now, we conclude that Kv9.3 does not alter the fraction of non-conducting Kv2.1 channels in HEK293 cells.